NASA Contractor Report No. 175030

Optical and Probe Determination of Soot Concentrations in a Model Gas Turbine Combustor

W.A. Eckerle
T.J. Rosfjord

UNITED TECHNOLOGIES RESEARCH CENTER
East Hartford, CT 06108

January 1986

Optical and Probe Determination of Soot Concentrations in a Model Gas Turbine Combustor

W.A. Eckerle
T.J. Rosfjord

UNITED TECHNOLOGIES RESEARCH CENTER
East Hartford, CT 06108

January 1986

NASA

National Aeronautics and
Space Administration

Lewis Research Center
Cleveland, Ohio 44135

ACKNOWLEDGEMENTS

Optical and Probe Determination of Soot Concentrations
In a Model Gas Turbine Combustor

Table of Contents

LIST OF FIGURES

LIST OF TABLES

LIST OF SYMBOLS

CDA	Effective Area of Liner Hole
D	Soot particulate characteristic diameter
f/a	Fuel-air ratio
I	Scattered light intensity
I_o	Incident light intensity at sample volume
l	Axial distance along combustor
L	Length of six-louver combustor
n	Complex refractive index
N	Soot particulate number density
NN	Fuel injector nozzle number
P	Local pressure
PC	Soot particulate concentration, mg/sm^3
PV	Soot particulate volume, sm^3
R	Measured radiance from soot particulates
R^2	Square of regression correlation
SMD	Fuel spray Sauter Mean Diameter
SMD_c	Critical SMD
SN	SAE smoke number
T	Local temperature
x	Light scattering size parameter
θ	Light scattering angle
τ	Wavelength of scattered light
ϕ	Complex light scattering function

SUMMARY

Contemporary gas turbine engines must be designed to meet both severe efficiency and fuel consumption requirements as well as advanced durability targets. These constraints are not easily satisfied at the same time. A compromise among these conflicting requirements is not easily developed during the design process because of a dearth of experimental data regarding certain aspects of the engine processes. One component that is particularly difficult to design is the combustor liner. An optimum combination of liner strength and liner coolant flow must be chosen so that the liner can withstand the high radiative loads generated by soot produced in the combustion process. Minimal liner weight and coolant flow rates are sought to achieve fuel consumption goals. Proper design of the liner, then, requires knowledge of the soot loading throughout the combustor. The program goal was to address this problem by tracking the variation in soot loading along the centerline of a generic gas turbine combustor.

Soot loading was measured inside a 12.7-cm diameter, six-sheet-metal-louver burner. A single pressure-atomizing injector and air swirler were centrally mounted within the burner's conical dome. Determination of soot loading along the burner length was achieved by acquiring measurements first at the exit of the full-length combustor and then at upstream stations by sequential removal of liner louvers to shorten the burner length. Alteration of the flow field approaching and within the shortened burners was minimized by maintaining a constant liner pressure drop achieved by bypassing flow that would have passed through removed louvers. In this manner, data were acquired at six combustor stations.

Two test phases were conducted. First, fuel effects tests were performed during which data were acquired with four test fuels. Fuel physical properties were de-emphasized by using fuel injectors which produced highly atomized, and hence, rapidly vaporizing sprays. The burner

exhaust flow was sampled at the burner centerline to determine soot mass concentration and smoke number. The characteristic particle size and number density of the centerline exhaust soot were determined by an optical technique which interpreted scattered light signals according to Mie thercy. Optical techniques were also used to measure the transmissivity of the exhaust flow as well as the local radiation from luminous soot particles in the exhaust. All data during this phase were acquired at a single airflow condition which simulated high-power operation of a gas turbine combustor, namely, combustor pressure = 1.3 MPa and inlet temperature = 700K. Test fuels were combusted at three fuel-air ratios, which were specified to achieved nominal exit temperatures of 1240K, 1340K, and 1470K.

The second test phase involved acquiring similar data at a reduced combustor pressure of 0.8 MPa. Airflows were flow-parameter scaled to maintain the same approach-flow Mach number at reduced pressure. Data were acquired at three burner lengths with two test fuels. The combustor approach flow was again maintained independent of combustor length by bypassing excess flow to retain constant liner pressure loss. The two test fuels were combusted at the same fuel-air ratios indicated above.

The particulate concentration data indicated a strong soot oxidation mechanism in the combustor secondary zone. Concentration measurements with three louvers removed were at least an order of magnitude higher than those measured for the full-length combustor. Samples collected with shorter burners were influenced by the dilution jets of this combustor. The jets effectively penetrated to the centerline and locally diluted the centerline region. Particulate samples representative of the average loading in the combustor front end, then, were not acquired via the centerline sampling technique. Transmissivity and radiation measurements, which were path-length diagnostics, indicated significantly higher loading near the primary zone. These optical data imply that mass loading in the vicinity of the primary zone was even more than one order of magnitude greater than loading measured in the full-length combustor exhaust. Secondary-zone oxidation was also a strong function of the flow temperature. Although increased levels of soot were produced at higher fuel-air ratios, higher exit temperatures, associated with higher fuel-air ratio, enhanced soot

oxidation so that full-length combustor exit concentrations were lower at higher fuel-air ratio. The influence of fuel chemical properties on soot production was directly related to the fuel smoke point, where fuels with the highest smoke point demonstrated less propensity to soot. Particulate concentrations measured at reduced pressure indicated less soot production at the lower pressure. The data also indicate that lower secondary-zone oxidation rates may be associated with reduced combustor pressure.

Particulate number density and SAE smoke number, which were also centerline measurements, displayed the previously noted trends. A good correlation was obtained between particulate concentration and smoke number. This agreement is attributed to the relatively small size distribution of the particulates, whose measured characteristic diameter varied from 0.25 μm inside the burner to 0.20 μm at the burner exit. Particulate number density and characteristic diameter were used to calculate particulate volume, which correlated with particulate concentration. Particulate density, calculated from particulate concentration and particulate volume, was nominally 20 percent that of pure carbon. This low value for density corroborates the concept that soot particulates are chain-like structures composed of tiny particles of pure carbon.

Optical and Probe Determination of Soot Concentrations in a Model Gas Turbine Combustor

SECTION I - INTRODUCTION

Substantial levels of soot are present within gas turbine combustors. High production rates occur in the dome region where zones of high fuel concentration exist. Coupled with the high temperature in this primary zone, such high soot levels produce intense radiative loads on the combustor liner, elevating its temperature and thereby reducing the time to failure. The level of soot produced is not known. A large fraction of it is oxidized in the secondary and tertiary zones of the combustor, producing soot levels which, by not being visible in the exhaust stream, are considered acceptable. The actual variation of soot loading within the gas turbine combustor has not been documented. Such data could be used to define the influence of chemical properties on primary zone soot production, and the effectiveness of the combustor oxidation mechanisms at reducing the soot loading upstream of the exit. Additionally, measured changes in soot particle size and number density along the combustor length would aid understanding of basic soot formation, growth, and oxidation mechanisms.

A previous NASA program (Ref. 1) documented that fuel chemical properties can influence the radiative load on the combustor liner by altering soot concentration in the primary zone. In that program, well-controlled combustor tests were performed with 25 test fuels. Data indicated that the primary influence of changing fuel chemical properties was to alter soot produced in the combustor. That is, fuels which displayed a high propensity to soot (i.e., low fuel specification smoke point) produced high radiative heat loads and exhaust soot concentrations. As a consequence, high liner temperatures and exhaust smoke numbers were also attained. While the exhaust soot concentrations were documented in that program, no measurements were made within the burner.

The work reported here represents a continuation of the above work. This program was directed toward documenting the soot loading in a gas turbine combustor. Optical and probing techniques determined characteristic size and number density of soot aggregates, soot mass concentration, and SAE smoke number along the centerline of a generic combustor. Optical techniques were also used to measure the tramissivity and radiance of the exhaust flow. Data were acquired from tests using four fuels with a significant variation in chemical properties. Tests were performed at two combustor pressures to document the influence of this variable. Fuel spray characterization studies supplemented the combustion tests.

This document reports results of this program. Section II describes the chemical analysis of the four test fuels along with the fuel spray characterization effort to determine appropriate fuel injectors. Sections III and IV describe the combustor, test facility and instrumentation, and the test conditions, procedures, and data handling, respectively. Results of the combustion tests are presented and discussed in Section V. Conclusions and recommendations are listed in Section VI.

SECTION II - FUEL CHEMICAL AND SPRAY PROPERTIES

In order to determine the effect of fuel chemical properties on soot loading within a combustor, tests were conducted with four fuels which offered a significant range in chemical properties. The four fuels used in these tests were Jet A, ERBS (Experimental Referee Broad Specification), ERBLS-2 (a 60/40 (vol) blend of ERBS and BLS (blending stock)), and XTB (Xylene Tower Bottoms). Jet A, which is a high-quality petroleum-derived fuel produced in accordance with ASTM and USAF specifications, is commonly used in gas turbine engines. ERBS fuel evolved from a NASA-directed workshop on alternative hydrocarbon fuels (Ref. 2). Unlike most fuel specifications, which place upper limits on certain chemical properties, a single level (and tolerance) of hydrogen content is specified for ERBS. This approach minimizes the chemical property variation of subsequent batches of ERBS production. ERBS has become a standard fuel for NASA-sponsored fuel-effects investigations. XTB is a specialty product consisting of various single-ring aromatic compounds (alkylbenzenes) and has been used in other fuel effects tests. BLS is a mixture of XTB and a gas oil that NASA had obtained to use for modification of fuel properties, and contains single-ring and double-ring aromatic compounds. The Jet A and XTB fuels were procured by UTRC while the ERBS and BLS fuels were provided by NASA. UTRC blended the ERBLS-2 fuel in the following manner. The volume fraction specifications were translated to mass fractions. A shipping scale was used to weigh the quantity of each component, which was then pumped into a 1000 liter mixing tank. The entire batch of the blend was mixed by pumping out of one end of the tank and into the other. Circulation time was sufficient to displace the blend volume at least ten times. The blended fuel was subsequently pumped from the mixing tank into drums.

Fuel Analysis

A sample of each test fuel was analyzed by Southwest Research Institute in accordance with the properties and procedures indicated in Table 1. The results of these analyses are presented in Table 2. The levels of total aromatics and naphthalenes presented for any fuel were obtained from mass spectrometric analysis. All hydrocarbons contained in the aromatic fraction of the sample contributed to the "total aromatics" level. The naphthalene compounds were assumed to include the acenaphthene (C_nH_{2n-14}) and acenaphthalene (C_nH_{2n-16}) hydrocarbons. Volume fraction values for total aromatics were determined from the reported mass fraction data and the following assigned specific gravity values:

Hydrocarbon Type	Specific Gravity
normal-paraffins	0.75
cyclo-paraffins	0.81
alkylbenzenes	0.87
Indans and tetralins	1.00
indenes	1.00
naphthalenes	1.00
tricyclic aromatics	1.28

The type of hydrocarbon species in the fuel was independently determined from more than one analysis. The mass spectrometric analysis (ASTM D2425) separated the fuel into twelve classes while the fluorescent indicator absorption (FIA, ASTM D1139) technique reported only on three general classes (saturates, olefins, total aromatics). The FIA was supplemented with the ultraviolet spectrophotometric technique (ASTM 1840) to determine naphthalene content. A comparison of the total aromatics and naphthalene contents obtained by the two techniques is shown in Figs. 1 and 2, respectively. The mass spectrometry and FIA results for aromatics agree well considering the wide range covered and the general acknowledgement that the FIA technique can be inaccurate for high aromatic levels. The agreement between naphthalene analyses was not as good for ERBS & ERBLS-2

fuels. This result is not surprising as the UV technique is strictly applicable to fuels containing only up to 5 percent naphthalene. Both ERBS & ERBLS-2 contain considerably higher levels of naphthalene.

Fuel Spray Characterization

Variations in either chemical or physical properties could influence the burner characteristics. Fuel chemical properties could primarily affect the type and concentration of hydrocarbon species within the burner. For example, hydrogen-deficient fuels might produce greater carbon concentrations, resulting in higher radiation heat loads (and subsequently higher liner temperatures). Fuel physical properties would primarily affect the level of atomization. That is, fuels with disadvantageous physical properties -- high levels of viscosity or surface tension -- would tend to form coarse sprays, with these relatively larger droplets penetrating deeper into the airflow and surviving for significantly longer time periods. Clearly the size, location and intensity of the combustion zone would respond to such fuel distribution alterations, and consequently the combustor characteristics would also change. In order to isolate chemical property influences, the processes dependent on physical properties must be minimized. Only by achieving highly-atomized and hence rapidly-vaporizing sprays can this goal be satisfied.

In principle the finest level of atomization possible should be used to truly minimize the influence of fuel physical properties on combustion efficiency. This extreme however, would have imposed unacceptable demands on the test program -- excessive fuel pressures and/or nozzle substitution for every fuel, for each fuel flow rate, would have been required. An atomization goal that would acceptably minimize the influence of fuel physical properties was sought.

The analytical technique of Ballal and Lefebvre (Ref. 3) can be used to analyze fuel sprays characterized by a Sauter Mean Diameter (SMD). In particular, this analysis includes system characteristics that define reaction-controlled and vaporization-controlled operation. Convective heat and mass transfer is included by assuming that the droplets do not respond

5

to the turbulent velocity fluctuations of the airflow. A critical SMD can be identified (SMD_c) with the analysis. That is, for $SMD < SMD_c$, fuel vaporization would not control heat release and, hence, combustion efficiency.

The critical droplet size to avoid vaporization control in the combustor used in this experiment was defined previously (Ref. 1). In particular, SMD_c values were sought that assured rapid vaporization within the combustor primary zone which, based upon the test conditions and flow splits, had a residence time of approximately 5 ms. Calculations indicated that for Jet A fuel, a 20 percent turbulence intensity, and a droplet lifetime half the primary zone residence time, $SMD_c = 52 \mu m$. That is, a Jet A spray with an $SMD < 52 \mu m$ would vaporize sufficiently fast so as not to limit the heat release rate. The least volatile fuel that was tested had distillation characteristics similar to a No. 2 oil. For the same conditions as described above, the critical diameter was calculated to be $SMD_c = 45 \mu m$. Based or these results a slightly conservative spray atomization goal cf $SMD = 40 \pm 5 \mu m$ was defined for the test fuels at the median fuel flowrate associated with the condition having a fuel/air ratio (f/a) of 0.018.

The four test fuels in this experiments d'd not exhibit a wide range in physical properties. For example, data acquired previously (Ref. 1) with a single fuel injector indicate a relatively small span of atomization quality:

Fuel	SMD (μm)
Jet A	39
XTB	52
ERBS	47
ERBLS-2	48
Median	46.5

However, combustion tests were to be performed both at the high-power condition achieved in the previous program (combustor pressure = 1.3 MPa)

as well as at reduced pressure levels. In order to assure meeting the atomization goal at reduced pressure, an injector characterization study was performed to guide selection of injectors that would achieve the desired high levels of spray atomization at two reduced pressure levels of 0.8 MPa and 0.3 MPa. For the same combustor inlet temperature (700K), airflow and fuel flow rates of 61.5 pct and 23.1 pct of the high power rates correspond to the two reduced pressure conditions, respectively.

Characterization of the fuel sprays was performed in the UTRC Ambient Pressure Fuel Spray Facility located in the Jet Burner Test Stand (JBTS). The pertinent components used in the present study are shown in Fig. 3. Fuel injectors were mounted in the facility and connected to the fuel delivery system. Jet A fuel was delivered to the injectors from an underground storage tank and metered via a turbine meter. Fuel pressure and temperature were measured at the injector. Fuel spray pattern and droplet distribution were documented as follows. A high power General Radio Strobolume illuminated the spray with a 10ms light pulse, substantially freezing the droplet motion. (Photographic records of the spray were obtained on Polaroid film to determine the included cone angle). Droplet size distribution was measured in a plane 6.4 cm downstream from the injector with a Malvern Model ST1800 Particle Size Analyzer. This instrument is based on Fraunhofer diffraction of a parallel beam of monochromatic light by moving or stationary particles. A He-Ne laser beam traversed the spray diameter and the diffracted light was sensed on a 30-element photoelectric detector. The data were acquired using a 300-mm focal length collecting lens which permitted detection of droplet sizes between 6 and 560 μm. The photocells were scanned 200 times (approximately 2.6 sec) to acquire a statistically meaningful average for each data point. A dedicated mini-computer stored the diffracted light data and, upon request, executed an analytical program to interpret these signals in terms of a Rosin-Rammler droplet distribution and to calculate a spray SMD.

Simplex pressure atomizing injectors produced by Hago Manufacturing, Inc. were used in these tests. All injectors produced hollow cone sprays with a rated included cone angle of 80 deg. Eight injectors, identified by nozzle number (NN, the volume flow (GPH) delivered at a pressure drop of 100 psid), were investigated. Two injectors (NN=35. and 32) were in a

range suitable for the high-power condition and three each were for the 0.8 MPa condition (NN=18, 20, and 22) and 0.3 MPa condition (NN=8, 9, and 10). Three fuel flowrates were investigated for each nozzle, representing the rate associated with fuel-air ratios of 0.015, 0.018, and 0.022 for each condition.

The data acquired in tests with the eight nozzles are presented in Table 3 and Fig. 4. Over the flow range investigated, SMD varied linearly with fuel flow, a trend consistent with data obtained previously (Ref. 1), but in conflict with the weaker relationship predicted by standard atomization correlations. In the prior study, it was concluded that surface tension forces, as represented by the nozzle exit Weber number, could significantly influence the atomization processes. It was demonstrated that for the very low fuel flows often used in developing the atomization correlations, this influence was not important while for larger (practical) flows, the influence was dominant. These recent data appear to again reflect this influence.

As previously indicated, the spray produced by the four test fuels is similar. Hence, for a given pressure condition, a single nozzle could be used to achieve acceptably fine atomization of the four test fuels. With an atomization goal of SMD = 40 ± 5 μm at the test condition corresponding to f/a = 0.018, the trends presented in Fig. 4 were used to determine a fuelflow - nozzle number relationship at constant SMD (Fig. 5). The flow rates of Jet A associated with the median f/a at each of the three combustor pressure levels are indicated. Since the mean atomization level for the four fuels (presented previously) was 19 pct greater than the Jet A value, nozzles which produce Jet A sprays with SMD=34 μm should satisfy the atomization goal for all fuels. Nozzles with NN = 30, 18, and 7 should produce the desired atomization levels at the three pressure conditions.

SECTION III - COMBUSTOR, TEST FACILITY, AND INSTRUMENTATION

This section of the report describes both the burner, specifying its geometry and performance, and the specialized test facility assembled for these efforts. A detailed description of the instrumentation is also included.

Combustor Description

The test combustor was nearly identical to the one used previously (Ref. 1). This combustor embodied the features of a gas turbine burner. That is, the burner was a high heat release device, with strong swirling-recirculating flow structure at the front end (i.e., primary zone) followed by penetrating jets of air to gradually reduce the local fuel-air ratio, and hence gas temperature, to levels acceptable to a turbine.

A photograph of the combustor is in Fig. 6. The cylindrical burner was louver-cooled with an inside diameter of 12.7 cm and a length of 41.1 cm. The combustor consisted of a dome, constructed from a frustrum of a 90-deg cone, and six conventional sheet-metal louvers. The dome cooling air was admitted through four rows of equally-spaced holes. Each louver was fed by a ring of equally-spaced holes with four of the louvers containing six larger holes to admit combustion air to the burner. These combustion air holes represented the greatest deviation from axisymmetry. The number and diameter of all combustor holes are listed in Table 4. This burner was created by modifying the hole pattern in a JT12 combustor to permit operation over a greater range of test conditions. That is, the original JT12 was rated for a combustor exit temperature up to 1145K. Alteration of the hole pattern to increase coolant flow permits routine use to exit temperatures up to 1480K.

A flange on the combustor dome was provided to centrally mount a fuel injector-swirler combination. As previously identified, pressure atomizing

Injectors produced by Hago Manufacturing, Inc. were used (Fig. 7a). All injectors produced hollow cone sprays with a rated included cone angle of 80 deg. Nozzle sizes were determined from spray characterization data described in Section II. The air swirler, which encircled the fuel nozzle, provided the swirl necessary to assure stable combustor operation. The swirler enhanced fuel-air mixing and distribution as well as established the recirculating primary zone flowfield. The swirler was a commercially available device developed by Pratt and Whitney Aircraft for the JT12 combustor (Fig. 7b). An annular clamp ring assured proper positioning and sealing of the injector-swirler combination to the combustor flange.

The airflow pattern in this burner was well documented in calibration tests (Ref. 1). First, a CO_2 tracer was used to determine the amounts of airflow from all sources which participated in the primary zone. Data from these tests indicated that 19.5 percent of the total air flow participated in the primary zone flowfield (Fig. 8). Hence, the primary zone equivalence ratio is 5.1 times the overall equivalence ratio. Second, calibration tests were performed to define the combustor airflow distribution over the entire burner length. The effective area of liner holes at each axial station (i.e., dome, louver cooling, combustion air holes) was determined as indicated in Table 5. The airflow swirler was calibrated in a separate test. The second column of Table 5 indicates the cumulative liner airflow. When used with a fuel injection rate this airflow schedule permits calculation of the global equivalence ratio at these combustor axial positions.

This burner operated quite stably in previous tests. Combustion efficiency was always greater than 99.9 percent, the nominal combustor exit pattern factor was 0.13, and the nominal liner pressure drop was 2 percent. By maintaining the 2 percent liner pressure drop, combustor operation of the shortened burners in this program was also stable.

Test Facility

The experimental test program was conducted in the JBTS, which is a self-contained facility with four test cells equipped for high-pressure combustion tests. The JBTS provides test cells with control rooms,

assembly areas, automatic data acquisition systems, and air, fuel, and gaseous nitrogen supply systems.

The test program primarily used hardware residual to the previous NASA program (Ref. 1), with some components fabricated for the needs of this program. The test facility consisted of three sections: an air preparation section, a test and instrumentation section, and an exhaust section (Fig. 9).

Air was supplied to the air preparation section through the system depicted in Fig. 10. Two multi-staged reciprocating compressors, capable of pumping a combined flowrate of up to 4.5 kg/s, provided air at pressures up to 2.7 MPa. The airflow for the combustion tests was heated by an indirect-oil-fired burner prior to entering the air preparation section; the typical preheat level was a 420K. The heated airflow was regulated in the test cell and metered by a venturi, with appropriate measurements of air pressure and temperature performed upstream and at the throat of this device. The temperature of the venturi body was also measured to account for thermal expansion of the throat diameter. The metered airflow was heated further by use of an electrical resistance-type heater. A plenum at the heater exit assured that uniform airflow velocity and temperature profiles were delivered to the test section.

The test section consisted of spacer spool sections, a combustor housing, and instrumentation rings. The spacer spools provided necessary access to remove the combustor housing. They also provided support for arrays of four total pressure probes and four thermocouples to document the airflow approaching the burner, and bosses to route out liner thermocouples and pressure lines.

The combustor housing (Fig. 11) was a simple spool section fabricated from commercially-available pipe with an inside diameter of 15.2 cm. A 1.3 cm annular gap between the liner and housing provided adequate backside convective cooling of the burner louvers. The housing contained a single boss to route fuel to the fuel nozzle. Fittings near the downstream end permitted insertion of pitot-static probes to measure the liner pressure loss and a bleed port to adjust the pressure loss.

11

The combustor attached to a mounting ring via a small flange attached to the liner at the burner exit (Fig. 11). Burner alignment was aided by centering tabs mounted on the dome. The fuel line, which was flexible to accommodate the liner thermal growth, consisted of two sections. An axial length incorporated two concentric tubes with fuel delivered through the inner tube and the outer tube providing an insulating air gap. A radial length included a steel braid/teflon tube flexible line, wrapped by a helix of copper tube to provide a water-cooled heat shield. In order to make measurements inside the burner, shortened combustors were produced by removing the complete downstream-most louver and welding a replacement flange at the new exit plane. Replacement lengths of the concentric tube fuel line enabled fuel to be delivered to the shorter burners. Since the shortened liners provided a reduced effective open area (CDA), less burner airflow was required for constant liner pressure drop. Reducing combustor airflow to match the decreased CDA, however, would have alterred the approaching flowfield, affecting both the penetration of jets through the liner and the internal flowfield. To eliminate this influence, the combustor total airflow (i.e., airflow approaching the burner) was held constant, with airflow greater than that required to match the full-length combustor pressure loss bypassed through orifice plates mounted in the annular region at the combustor exit (Fig. 11). Each plate contained equally-spaced holes sized to compensate for the decreased liner open area of shortened burners. Hole sizing was based on the calibration results obtained previously (Table 5). Liner pressure drop was determined from pitot-static tubes placed in the annulus between the liner and housing and static tapes installed in the combustor dome. A remotely adjustable bypass bleed was available to fine tune the total bypass to achieve desired liner pressure drop.

This technique of shortening the liner to make measurements inside the burner incurred significantly reduced cost relative to designing and fabricating elaborate combustor housings that would have allowed optical and probe diagnostics to transverse parallel to the combustor centerline. That is, instead of moving the diagnostics toward the fuel nozzle, the fuel nozzle was moved toward the diagnostics, which remained fixed. By exercising the indicated test procedures, the flowfield between the nozzle

and measurement planes is not believed to have been significantly altered by removal of downstream louvers.

Two instrumentation rings, designed and fabricated previously (Ref. 1), were mounted to the combustor housing. These rings were specially constructed, flange-cooled units (Fig. 11). The particle sizing ring provided optical access for scattered light signals. The probe mounting ring provided fittings to mount up to three probes. In this program, a single probe was utilized, with its sampling orifice located on the rig centerline.

The exhaust section consisted of an adapter followed by a water-cooled T-section and a backpressure value. The T-section provided a 7.6 cm diameter viewport to permit direct observation of the combustor exit plane. A remotely-operated butterfly valve was used to control the test-section pressure. A high-pressure water quench reduced the gas temperature upstream of the valve to less than 700K to prevent damage to it.

The fuel delivery system consisted of three subsystems: a startup fuel subsystem, a test fuel subsystem and a nitrogen purge subsystem. Jet A was supplied to the test cell from underground storage tanks by positive displacement pumps. This fuel, referred to as Jet A-U, was the startup fuel used prior to switching over to the test fuel. Data were acquired with the combustor operating on Jet A-U prior to operation on any test fuel to verify consistant combustor operation. Jet A-U had properties nearly identical to the Jet A test fuel. Drum quantities of the test fuel were delivered by the test fuel subsystem, which was capable of delivering 4.6 liter/min at a pressure of 6 MPa. Two solenoid valves, one in each fuel subsystem, were actuated by a common electrical circuit. A normally-open valve in the Jet A-U system and normally-closed valve in the test fuel system were switched in unison to provide a rapid, positive change in fuel. The nitrogen subsystem was available to purge the fuel nozzle and delivery lines inside the combustor rig and to cool these components during the setup of the test condition. The fuel system is depicted as part of Fig. 12.

Instrumentation

The test facility was instrumented as described below. The parameters measured are indicated in Fig. 12.

Measurements were made to document the airflow rate, pressure and temperature approaching the model combustor. The airflow rate was determined using a venturi with a 2.286-cm throat diameter; pressure and temperature upstream and pressure at the venturi throat were measured. The distribution of temperature and total pressure at the test section inlet were documented using arrays of four thermocouples and four total pressure probes. The test-section housing contained two fittings, located 180 deg apart near the downstream end of the housing (Fig. 11), for mounting pitot-static probes to document the total and static pressure of the airflow proceeding through the annulus. Several thermocouples installed in the adapter section indicated the combustor exhaust temperature.

The fuel supply contained provisions for acquiring pressure and temperature measurements necessary to control the flow. Fuel flowrate was measured with a turbine meter. A mass flowmeter was not required since the viscosity variation among the test fuels was small. A dc voltage source, interlocked with the fuel switchover valves, produced a signal to identify data points acquired when operating with test fuel.

The combustor liner was instrumented with thermocouples and internal pressure taps. Twelve type K thermocouples were attached along an axial line at one angular position of the burner, with another six attached along a line on the opposite side of it. In the twelve thermocouple array, two were placed on each of the six louvers, with one thermocouple opposite the edge of the inner film slot lip and the second approximately 2.5 cm farther downstream. The six thermocouple array contained one sensor on each louver at the second axial position. Two static pressure taps were attached to the first louver to provide a measurement of burner static pressure, which was used to determine and monitor the liner pressure loss for the different burner lengths. The twelve thermocouple array and one pressure line are visible in the photograph contained in Fig. 6.

14

Soot particle size and concentration (number density) were determined from the scattered light emanating from a 15 mm^3 sample volume located 7 cm downstream of the combustor exit centerline. The scattered-light signals were interpreted according to Mie theory of light scattering. This technique has been detailed by several authors (Refs. 4, 5, and 6) with a critical assessment of its accuracy given by Bonczyk (Ref. 7). In brief, this theory predicts the intensity of light scattered by particulates as a function of the scattering particle properties, scattering geometry and the incident intensity:

$$I = K * I_0 * N * \phi$$

where:

I = light intensity scattered by particles

K = constant including scattering solid angle

I_0 = incident light intensity

N = particulate number density

ϕ = complex scattering function

The scattering function, ϕ, is dependent upon the size parameter, x, the scattering angle, θ, and the complex refractive index, n:

$$\phi = \quad (x, \theta, n)$$

where: $x = \pi D / \tau$, D = particle diameter

τ = wavelength of scattered light

ϕ is also responsive to the polarization of the light. Strictly, this description is accurate only for spherical particles of uniform size. The extensions of the theory to permit definition of polydispersions result in greater analytical and experimental complexity. For combustion

15

applications, where the particulate shape is non-spherical, it is difficult to determine all the parameters of the polydispersion. Therefore, for such applications, it is common to assume a monopdisperse particulate size distribution. This approximation (and the accompanying assumption of spherical particles) limits the accuracy of size and concentration determinations.

The evaluation of particulate size and number density relied upon the angular disymmetry of the scattered light. From the above description, for a fixed polarization of the light (chosen to be perpendicular to the scattering plane), the ratio of light intensity at two different angles, θ_1 and θ_2 is:

$$I(\theta_1)/I(\theta_2) = (D,\theta_1,n)/(D,\theta_2,n)$$

This ratio is a function of D alone for given values of the complex refractive index and scattering angles. In this program, values of $\theta_1 = 45$ deg and $\theta_2 = 135$ deg were used; the scattered light had a wavelength of 514.5 nm. The dependence of the ratio of scattered light on D is depicted in Fig. 13 for two values of n. Note that the theory permits size determination for $D < 0.3 \mu m$; for larger diameters, the ratio is multivalued and unambiguous size determination cannot be made. The proper value for the complex index of refraction of the combustor exhaust particles was not known; the value likely depended on the chemical composition of the particulates. The two values used to generate the curves in Fig. 13 were obtained from measurements either on graphite or on soot from an acetylene flame. For the valid range of diameter determination, the uncertainty introduced by these two n values was not great, however. The value for graphite ($n = 1.94 - 0.66i$) was used in the data reduction. Once D had been determined, the particulate number density, N, was calculated from the scattered light intensity measured at θ_1 and the known geometry of the scattering setup.

The particle sizing apparatus assembled for this program is shown in Figs. 14 and 15. The incident light was produced by an argon-ion laser with an output power level of approximately 1w at a wavelength of 514.5 nm.

The polarization of the output beam was rotated to be perpendicular to the scattering-plane. The beam, which was chopped at a frequency of 2008 Hz, was directed through a recess sapphire window and across the combustor exhaust. Two scattered light detector assemblies were rigidly attached to the test duct, one at 45 deg and one at 135 deg from forward scattering. The fabrication tolerances of the assembly mountings were specified to assure precise alignment of them. During installation of this apparatus it was observed that beams from two He-Ne alignment lasers intersected on the test duct centerline. Each detector assembly contained a sapphire window, a polarizing disk, a narrow-pass filter (centered at 514.5 nm) and a fast linear focused (EMI type 980/B) photomultiplier tube (PMT). The solid angle of the scattered light was defined by two 3.1 mm dia appertures (separated by a distance of 20.0 cm) located along the detector centerline. The output from each PMT was input to a lock-in amplifier which was referenced to the chopper frequency. This setup enhanced the signal-to-noise ratio by providing an output voltage proportional to the difference between the laser-stimulated scattered light and any random light which might have been detected.

The laser beam path also contained a focusing lens. Combustor shakedown tests conducted without a lens in the previous program (Ref. 1) indicated substantial beam diameter growth at the alignment window. That is, the 1.3-mm diameter laser beam had grown to fill the 12-mm diameter exit port. This growth was attributed to "thermal blooming" which occurs as light passes through gases which possess large temperature gradients. The thermal gradients produce gradients in the index of refraction which result in a lens-like expansion of the ray. It was suspected that the blooming occurred in the window recesses where cool nitrogen purge flow and hot combustion gases were unavoidably mixed. The lens focused the laser beam on the test duct centerline to minimize this problem.

In addition to the scattering diagnostics, transmission measurements of the laser source light used for the scattering measurements were analyzed. This setup is depicted in Fig. 16 which shows the placement of a detector to sense the transmitted light. Data were acquired both with and without combustion to determine the absorption of the laser beam as it traversed the combusting flow. In these measurements a neutral density

17

filter was used to reduce the signal level to within detector limits. A lock-in amplifier referenced the detector signal to the chopper located on the laser side of the test rig. Radiance measurements were also made by blocking the laser source and inserting a chopper in front of the detector (Fig. 16); the filter was withdrawn to increase detector sensitivity. The devices were driven by pneumatic cylinders actuated from the control room. The detector, sensitive only to visible and near IR radiation, sensed radiation generated by the luminous soot particles only.

Combustor exhaust products were probed near the combustor exit to determine gaseous emission levels, smoke emission levels, and soot mass loading. A sampling probe was positioned to locate its inlet orifice on the rig centerline approximately 8 mm downstream of the scattering sample volume (Fig. 11). The probe had a 1.3-cm OD with a 3.7-mm sampling port (Fig. 17). The probe body was water-cooled to assure its survival in the high heat load condition created with shortened burners. The outside of the sample tube in the probe was coated with 0.3-mm thick ceramic to reduce heat exchange between the sample and coolant and, hence, to avoid low local sample temperatures that could promote condensation. Nitrogen diluent could be added to the sample near the probe tip to quench the oxidation processes and reduce the sample dew point. The sample temperature measured at the probe exit was used to determine when nitrogen dilution was required. If the sample temperature measured with the shortened burners was significantly larger (more than 80K) than that measured with the full-length burner, diluent was added to deter soot oxidation in the sampling system.

Particulate laden flows were extracted through the probe. The sample was divided and passed through two heat exchangers, as shown in Fig. 12, before entering transfer lines to pass out of the test cell. Heat exchangers were required to reduce the sample temperature below 400K in order to ensure that the teflon coating over the transfer line interior did not melt. Separate transfer lines and sampling systems for the smoke and soot measurements were determined to be necessary during shakedown tests. The flowrates and sampling times to acquire mass samples were much greater than the flowrates prescribed by SAE ARP 1179 for measuring smoke number. The amount of soot collected in a typical smoke sample was

calculated to be less than one percent of a typical soot mass sample. During tests where both measurements were made with the same transfer line, soot, which tended to adhere to the transfer line walls, would randomly break loose. This effect, which was a negligible perturbation on mass samples obtained over extended sampling periods at high flowrates, had a significant influence on smoke number measurements. Consequently, to overcome the erratic smoke number results that were being acquired, a separate transfer line and filter system was dedicated to smoke number sampling. Repeatable smoke number measurements were gathered with the dedicated system.

During shakedown tests, soot samples were acquired using four different filters -- two paper filters and two Fluoropore teflon filters. One of the paper filters was Watman No. 4, the membrane specified for SAE smoke number determination. This material had insufficient filtration efficiency as indicated by significant soot stains that were collected on the second of two stacked filters. The other paper filter, Millipore HA, had sufficient efficiency but suffered form the problem of all paper filters -- it absorbed water form the atmosphere. Subsequent weighings of new filters indicated an increasing tare because of this tendency. Rather than drying the paper filters before and after sampling to overcome the water absorption problem, teflon membrane filters, which are hydrophobic, were investigated. These filters, with a nominal pore size of 0.5 m, have demonstrated a filtration efficiency of greater than 99 percent for particles down to $0.03 \mu m$ (Ref. 8). This performance arises from the fibrous structure of the filter which is apparently formed from $0.2 \mu m$ fibers. Both Millipore Type FA and FH filters were investigated. The former, which had a polyethylene backing, was unacceptable because the backing melted in the heated filter holder. The Type FH collected samples efficiently and was used successfully throughout the program.

Though the concern of water absorption by the filters was eliminated by using teflon filters, the potential for water absorption by the collected soot also needed to be addressed. To determine whether water absorption by the soot was a problem, several of the acquired samples were weighed immediately before and after drying the samples in an oven. The weights agreed to within 10^{-2} mg indicating that water absorption by the soot was insignificant.

SECTION IV - TEST CONDITIONS, PROCEDURES, DATA ACQUISITION AND REDUCTION

Soot loading in the burner was documented In terms of three variables: fuel chemical properties, fuel-air ratio, and combustor pressure. Soot loading was documented for six different combustor lengths. This section of the report details the test conditions and procedures for setting up and conducting tests as well as for acquiring data.

Test Conditions and Procedures

Two phases of combustor tests were performed: fuel-effects tests and pressure-effects tests. The fuel-effects tests determined the influence of fuel chemical properties on soot loading. A single airflow condition, simulating high-power operation of a gas turbine engine, was used for the fuel effects tests. The approach airflow pressure, temperature and flowrate for this condition, designated Test Condition 1 in Table 6, were identical to those used previously (Ref. 1). These parameters were independent of combustor length. Bypass flow, set by the open area in the mounting ring, was adjusted to achieve a relatively constant liner pressure drop for all burner lengths. Soot loading was documented for four test fuels: Jet A, ERBS, ERBLS-2, and XTB. Each fuel was tested at three flowrates that produced full-length combustor ideal exhaust temperatures of approximately 1240K, 1340K, and 1470K. These three temperatures were the ideal temperature levels associated with combusting Jet A at fuel-air ratios of 0.015, 0.018, and 0.022, respectively. The flowrates for the other three fuels required to achieve the same exit temperatures were slightly different. Required flowrates for each fuel were determined from thermochemical calculations using chemical properties identified by the fuel analysis. A listing of these fuel-air ratios is contained in Table 6.

Tests were performed at a reduced combustor pressuring of 0.8 MPa to document the influence of combustor pressure on soot loading. The same inlet temperature of 700K was used with the mass flow decreased In

20

proportion to the pressure reduction, i.e., the Mach number of the approach flow was held constant. This condition is denoted as Test Condition 2 in Table 6. The combustor approach flow was again independent of burner length, with excess air bypassed to retain constant liner pressure loss for each of the three burner lengths investigated at reduced pressure. Two fuels, Jet A and ERBLS-2, were combusted at reduced pressure with each injected at flowrates required to achieve the same full-combustor ideal exit temperatures noted above.

Shakedown tests were conducted to initially check out combustor operation and instrumentation systems. Also during these tests, sampling times (nominally 10 min.) and flowrates (nominally 0.082 sm^3/min) were established to gather a satisfactory sample for the mass concentration measurements. A minimum of 1 mg of sample was sought so that the sample weight could accurately be discerned from the nominal 50 mg tare weights of the teflon filters. As soot loading increased with shortened burners, these sampling times, which were the primary determinant of test duration, were reduced to minimize fuel usage.

Startup procedures were standard for each test day. The data acquisition system was set up with pressure tranducer and thermocouple references checked, flowmeter and analyzer outputs zeroed, and signal amplifiers calibrated. If optical data were to be acquired, the laser was aligned and all mirror, window, and filter surfaces were cleaned. Appropriate JBTS support systems were activated and purge flows were established through the sample probes, ducts providing optical access, and fuel delivery line. Airflow from the 2.7 MPa facility system was initiated and heated by both indirect-fired and electrical heaters. After air temperature increased to approximately 730K, the backpressure value was closed to raise the pressure to approximately 1 MPa. The fuel purge was then terminated and Jet A fuel, supplied from a large underground tank at the JETS, was slowly introduced. (This fuel is termed Jet A-U). At these conditions, the fuel ignited spontaneously at a minimal flow, avoiding a sudden increase in burner pressure. The fuel flowrate was increased and the airflow parameters (pressure, temperature, flowrate) were adjusted to desired setpoints. Probe purge flows were terminated and the exhaust gas temperatures observed to confirm stable steady-state conditions had been established.

Performance at each burner length were initially investigated with Jet A-U. Detailed data, including pressures, temperatures, soot samples, smoke samples, and gas emission analysis for selected burner lengths, were acquired at Test Condition 1 for all three fuel-air ratios. The data were acquired to document the burner performance as well as to establish a small data base for referencing the combustor operation.

Measurements with the test fuels were initiated by acquiring data with Jet A-U at a f/a = 0.018. Comparison of these data with the initial data set aided in verifying that the burner performance remained constant. The fuel supply was then switched to operation on a test fuel. Switchover was accomplished by the simultaneous activation of solenoid valves which provided for an uninterrupted flow of fuel so that the burner never extinguished. The test fuel was fed from two drums, each containing approximately 190 liters of fuel, to provide enough fuel to achieve the relative long test time required to acquire soot samples. Upon completion of measurements with the test fuel, the fuel supply was switched back to Jet A-U in a similar manner. Data were again gathered at f/a = 0.018 before terminating the test to ensure that combustor performance had not changed. Testing was conducted in this manner with the four test fuels at the high pressure condition for each burner length to establish the effect of fuel chemical properties on soot loading. Upon completion of fuel-effects testing with a given burner configuration, either similar tests were conducted at reduced pressure, or the burner was shortened and similar tests performed with the shortened burner. For the reduced-pressure tests, the fuel nozzle was replaced with the appropriate nozzle defined for the 0.8 MPa pressure condition during spray evaluation tests. Each of the reduced-pressure tests was again initiated with Jet A-U to ensure consistant burner performance before gathering data with Jet A and ERBS test fuels.

Data were not gathered at the 0.3 MPa pressure. During tests at 0.8 MPa, the soot loading was quite low at certain conditions so that determination of fuel effects was difficult. Since soot concentration at a lower combustor pressure would have been further reduced, the benefits of testing at 0.8 MPa were minimal.

For a given fuel, fuel-air ratio, and combustor pressure, data were acquired in the following manner. With airflow and fuelflow parameters properly set, the probe flow was delivered a through the soot sampling system (but bypassing the filter) at a rate equivalent to the sampling rate. The coolant flow through the heat exchanger was also adjusted as necessary to maintain sample flow temperature below 400K at the transfer line entrance. The sample temperature at the probe exit was observed, and quench flow added with the shorter burners if this temperature was significantly higher than that measured with the full-length burner. With the sample flow properly conditioned, a minimum of three mass samples were acquired on preweighed teflon filters. Since the sampling times to acquire the mass loading were were relatively long, three smoke samples and three data scans were normally acquired during each of the mass sampling periods. Mass samples were weighed and smoke numbers were calculated from the smoke samples immediately after acquisition. These data were checked for consistency, with more samples gathered if any sample weights differed more than approximately 20 percent of the mean. For test conditions where optical data were acquired, the laser beam was passed through the combustor exhaust to permit scattering and transmissivity data to be acquired with the data system for most of the data scans. Several data scans, however, were acquired with the laser beam blocked in order to acquire radiation data.

After completion of a test sequence, the burner was shut down in the following manner. Purge gas was reestablished through the sampling probes to avoid ingestion of unburned fuel. Fuel flow was terminated and the fuel lines immediately purged. All systems were secured if tests planned for the day were completed. Otherwise, the test fuel was changed and the Jet A-U/ test fuel sequence described above was executed again.

Data Acquisition and Reduction

The complete set of test data was recorded by means of an automatic data acquisition system which stored the information on magnetic tape for subsequent computer processing. The data system accepted data on up to

25 channels, 10 provided with signal conditioners, and the remainder compatible with preconditioned input signals. The system was capable of controlling and accepting data from submultiplexers such as pressure and thermocouple scanning switches. The data channels were scanned sequentially at a rate of 12 channels per second and whenever a submultiplexer was connected to a channel, all ports were sampled before preceeding to the next channel. An analog-to-digital converter digitized the data and an incremental magnetic tape recorder stored it for subsequent computer processing. The format of the tape was structured for compatibility with the UTRC UNIVAC 1110 digital computer.

The data system magnetic tape was reduced by use of an existing computer program. This code applies the appropriate calibration factors to each signal to provide engineering units for pressures and temperatures for calculation of parameters of interest. Among those selected for this program were: airflow rate, fuel massflow rate, combustor reference velocity, fuel-air ratio from metered flows, particulate size and number density (using look-up tables generated by a code for Mie-scattered light), and ideal combustion temperatures for the overall combustor. Averages of pressures and temperatures which characterized the inlet airflow or combustor exhaust were also calculated. The output from this data reduction code was a Summary Table which displayed all measured and calculated parameters for every data point. This Table was reviewed for spurious measurements (e.g., open thermocouples) with hand-recorded data input if available. Also, items not acquired by the data system (e.g., SAE smoke number) were entered into the Summary Table.

Particulate Concentration and Smoke Number

Metered samples from a probe positioned 7 cm downstream of the combustor exit centerline were filtered to determine soot mass loadings. The data are presented as particle concentrations (PC) at standard conditions, mg of soot per standard cubic meter of sample. Figures 18-21 show the concentrations as a function of normalized combustor length for the four fuels that were burned. Each data point represents an average of 3 to 5 samples. Data are shown for the full-length combustor (l/L = 1.0) and five length reductions corresponding to the sequential removal of five louvers.

The soot loading generally increased with the removal of each of the first three louvers. Concentrations measured with three louvers removed (l/L = 0.554) are an order of magnitude larger than those gathered with the full-length combustor. This trend indicates that significant soot oxidation occurred in the secondary zone. Soot masses gathered with the five-louver combustor operating at the high fuel/air ratio with all four fuels (and at all three fuel/air ratios with Jet A) are not appreciably different from the full-length results. Evidently little soot oxidation occurred near the combustor exit for these conditions.

Concentrations measured with the two shortest burners do not follow the trend of increasing soot loading inside the combustor. With the exception of data gathered with the one-louver combustor (l/L =0.27) at the highest fuel-air ratio, concentrations are comparable with levels measured with three louvers on the burner. However, these levels are not considered to be representative of the overall soot concentration in the combustor front end. This combustor utilizes a diffusion flame in the primary zone located upstream of air jets admitted in the first louver. Soot production in such a diffusion flame apparently involves fuel pyrolysis followed very quickly by nucleation and growth near the flame front (Ref. 9). Soot levels should peak in the vicinity of the production sites in the primary zone and then decrease due to oxidation in the combustor secondary zone. This trend was indicated by case-mounted radiometer measurements in the

previous program (Ref. 1). Since all measurements in this experiment were obtained downstream of the primary zone, soot concentrations were expected to increase as the combustor was shortened for all configurations tested.

The low concentrations measured with short burners can be explained by recognizing that the flow field in the front end of a practical combustor tends to be nonuniform. Calculations using the nominal liner pressure drop of 17 KPa indicate that the combustion air jets penetrating through the louvers will reach the combustor centerline. The centerline region would be diluted by the jets and exhibit lower soot concentrations. In addition, the diffusion flame, which follows the fuel spray, tends to be spacially nonuniform within a transverse plane and could reinforce the nonuniformities created by the dilution jets near the combustor centerline. The sampling probe was located near the burner exit plane on the centerline and it appears that the flow field was not fully mixed at this point. One-point measurements at the centerline, then, probably were not representative of the average flow condition in the combustor front end.

In order to gain more insight concerning the flow field in the combustor front end, gas samples were obtained in conjunction with soot samples for the two short burners. With the combustor burning Jet A fuel. a portion of the sample from the the probe was removed upstream of the soot filter location and analyzed to determine carbon monoxide, carbon dioxide, oxygen, and total nitric oxide concentrations. The carbon dioxide and oxygen data were used to separately calculate the local centerline fuel-air ratio (f/a). As shown in Fig. 22, the two emission measurements indicate nearly the same f/a. These fuel-air ratios, however, are considerably lower than the flagged symbols, which represent the expected average f/a at those axial positions based on the flow splits identified in combustor airflow calibrations (Ref. 1). This f/a comparison indicates that the centerline region was diluted and contained below-average particle concentrations. Centerline soot measurements with the two shortest burner lengths, then, cannot be viewed as being representative of soot levels in those measurement planes.

Optical diagnostics also indicate that soot mass loadings were highest in the combustor primary-zone region. Transmission measurements of the

laser source light both with and without combustion were used to determine
the combusting stream spectral emissivity (ϵ) at the light source
wavelength (τ) according to:

$$\epsilon_{514} = \frac{R_{\tau, \text{ w/o comb}} - R_{\tau, \text{ w comb}}}{R_{\tau, \text{ w/o comb}}}$$

where R_τ = measured radiance either without (w/o) or with (w) combustor
operation. The emissivities for Jet A and XTB fuels, displayed in Fig. 23,
increase with decreasing combustor length. This path-length measurement,
then, indicates that soot loading was highest in the burner primary zone
($l/L < 0.3$) and then decreased via oxidation through the remaining burner
length.

Radiation measurements were also made with a narrow-angle detector
sensitive only to visible and near IR radiation. The detector, then,
sensed only radiation generated along a combustor diameter by luminous soot
particles. The measured detector output is shown in Fig. 24 for operation
with Jet A and XTB fuels. Radiation levels, though quite low with the
longer combustor lengths, increase slightly with the two-louver
configuration and increase significantly with one louver on the burner.
Though higher temperatures at the one-louver combustor exit contributed to
the increased radiation, temperature effects cannot account for all of the
increase. For example, the average exit temperature for the one-louver
configuration would have to be 2.8 times that of the two-louver burner to
account for the increased detector output at the lowest f/a. Using the
calibrated air splits, the calculated average temperature increase is only
a factor of 1.25. The radiation measurements, then, also indicate higher
soot loading in the vicinity of the primary zone.

The optical diagnostics also show that soot production increased with
increasing f/a. For example, the radiation levels (Fig. 24) increase with
higher f/a ratios for the one-louver combustor. Since the primary-zone
equivalence ratios are greater than unity for all three f/a ratios, the

temperatures in the diffusion flame structure are nearly the same for the three cases. Soot located near the primary zone radiates at nearly the same temperature and, therefore, the increased radiation can be attributed to higher soot production. Radiation detected by radiometers mounted in the combustor dome during the previous program (Ref. 1) also increased with increasing f/a, indicative of higher soot loading at higher f/a. This trend is expected because higher f/a was achieved by increasing fuel flow while maintaining constant airflow. Higher fuel concentration in the primary zone led to increased soot production.

The effect of temperature on soot oxidation can be seen in Figs. 18-21. Particulate concentrations for the three-louver burner are comparable for the three f/a ratios. With the longer burners, however, the concentrations decrease with increasing f/a. This trend is directly attributable to higher combustor exit temperatures, associated with higher f/a, promoting soot oxidation. Thus, even though more soot was produced in the primary zone at the higher f/a ratios, higher temperatures in the secondary zone enhanced particle burnout to overcome the increased production.

Particulate concentration distributions obtained with the four test fuels burned at f/a = 0.018, shown in Fig. 25, indicate the effect of fuel chemical properties on soot formation and oxidation. Since soot measurements with the one-louver combustor are not believed to be representative of the loading in the dome region, soot production rates for the four fuels cannot be deduced from those data. Although soot oxidation occurred upstream of the three-louver burner measurement location, data from the longer burners indicate that oxidation rates for the four fuels are similar. A ranking of the fuels relative to soot production can be made, then, using the data gathered with the three-louver combustor. A general ranking in increasing order of soot production is Jet A, ERBS, ERBLS-2, and XTB. This ranking is consistant with the correlation developed in the previous program (Ref. 1) where radiation levels in the dome region were found to be inversely proportional with fuel smoke point.

Particulate concentrations associated with burning Jet A and ERBLS-2 at a reduced combustor pressure of 0.8 MPa (Figures 18 and 20) are

generally lower. The change in particulate concentration due to the pressure reduction is shown in Fig. 26. The data are expressed in terms of the change in concentration normalized by the concentration measured at the higher pressure. Data for the three-louver combustor (l/L = 0.554) show lower soot loadings at lower pressure for all three fuel-air ratios. Though soot oxidation occurred inside this combustor upstream of the sampling location, these data indicate that less soot was produced at the lower combustor pressure. This trend is logical since the reactants are less concentrated at the soot production site for lower pressure. With longer burners, the effect of lower pressure is not as strong. Concentrations measured at the two lower fuel-air ratios are reduced at lower pressure, with the more significant reduction at the lowest f/a. At the highest f/a, however, either the reduction of soot with lower pressure is small or an increased concentration was measured at lower pressure. The implication of these data is that although less soot was produced at lower pressure, as indicated by the data at l/L = 0.554, the oxidation rates at the higher fuel-air ratios were also appreciably reduced resulting in similar concentrations at the full-length combustor exit for the two pressure conditions. The scatter in the high-f/a data for the longer burners is associated with attempting to ascertain a pressure effect at rather low soot loading conditions. The uncertainty in the concentration measurements at these low soot loadings is equivalent to a significant portion of the sample. For example, PC for Jet A at f/a = 0.022, l/L =0.834, and P_3 = 1.3 MPa is 0.49 mg/sm^3 whereas at P_3 = 0.8 MPa PC is 0.73 mg/sm^3 . The measurement uncertainty at these loadings is approximately ± 0.15 mg/sm^3. Most of the difference in loading, then, could be due to measurement uncertainty.

In conjunction with gathering particulate concentration data, SAE smoke number data were acquired as prescribed by SAE ARP 1179. Data are shown for the four test fuels in Figures. 27 - 30. Valid smoke samples were not acquired with the full-length burner because of leaks in the sampling system for those tests. Data from the previous program (Ref. 1) are shown for that configuration. Some smoke samples were gathered while burning Jet A fuel with the one-louver combustor. These samples yielded smoke numbers close to 100. Since this technique has low resolution at high smoke number (SN) and the other more sooting fuels would have provided

even darker deposits on the filter, detailed smoke samples were not acquired with the one-louver combustor.

The SN data follow trends similar to those noted with the PC data. SN increased as the combustor was shortened except when the first louver was removed. SN's for the five and six-louver burners are nearly the same. SN's gathered with the two-louver combustor again are not representative due to dilution of the combustion products near the centerline by the dilution jets and nonuniformities in the flame pattern. SN varies inversely with f/a for the longer burners but is nearly constant for the three fuel-air ratios with the three-louver burner. The effect of fuel chemical properties and the effect of reduced pressure, as shown in Figs. 31 and 32, respectively, are also similar to the observations developed concerning the PC data.

Smoke number is a common and a relatively easily acquired measurement to document turbine engine exhaust smoke. A smoke number, however, does not reflect any of the physical properties of soot. A correlation between PC and SN would allo determination of soot mass loading from SN data. For this reason, the correlation of PC and SN data from this experiment was quantified via a regression analysis. Fig. 33 depicts the variation of particulate concentration with smoke number. The data points represent all test conditions: four fuels, three fuel-air ratios, and two combustor pressures. The relationship determined from the regression analysis, shown in Fig. 33, is:

$$PC = \frac{0.177 \; SN^{1.234}}{(100 - SN)^{0.360}}, \quad R^2 = 0.91$$

where R is the correlation coefficient. This formulation correctly models the asymptotes of the PC/SN relationship. As SN decreases to zero, PC must also approach zero. Similarly, at high soot loadings, PC must approach infinity as SN approaches 100. Thus, the function has an "S" shape in Fig. 33. The high value of the square of the correlation coefficient indicates that this expression is an excellent fit to the data.

Champagne (Ref. 10) has also looked at the relationship between soot loading and smoke number using data gathered by C. Stamforth from the exhaust of a J79 turbojet engine. A correlation of Stamforth's initial data was very poor. Assuming that variations in carbon particulate size caused the poor correlation, data were gathered using a two-staged particle separator. The division of particle diameter was estimated at one micron. A good correlation with smoke number was obtained using only the small particle weights. This correlation is shown as the middle curve in Fig. 33. Stamforth concluded that the large particles, which accounted for zero to 50 percent of the total carbon weight, added little to the smoke number values. The actual particle concentrations for a given smoke number, then, were assumed to be anywhere from zero to 100 percent greater than the small particle concentrations. This upper limit is indicated by the upper curve in Fig. 33.

A main conclusion from Champagne's work is that the correlation between SN and PC will depend on particle size. Mie scattering data, which will be shown below, indicate that the particle diameter in this experiment only varied from 0.2 to 0.25 micron for all test conditions. This relatively uniform particle size strongly contributed to the good correlation of the data from this experiment. The difference between Stamforth's correlation and that from this work can probably be attributed to the presence of smaller particles in this experiment.

Particulate Size and Number Density

A characteristic size and number density of the soot exiting the burner on its centerline were determined from light scattering measurements. Number density data gathered for the test fuels is shown in Fig. 34 - 37. Data obtained during the previous program are also shown and agree reasonably well with results from this test. Differences are indicative of the uncertainty associated with this measurement.

Trends described previously concerning the soot loading and smoke number data are evident. The lowest number density at the exit of the full combustor was measured at the highest f/a. This again points out the vigorous oxidation mechanism in the burner secondary zone. Number densities associated with the three-louver combustor are less affected by f/a and are higher than those measured with the full-length combustor. Number densities calculated for the two-louver combustor are lower than those obtained with the three-louver burner due to the nonuniformities described previously. Limited data taken with the one-louver combustor operating with Jet A fuel at f/a = 0.018 show a drastically reduced number density. Evidently the high particle concentrations in this region, indicated by the emissivity and radiation data (Figures 23 and 24), scattered the laser beam resulting in significantly reduced power at the probe volume. The scattered signal from the probe volume, then, was also reduced yielding abnormally low number density. Number density as a function of fuel type is displayed in Fig. 38 for f/a = 0.018. As indicated by the soot and smoke measurements, number density responded to fuel chemical properties, increasing for fuels with decreased smoke point.

Limited number density data were acquired with Jet A and ERBLS-2 fuels at reduced combustor pressure (Figures 34 and 36). As expected, number density is lower at reduced pressure. Reductions with Jet A, however, are disproportionately larger than reductions observed with soot loading and smoke number at this pressure condition. An explanation for these low number densities has not been established.

Particle size, as determined from scattering measurements, is shown in Fig. 39. Based on Ref. 11, combustor soot particles are mature agglomerates of large numbers of primary soot spheroids. These diameters are assumed to be representative of the size distribution of the agglomerates. It must be recognized, however, that since light scattering signals are greatest for large particles, these diameters are biased toward the larger particles of the distribution. These data show that particle size is invariant with respect to fuel chemical properties and combustor pressure. Using Jet A data as the reference, particle diameter is approximately 0.25 μm for the three shorter burners. The relative

constancy in particle size immediately downstream of the primary zone indicates that the spheroids agglomerated quickly. The average particle diameter evidently decreased between the third and fourth louvers and then remained constant. Particle diameter for the full-length burner is approximately 0.21 μm. This size, which is nearly identical with the particle size determined in the previous program, is apparently much smaller than that measured by Stamforth, where a significant portion of the sample consisted of particulates larger than one micron. The correlation between soot loading and smoke number in this experiment (Fig. 33), then, should and does fall below Stamforth's correlation.

Number density and particle size can be used to calculate the volume fraction occupied by the soot particles. In order to correlate this volume fraction with the particulate mass concentrations previously presented, however, the volume fraction must be calculated for standard conditions. Temperature at the probe volume is required to perform this calculation. This temperature was not measured during the test program because of the high exit temperatures that were produced as the combustor was reduced in length. The emission data gathered with the two-louver combustor (l/L = 0.413 in Fig. 22) was used to calculate temperatures for that configuration. Temperatures at the exit of the full-length burner were calculated based on the measured overall fuel and air flows. Temperature was assumed to decrease linearly between these two points. The resultant correlation obtained with this temperature distribution is shown in Fig. 40. With the exception of the low-pressure data gathered with Jet A fuel, concentration and volume fraction correlate well. A reasonably good representation of the data (not including the low-pressure Jet A data) was generated via a regression analysis.

The ratio of particulate concentration to particulate volume fraction is particle density. The density distribution obtained from the data shown in Fig. 40 is contained in Fig. 41. The data indicate that the average particle density only decreased slightly as the particles moved through the combustor. That the particle density tended not to change can also be deduced from the expression developed in the regression analysis (Fig. 40) of data from all combustor lengths. The exponant in that expression is close to unity indicating that concentration is nearly proportional to

volume fraction and, hence, that density does not change significantly over the range of test conditions. The value of the particle density is lower than that for solid carbon, which is approximately 2 g/cm^3. The lower particle density is consistant with the concept that the particles are agglomerates of smaller solid spheroids. The particle density will always be less than 2 g/cm^3 because of the space between spheriods and will be a function of the type of chain-like structure created during the agglomeration process. Samples collected by Wyatt et. al. (Ref. 12) downstream of a disk-stabilized flame also contained particulates with densities lower than that of carbon by a factor of 3 to 5. Note that the low-pressure Jet A results yield particle densities 5 to 7 times that calculated for the high-pressure tests. Since the particle diameter for the two pressure conditions is nearly the same, these data imply that these agglomerates were more tightly packed at low pressure. There are apparently no physical arguments that can be used to explain this tendency.

The number of small spheroids in the agglomerates of this experiment can be estimated. Bonczyk and Sangiovanni (Ref. 11) determined from photomicrographs of typical soot samples that the average spheroid diameter is approximately 200 Å. These small particles can be assumed to be solid carbon with a density of 2 g/cm^3. For an average agglomerate density of 0.4 g/cm^3 and diameter of 0.2 μm, the average number of spheroids per agglomerate is 200.

SECTION VI - CONCLUSIONS AND RECOMMENDATIONS

Based upon data acquired in the combustion test program, the following conclusions have been made:

1. The soot oxidation mechanism in a gas turbine combustor secondary zone is very vigorous and strongly dependent on the combustion product temperature. Oxidation rates do not depend strongly on fuel type.

2. Soot particulate size distribution decreases from a characteristic diameter of 0.25 m to 0.20 m as the soot particulates oxidize.

3. Soot mass loading and SAE smoke number correlate well for gas turbine combustors that produce small particulates.

4. Soot particulate density is approximately 20 percent that of pure carbon. This lower density is consistent with the concept that the particulates are chain-like structures composed of small particles of pure carbon.

5. Combustor pressure affects soot production, with more soot produced at higher pressure. Combustor pressure may also affect soot oxidation rates.

6. Fuels with a higher smoke point produce less soot in a gas turbine combustor.

7. Soot loading near the primary zone of a gas turbine combustor is three-dimensional due to the combustion jets passing through the louvers.

It is recommended that the following investigations be conducted to address the following technology needs as indicated in this program:

1. A phenomenological model of soot production and consumption in a gas turbine combustor needs be developed and evaluated. As chemical and fluid mechanical processes together control soot production, both influences must be included. Data are required to evaluate the model.

2. Development of fundamental mechanisms and models of soot production from aviation type fuels.

3. Quantitative evaluation of pressure influence on soot production.

4. Data to identify fuel chemical property influences associated with the use of air-blast fuel injectors in gas turbine combustors.

REFERENCES

1. Rosfjord, T. J.: Avietior - Fuel Property Effects on Combustion. NASA CR 168334, February, 1984.

2. Clark, J. A.: Fuel Property Effects on Radiation Intensities In a Gas Turbine Combustor. AIAA Journal, Vol. 20, No. 2, pp. 274-281. February, 1982.

3. Ballal, D. R. and A. H. Lefebvre: Combustion Performance of Gas Turbine Combustors Burning Alternative Fuels. AIAA Journal of Energy, Vol. 3, No. 1, pp. 50-54. January, 1979.

4. Van de Hulst, H. C.: Light Scattering by Small Particles. Wiley, New York, NY 1957.

5. Kerker, M.: The Scattering of Light and Other Electromagnetic Radiasions. Elsevier, New York, NY, 1969.

6. Diermendjian, D.: Electromagentic Scattering of Sperical POlydispersions. Elsevier, New York, NY 1969.

7. Bonczyk, P. A.: Measurement of Particulate Size by In Situ Laser Optical Methods: A Critical Evaluation Applied to Fuel Pyrolyzed Carbon. Combustion and Flame, Vol. 35, pp. 191-206. 1979.

8. Lin, B. Y. H. and K. W. Lee: Efficiency of Membrane and Nuclepore Filters for Submicrometer Aerosols. Enviornmental Sciences and Technology, Vol. 10, No. 4, April, 1976.

9. Glassman, I.: Phenomenological Models of Soot Processes In Combustion Systems. AFOSR TR 79-1147, 1979.

10. Champagne, D. L.: Standard Measurement of Aircraft Gas Turbine Engine Exhaust Smoke. Presented at the ASME Gas Turbine and Products Show, Houston, Texas, Mar. 28 – April 1, 1971.

11. Bonczyk, P. A. and J. J. Sangiovani: Optical and Probe Measurements of Soot In a Burning Fuel Droplet Stream. UTRC Rep. UTRC 83-25, June, 1983.

12. Wyatt, W. R., J. A. Clark, J. E. Peters, and A. M. Mellor: Size Distribution and Surface Area Measurements of Gas Turbine Combustor Smoke. Journal of Energy, Vol. 3, No. 6, pp. 285-290. September – October, 1979.

TABLE 1 - FUEL ANALYSIS METHODS

Property	Method
Hydrogen (wt pct)	ASTM D 3178
Flash point, tag closed (K)	D 56
Distillation (vol pct at T [K])	D 86
Freeze point (K)	D 2386
Smoke point (mm)	D 1322
Specific gravity (at 289K)	D 1298
Viscosity at 293 (cst)	D 445
Viscosity at 253K (cst)	D 445
Net heat of combustion (MJ/kg)	D 240
Mercaptan sulfur (wt pct)	D 3227
Total sulfur (wt pct)	D 2622
Nitrogen (wt pct)	Antek Chemiluminescence
Saturates (vol pct)	D 1319
Olefins (vol pct)	D 1319
Aromatic (vol pct)	D 1319
Naphthalenes (vol pct)	D 1840
Mass spectrometry for hydrocarbon types (wt pct)	D 2425
Surface tension (dyne/cm)	Tensiometer

TABLE 2 - Fuel Analyses

	Jet A	ERBS	ERBLS-2	XTB
Specific Gravity at 289K	0.8165	0.8388	0.8612	0.8751
Flash Point (K)	319	326	316	315
Freeze Point (K)	226.5	243	247	<206
Smoke Point (mm)	20.3	12.7	10.3	7.4
Net Ht of Combustion (MJ/kg)	42.88	42.48	41.86	40.78
Viscosity at 253K (cst)	5.39	5.69	5.00	1.85
Viscosity at 293K (cst)	2.02	2.07	1.89	0.95
Surface Tension (dynes/cm)	26.3	27.1	27.6	28.50
C (wt pct)	86.04	87.02	87.85	90.30
H (wt pct)	13.70	12.84	11.76	10.24
Mercaptan Sulfur (10^{-4} wt pct)	<5	<5	<5	<5
Total Sulfur (wt pct)	0.06	0.12	0.11	<0.01
Nitrogen (g/m)	7	81	75	<5
Saturates (vol pct) HC-FIA	78.1	67.2	47.7	0
Olefins (vol pct)	1.7	1.4	1.3	0
Aromatics (vol pct)	20.2	31.4	51.0	100
Naphthalenes (wt pct) - UV	2.44	16.34	17.41	0.43
Aromatics (vol pct) HC-Mass Spec	22.0	29.9	47.5	100
Naphthalenes (wt pct)	1.68	11.71	22.97	0.01

Hydrocarbon Type by Mass Spectrometry (wt pct)

	Jet A	ERBS	ERBLS-2	XTB
Total Saturates	75.4	65.8	47.3	0.0
Paraffins	34.9	42.6	31.1	0.0
Moncyclo Paraffins	33.7	15.3	10.5	0.0
Dicyclo Paraffins	6.2	7.1	5.3	0.0
Tricyclo Paraffins	0.6	0.8	0.3	0.0
Total Aromatics	24.6	34.2	52.7	100.0
Akyl Benzene	18.0	16.9	20.1	100.0
Indanes	4.9	4.7	7.5	0.0
Indenes	0.0	0.2	0.9	0.0
C10 Napthalene	1.7	0.4	0.5	0.0
C11+ Napthalenes	0.0	9.2	17.5	0.0
Acenanapthenes	0.0	1.3	3.2	0.0
Acenanapthalenes	0.0	0.8	1.8	0.0
Tricylic Aromatic	0.0	0.6	1.3	0.0

TABLE 2 - Fuel Analyses

(continued)

Distillation (K)

Vol Off	Jet A	ERBS	ERBLS-2	XTB
IBF	438	446	424	430
5	452	457	437	432
10	459	462	442	433
15	463	465	448	434
20	466	467	452	434
30	473	473	462	435
40	479	479	473	435
50	486	486	486	436
60	492	493	499	437
70	500	502	514	439
80	509	514	530	439
90	521	537	556	442
95	531	563	580	445

TABLE 3 - Nozzle Characterization

Nozzle No.	SMD (μm)/Included Cone Angle (deg) Fuel Flowrate (kg/hr)								
	27	30	37	73	82	100	118	133	162
8	48/82	40/80	28/77						
9	60/80	52/77	35/78						
10	66/80	60/78	44/78						
18				42/82	30/80	6/77			
20				53/80	42/80	16/79			
22				67/75	53/76	31/74			
32							57/81	42/82	9/77
35							71/78	56/76	23/74

TABLE 4 - Combustor Open Area Distribution

Section		Number	Area Distribution Diameter (mm)	Area (cm^2)
Dome	Cooling	60	1.78	
	(4 rings)	60	1.47	
		60	1.47	
		60	1.09	4.09
Louver 1	Cooling	96	1.98	2.96
	Combustion	6	12.7	7.13
Louver 2	Cooling	96	1.98	2.96
	Combustion	6	12.7	7.13
Louver 3	Cooling	96	1.98	2.96
	Combustion	6	12.7	7.13
Louver 4	Cooling	96	1.98	2.96
Louver 5	Cooling	48	1.98	1.48
	Combustion	6	12.7	7.13
Louver 6	Cooling	48	1.98	1.48

TABLE 5 - Liner Effective Area Distribution

Section		Effective Area (cm^2)	Percent of Total (with Swirler)
Swirler		3.0	8.2
Dome	Cooling	3.0	16.3
Louver 1	Cooling	2.5	23.1
	Combustion	4.6	35.6
Louver 2	Cooling	2.5	42.4
		4.6	54.9
Louver 3	Cooling	2.4	61.4
	Combustion	4.5	73.7
Louver 4	Cooling	2.6	80.7
Louver 5	Cooling	1.2	84.0
	Combustion	4.6	96.5
Louver 6	Cooling	1.3	100.0
Total Liner with Swirler		36.8	100.0

TABLE 6

AirFlow and FuelFlow Conditions

Airflow Conditions

Condition	Mass Flow (kg/s)	Approach Pressure (MPa)	Approach Temp. (K)
1. High Power	1.82	1.3	700
2. Reduced Pressure	1.45	0.8	700

Fuel-Air Ratios

Exit Temperature (K)	Fuel			
	Jet A	ERBS	ERBLS-2	XTB
1240	0.0150	.0153	.0153	.0156
1340	0.0180	.0182	.0184	.0188
1470	0.0220	.0223	.0224	.0230
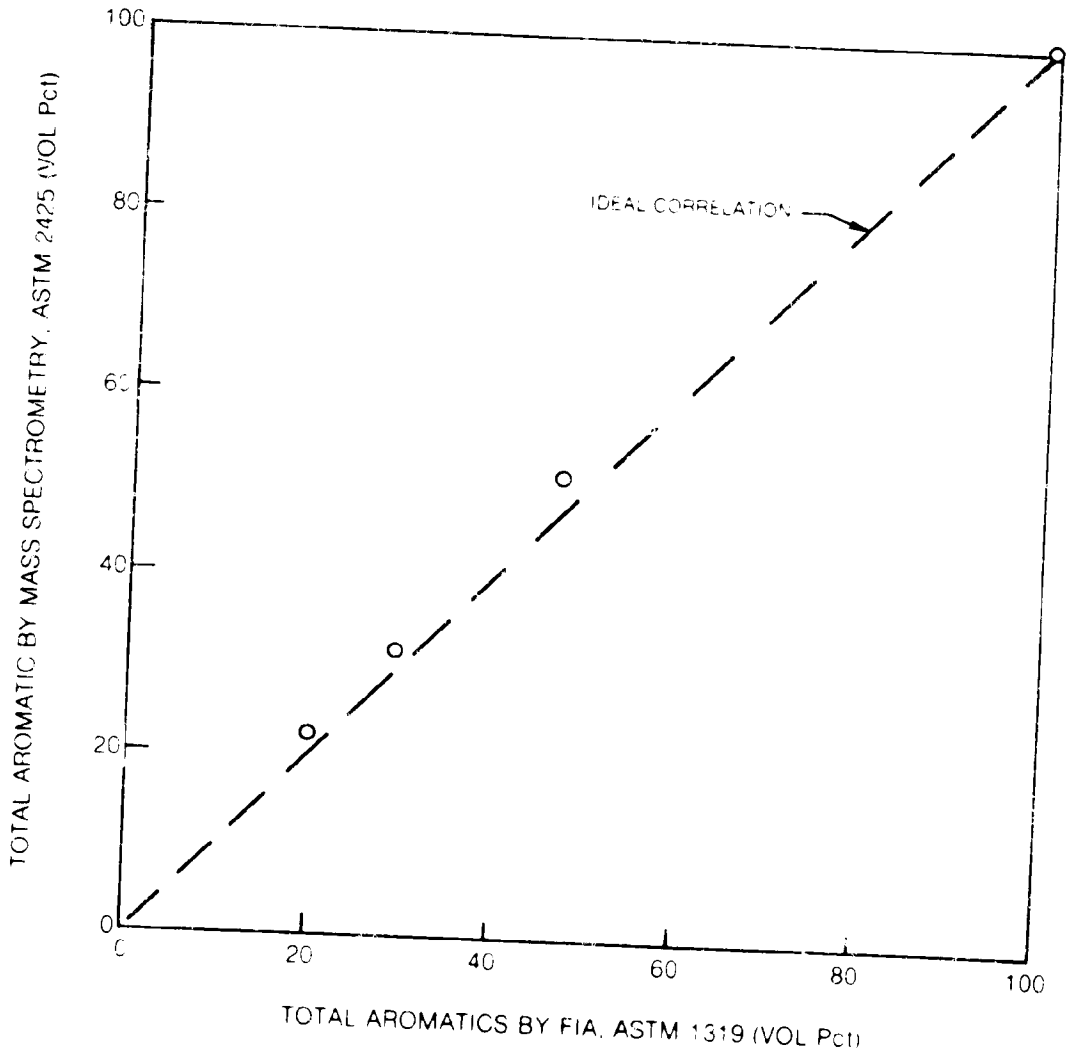
Fig. 1 Comparison of Total Aromatic Content for Two Analysis Techniques
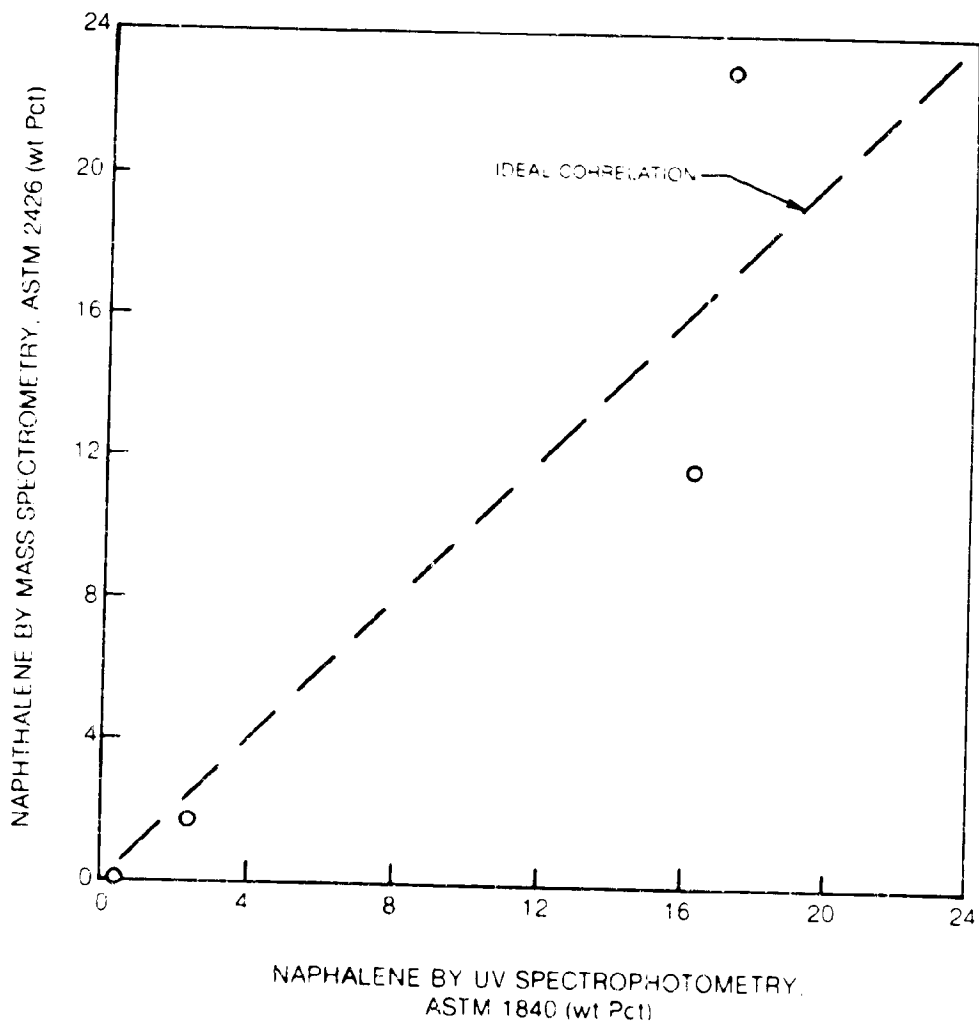
Fig. 2 Comparison of Naphthalene Content for Two Analysis Techniques

TURBINE
METER

JET A
(UNDERGROUND
STORAGE)

TM

P T

NOZZLE

LASER

MALVERN PARTICLE
SIZE ANALYZER

SCRUBBER
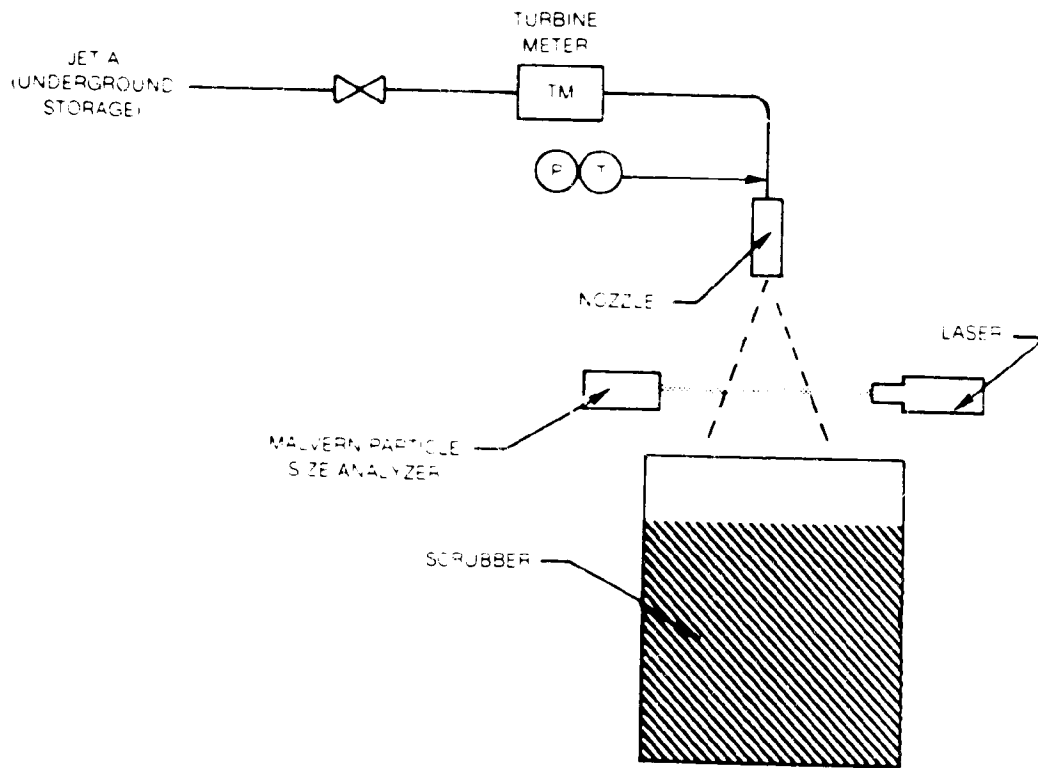
Fig. 3 Fuel Spray Characterization Facility

JET A FUEL
80 deg. HOLLOW CONE SIMPLEX
INJECTORS WITH INDICATED
NOZZLE NUMBER
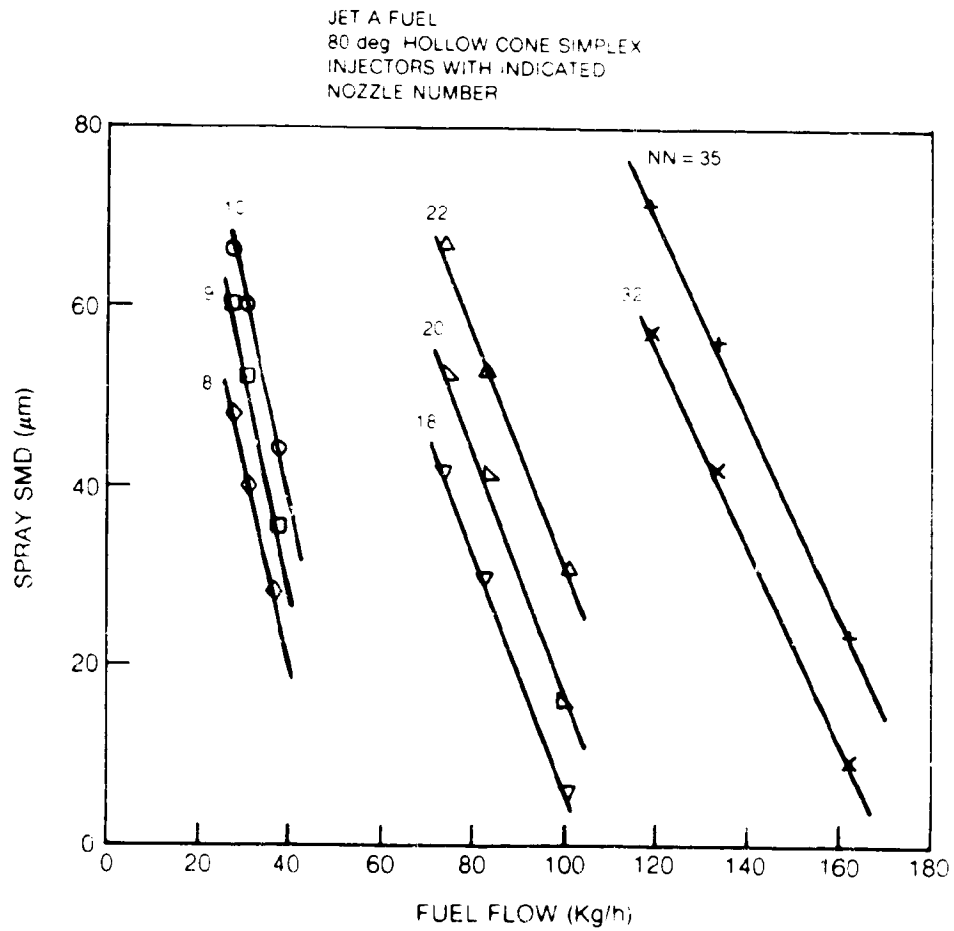
Fig. 4 Influence of Fuel Flow on Jet A Spray SMD for Several Nozzle Sizes

84-5-49-1

JET A FUEL
80 deg HOLLOW CONE
SIMPLEX INJECTORS
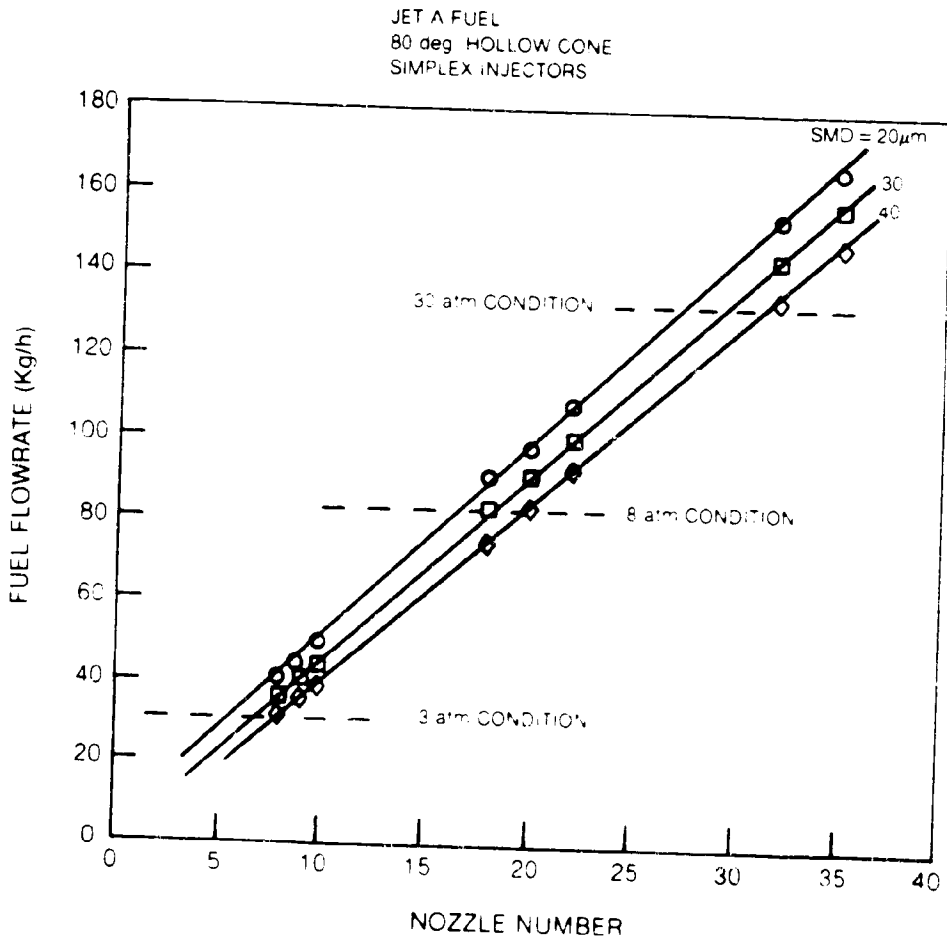
Fig. 5 Injector Size Required to Achieve Atomization Level

R85-956760-21

Fig. 6 Generic Gas Turbine Combustor

85-9-57 4
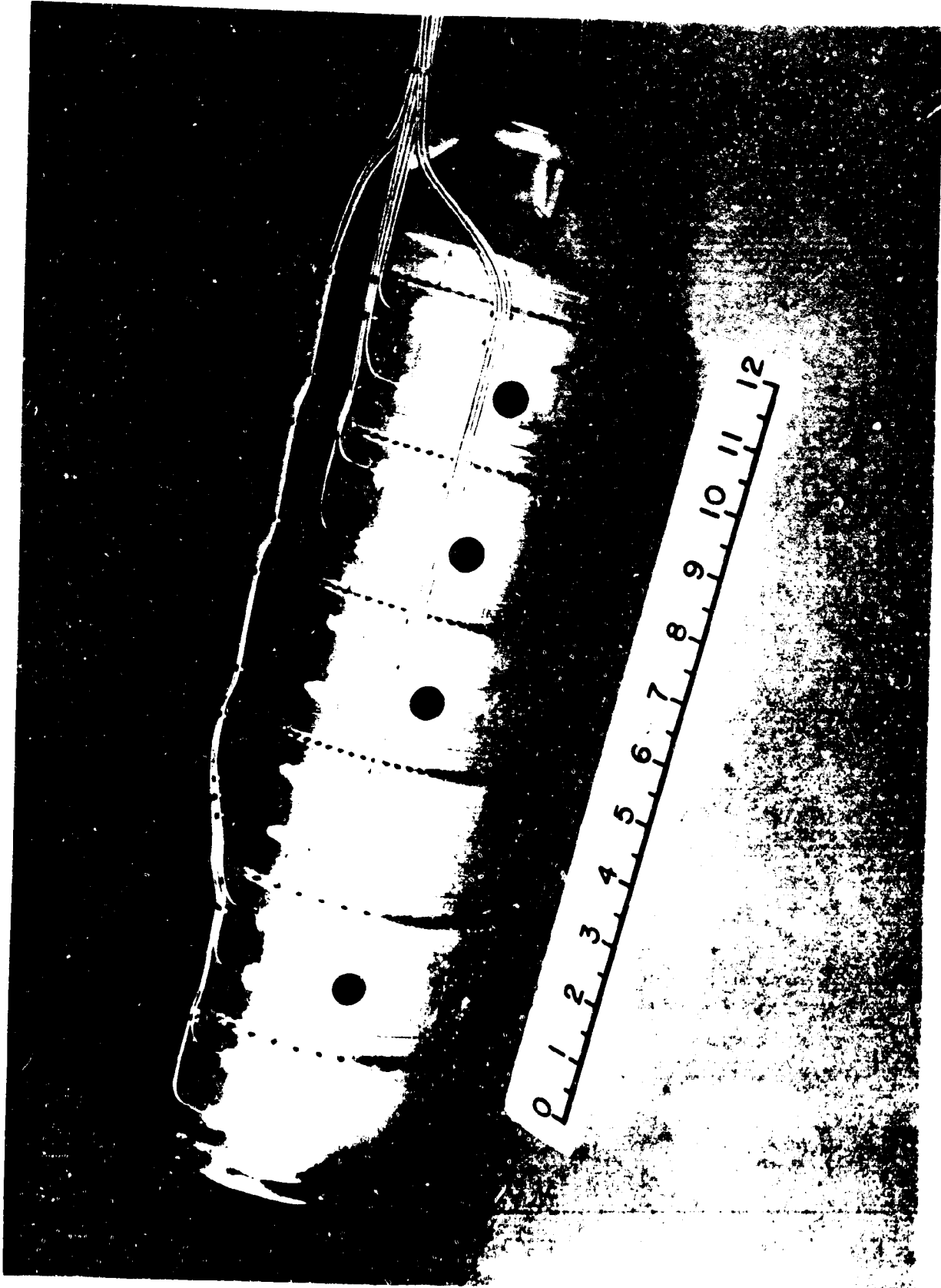
a) SIMPLEX PRESSURE ATOMIZING INJECTOR

b) AIRFLOW SWIRLER

Fig. 7 Fuel Nozzle and Air Swirler
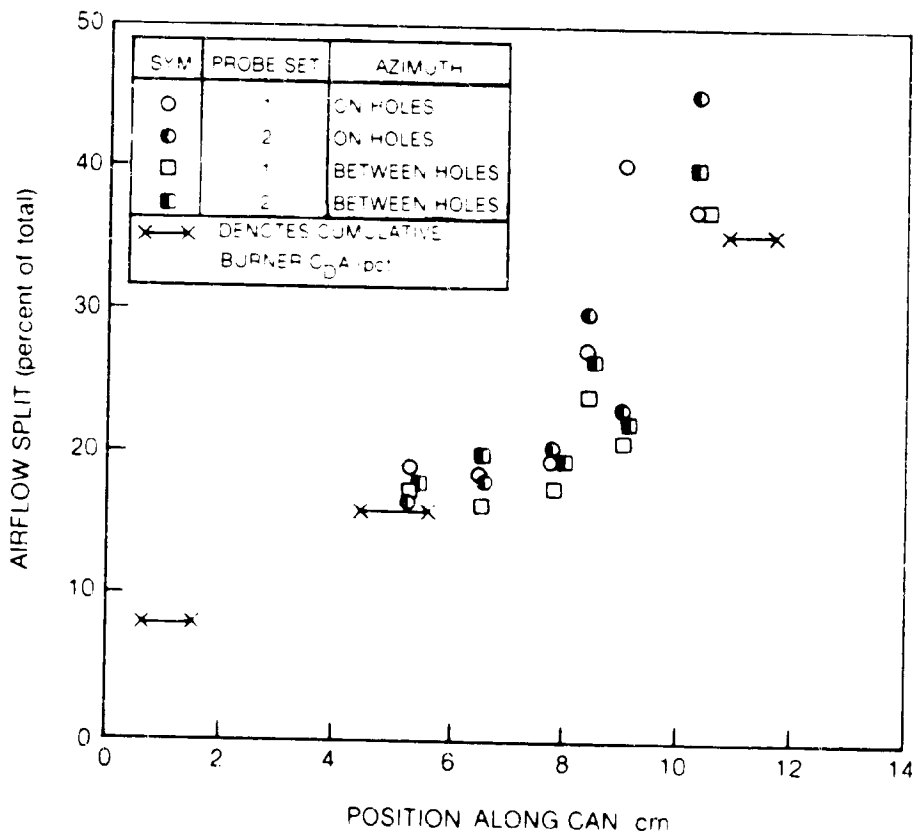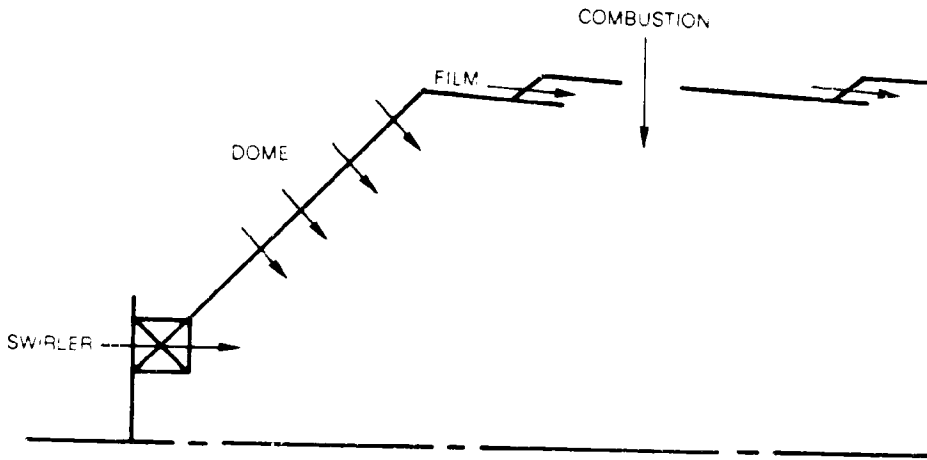
Fig. 8 Primary Airflow Split in Generic Combustor

BURST
DISC

15.2 cm ID (TYPICAL)

ADAPTER

VIEWING
PORT

HEATER

PLENUM

ACCESS SPOOLS

EXHAUST

BACK
PRESSURE
VALVE

```
                    |                 |
AIR PREPARATION     |   TEST AND      |
    SECTION         | INSTRUMENTATION |   EXHAUST
                    |    SECTIONS     |   SECTIONS
                    |                 |
                    |                 |
```
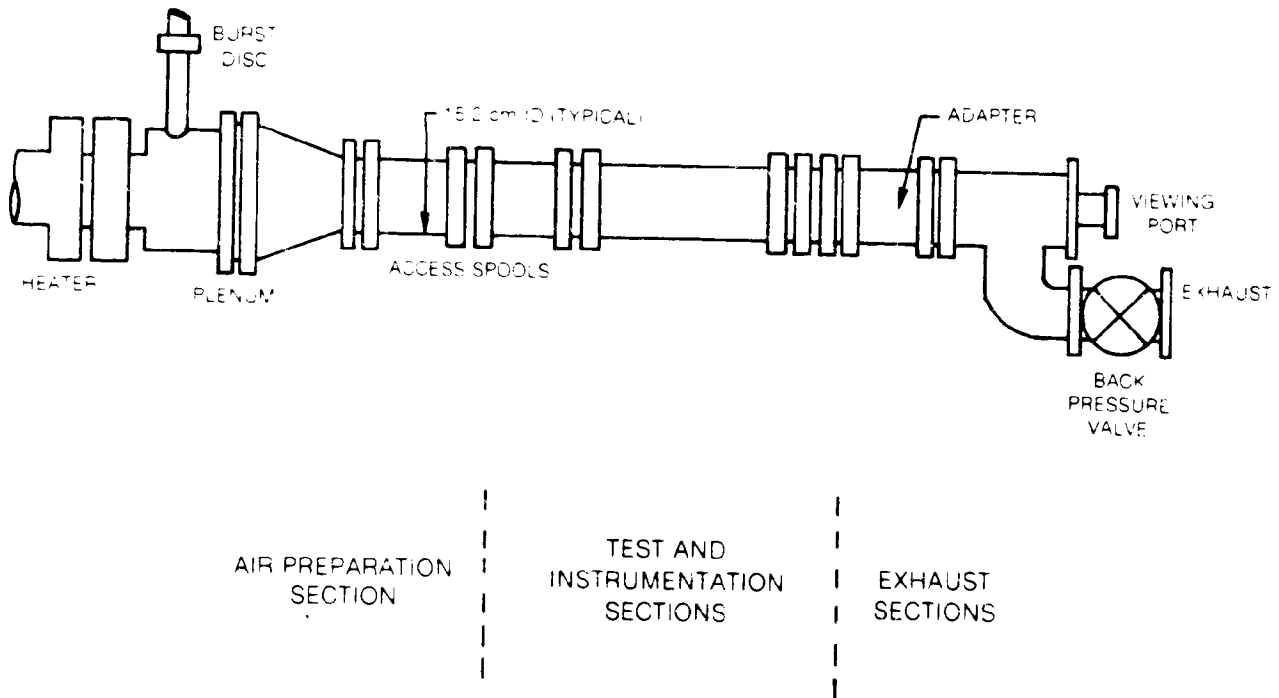
Fig. 9 Aviation-Fuel Property Effects Test Facility

85-9-57-5
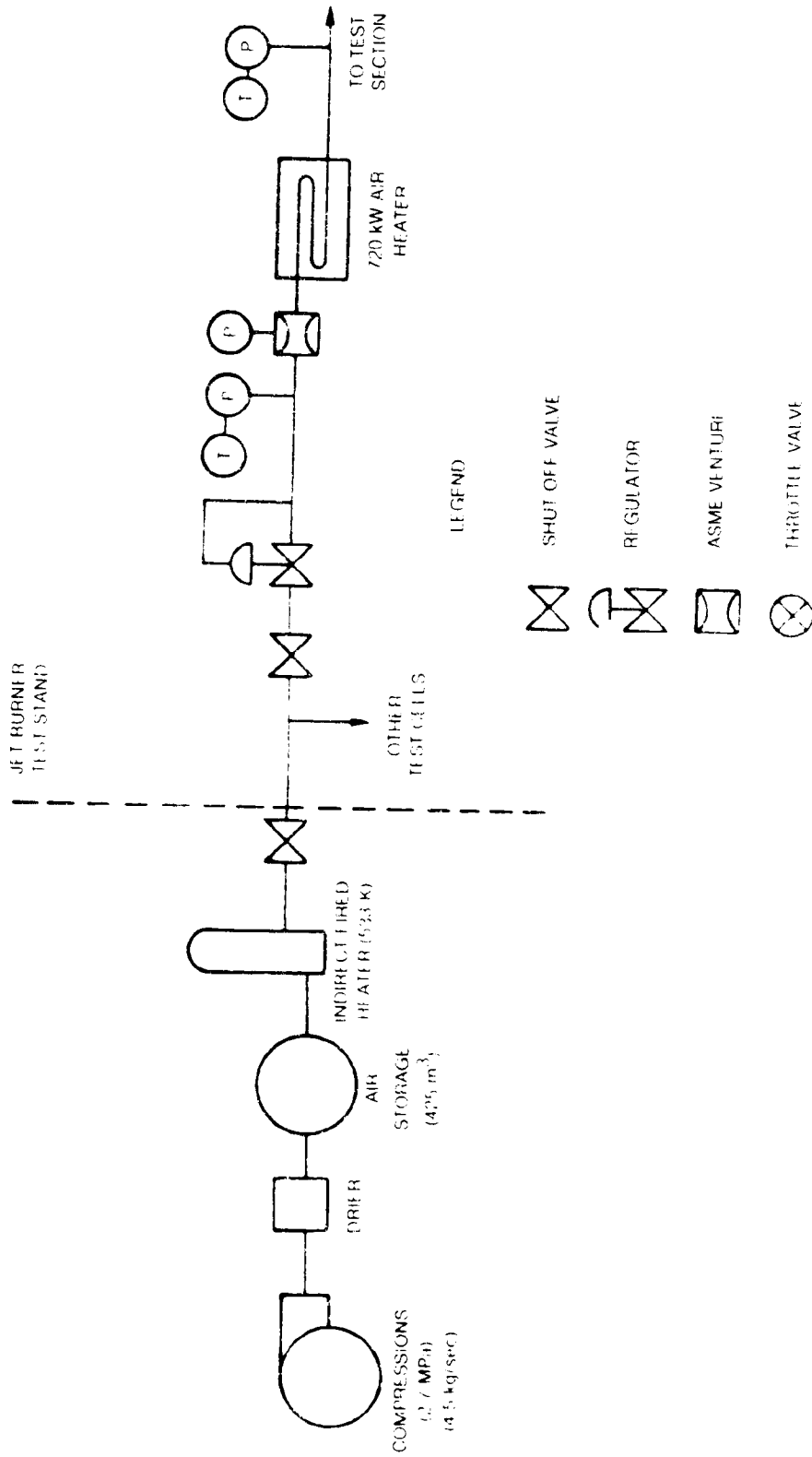
Fig. 10 Air Supply System for Test Rig

LEGEND

SHUT OFF VALVE

REGULATOR

ASME VENTURI

THROTTLE VALVE

COMPRESSORS
(2.7 MPa)
(4.5 kg/sec)

DRIER

AIR STORAGE
(42.5 m³)

INDIRECT FIRED
HEATER (533 K)

JET BURNER
TEST STAND

OTHER
TEST CELLS

720 KW AIR
HEATER
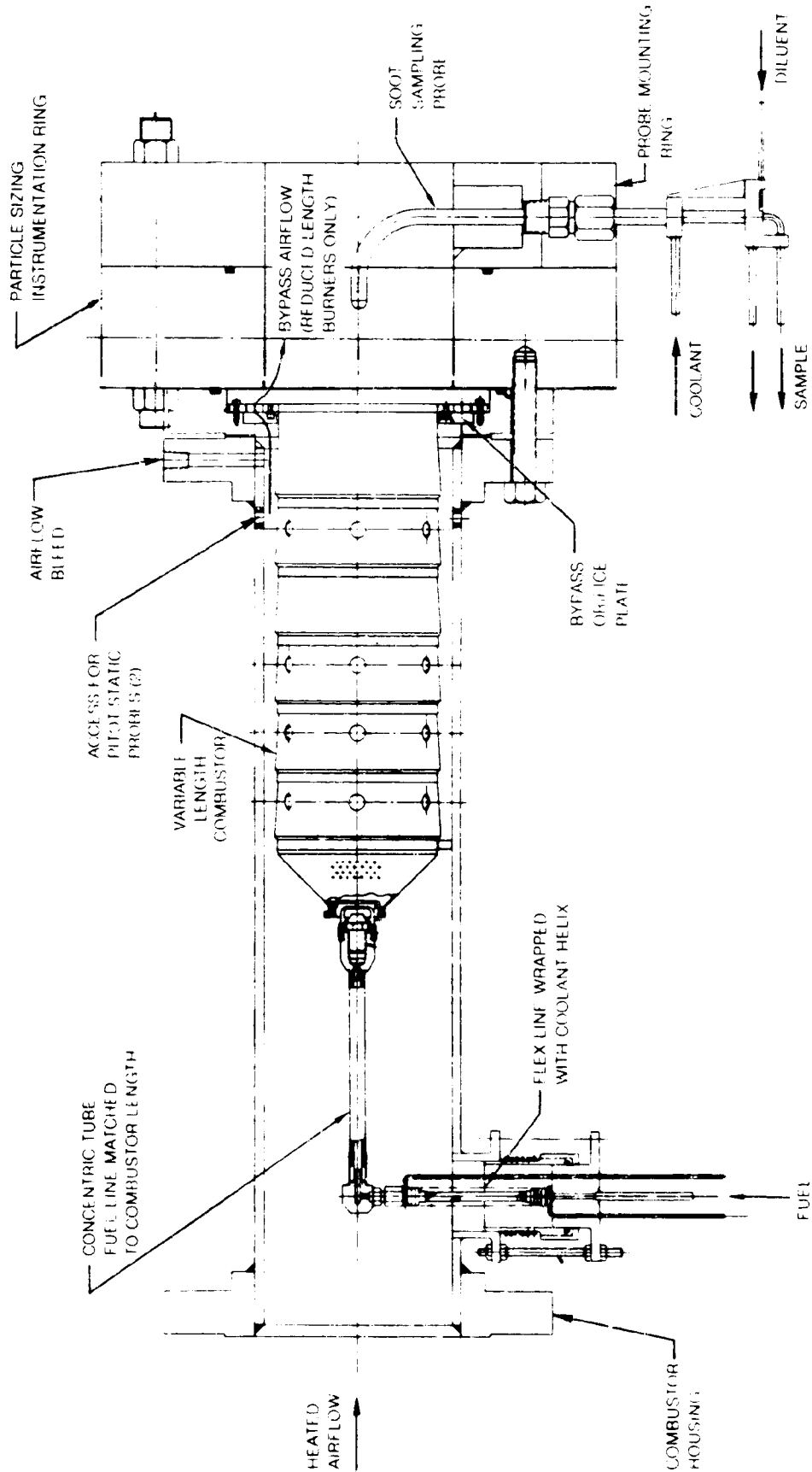
TO TEST
SECTION

Figure 11 Combustor configuration for soot sampling

Labels in figure:

PARTICLE SIZING INSTRUMENTATION RING

SOOT SAMPLING PROBE

PROBE MOUNTING RING

DILUENT

BYPASS AIRFLOW (REDUCED LENGTH BURNERS ONLY)

COOLANT

SAMPLE

AIRFLOW BLEED

BYPASS ORIFICE PLATE

ACCESS FOR PITOT STATIC PROBES (2)

VARIABLE LENGTH COMBUSTOR

CONCENTRIC TUBE FUEL LINE MATCHED TO COMBUSTOR LENGTH

FLEX LINE WRAPPED WITH COOLANT HELIX

FUEL

HEATED AIRFLOW

COMBUSTOR HOUSING

84-4-34-2

AIR SUPPLY

SOLENOID VALVE

PUMP

FILTER

REGULATOR

STRAINER

CHECK VALVE

PHOTOMULTIPLIER TUBE

HEAT EXCHANGER

VENTURI

TURBINE METER

SOOT AND EMISSION MEASUREMENTS

GAS SMOKE ANALYSIS

ELECTRICAL AIR HEATER

COMBUSTOR

EXHAUST

PURGE

PURGE

PURGE

FUEL SYSTEM

JET A

N2 PURGE

NO

NC

TEST FUEL

NOTES: SUPERSCRIPT INDICATES MULTIPLE MEASUREMENTS, COOLANT TEMPERATURE MEASUREMENTS NOT INDICATED

Fig. 12 Test Rig Support Systems and Instrumentation

82-7-68-1

$$\frac{I(45)}{I(135)}$$

n = 1.94 – 0.66

n = 1.56 – 0.46

PARTICLE DIAMETER (μm)
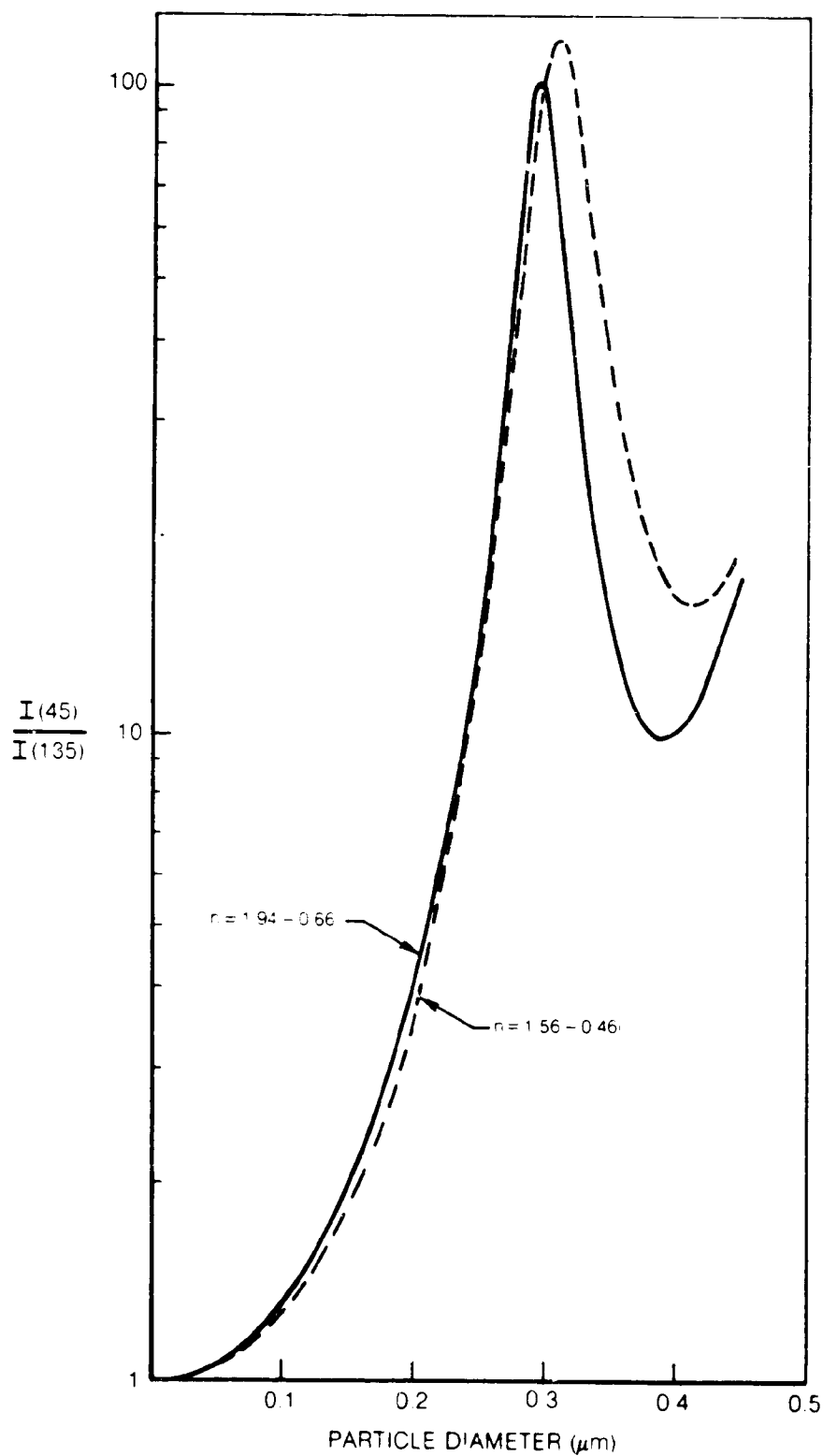
Fig. 13 Scattered-Light Ratio Dependence on Particle Diameter

83–7–29–13

OUTPUT TO LOCK-IN AMPLIFIER
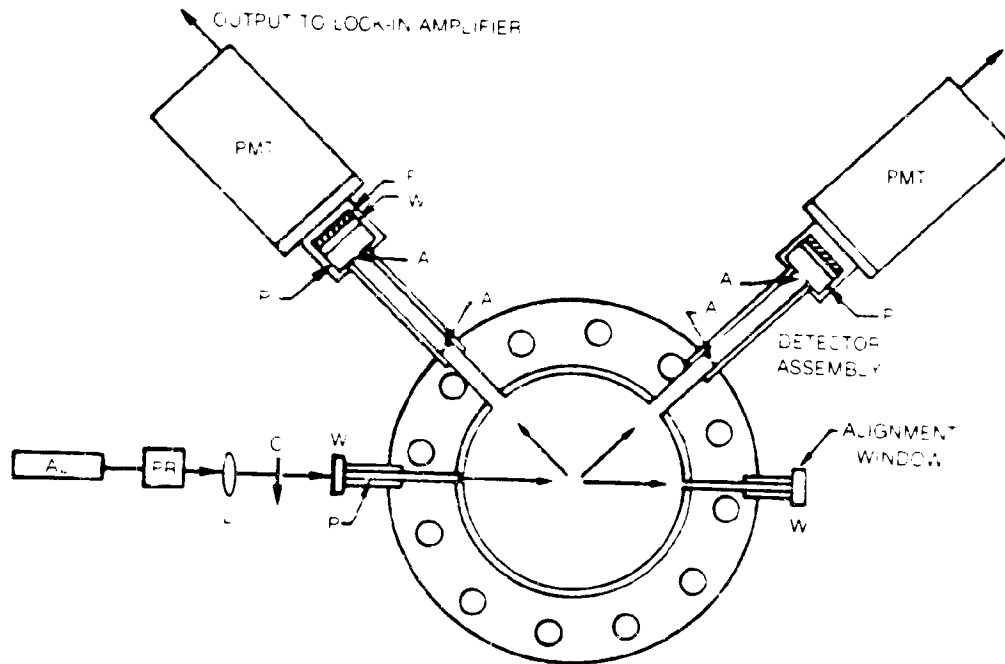
A	APERTURE
AL	ARGON ION LASER
C	MECHANICAL CHOPPER
F	NARROW BAND OPTICAL FILTER AND POLARIZER
L	LENSE
P	NITROGEN PURGE
PM	POWER METER
PMT	PHOTOMULTIPLIER
PR	POLARIZATION ROTATOR
W	WINDOW

Fig. 14 Layout of Particle Sizing Apparatus
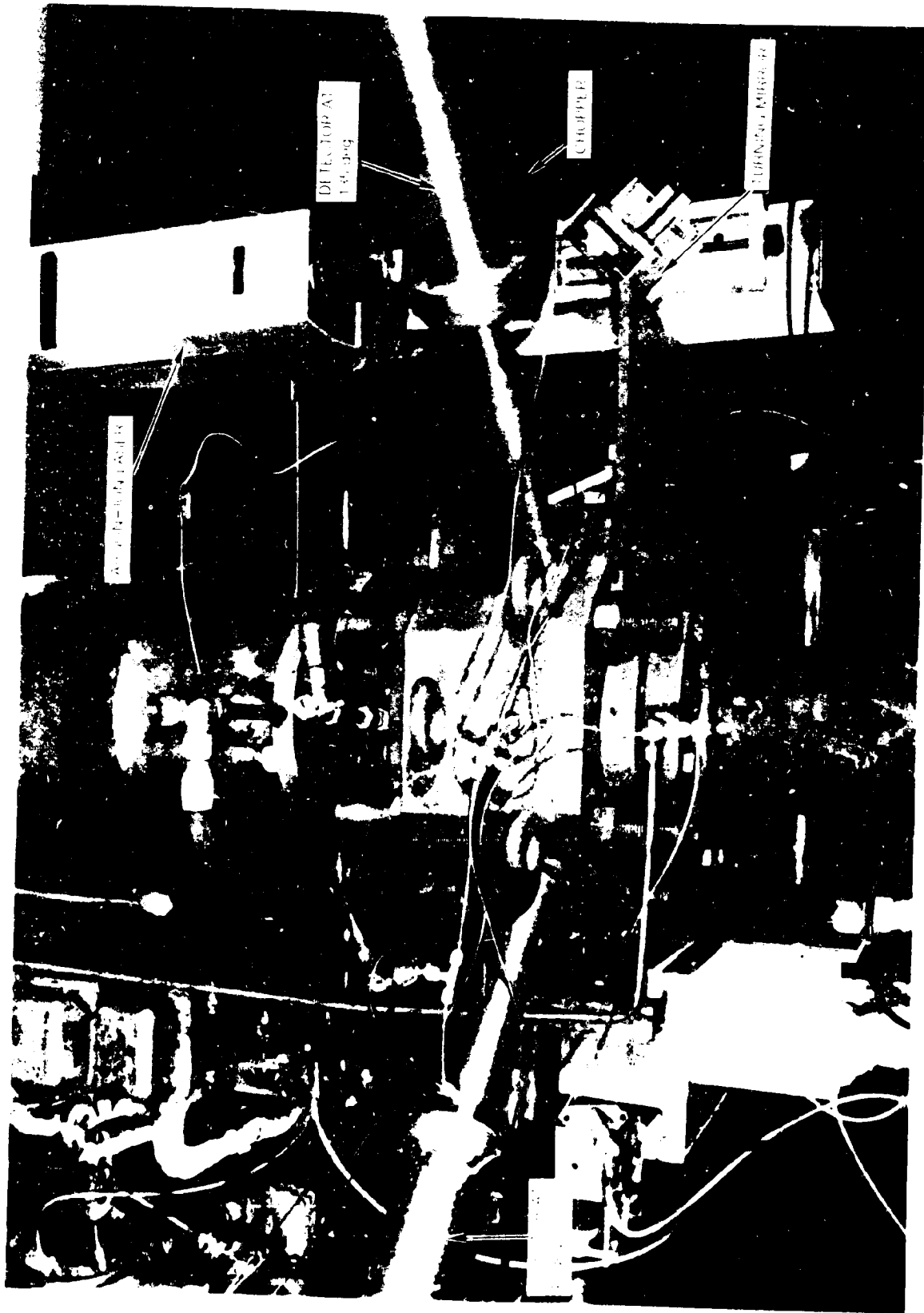
Fig. 15 Light Scattering Particle Sizing Diagnostic

85-3-72-15
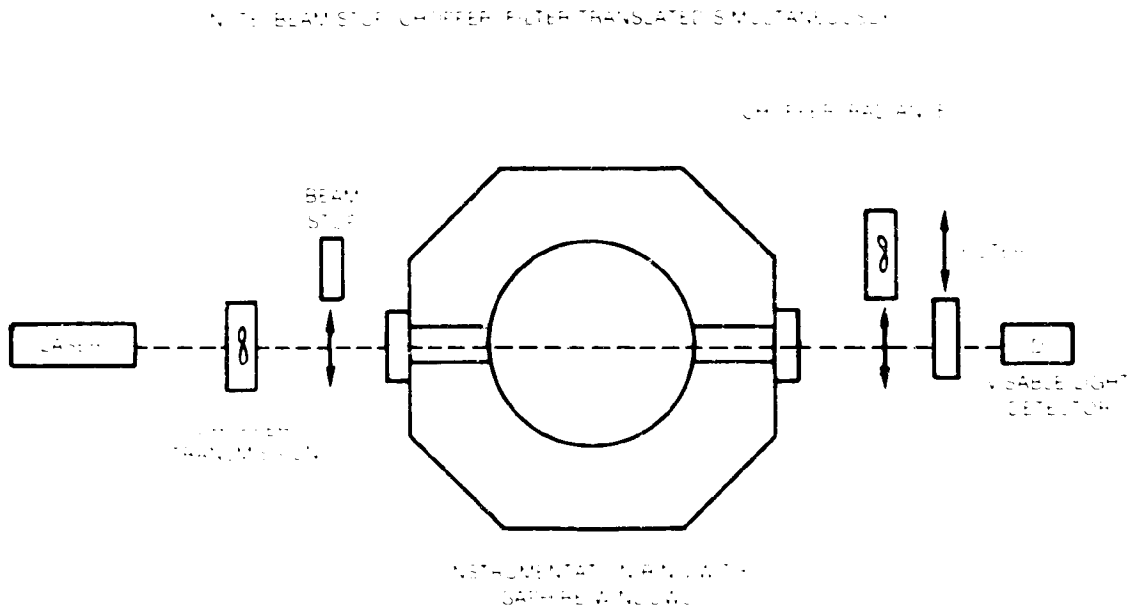
Fig. 16 Optical Setup for Visable Transmission/Radiance Measurements

MIXTURE

NITROGEN
DILUENT

COOLANT

CERAMIC
COATING
(0.3 mm)

A

A

SAMPLE

13 cm OD

SAMPLE TUBE
(3.7 mm ID)

DILUENT
MANIFOLD

SECTION A-A
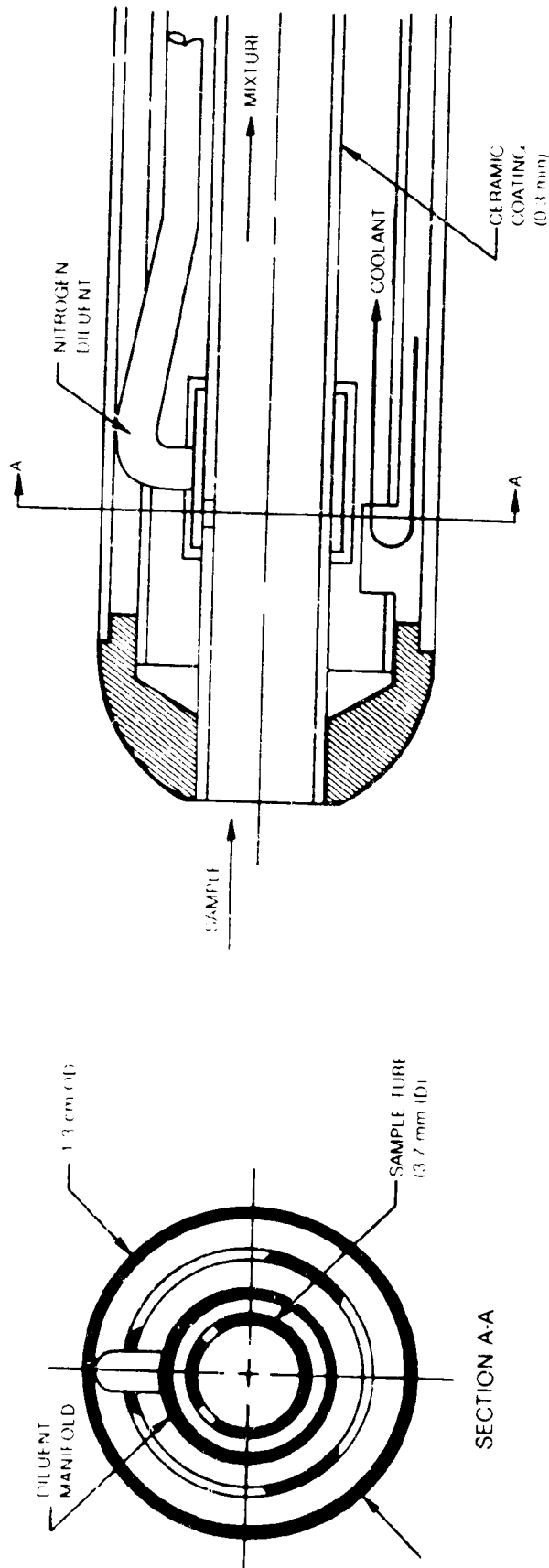
Fig. 17 Combustor Exhaust Sampling Probe Tip
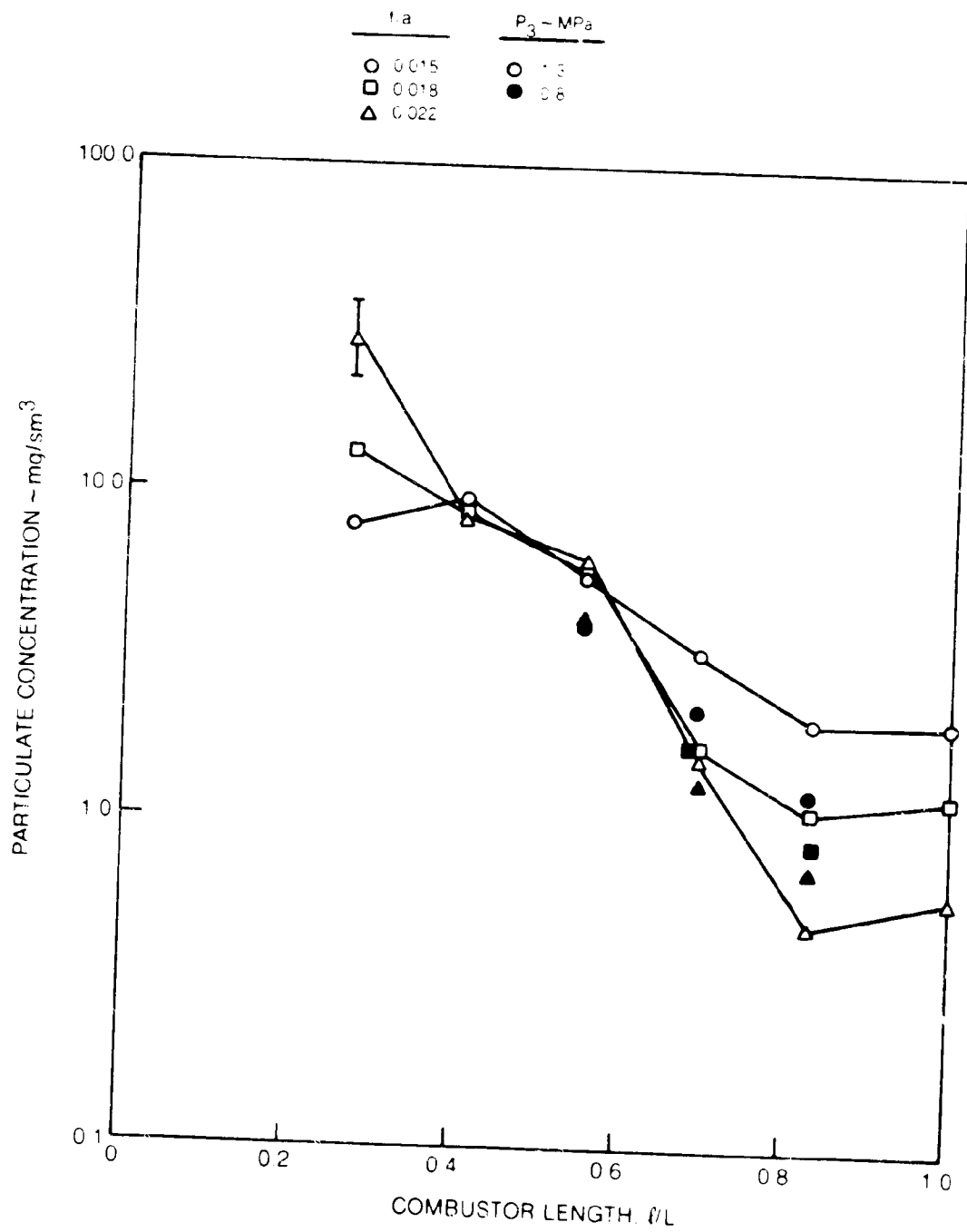
Fig. 18.   Soot loading for Jet A fuel
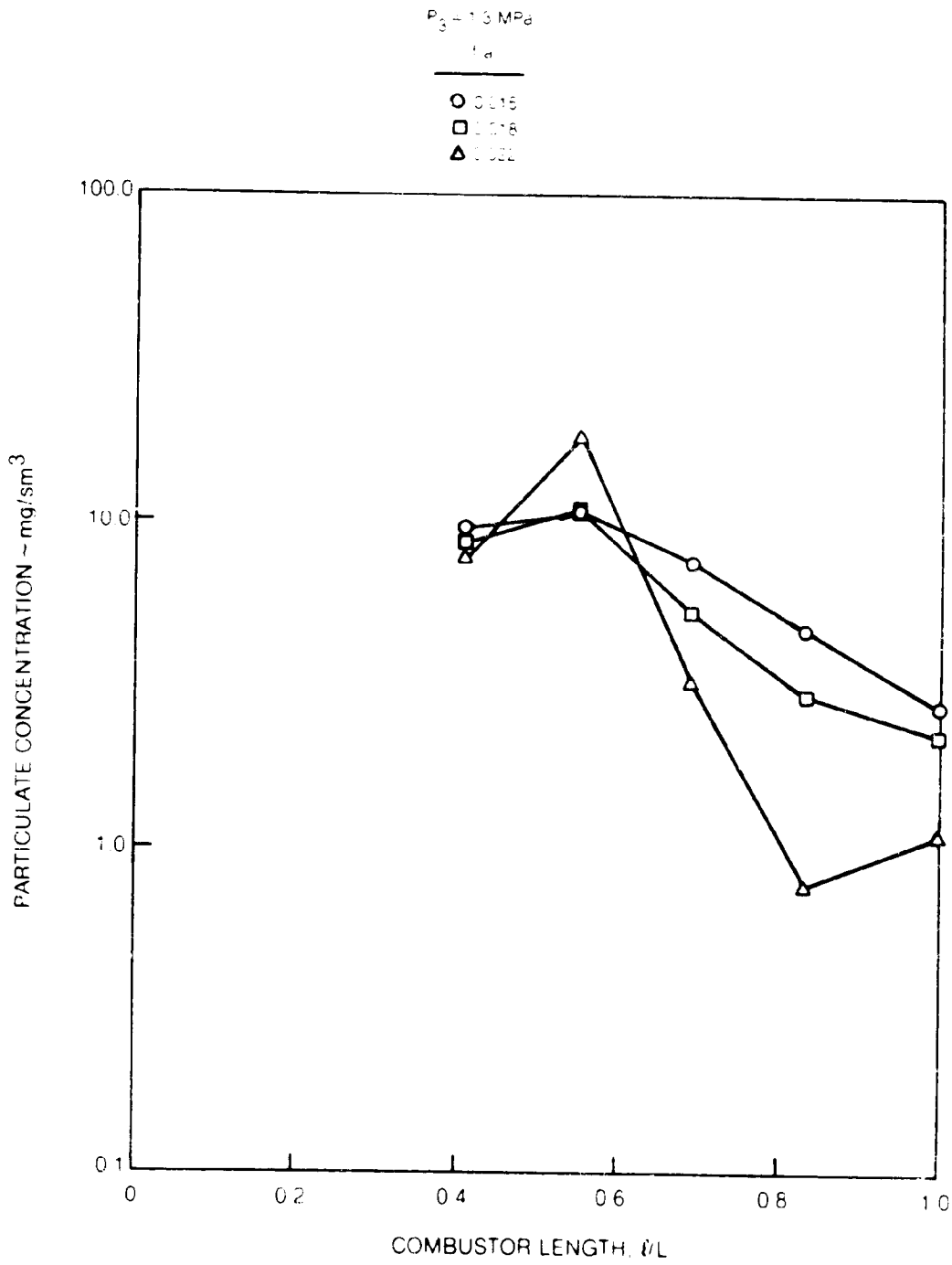
Fig. 19. Soot loading for ERBS fuel
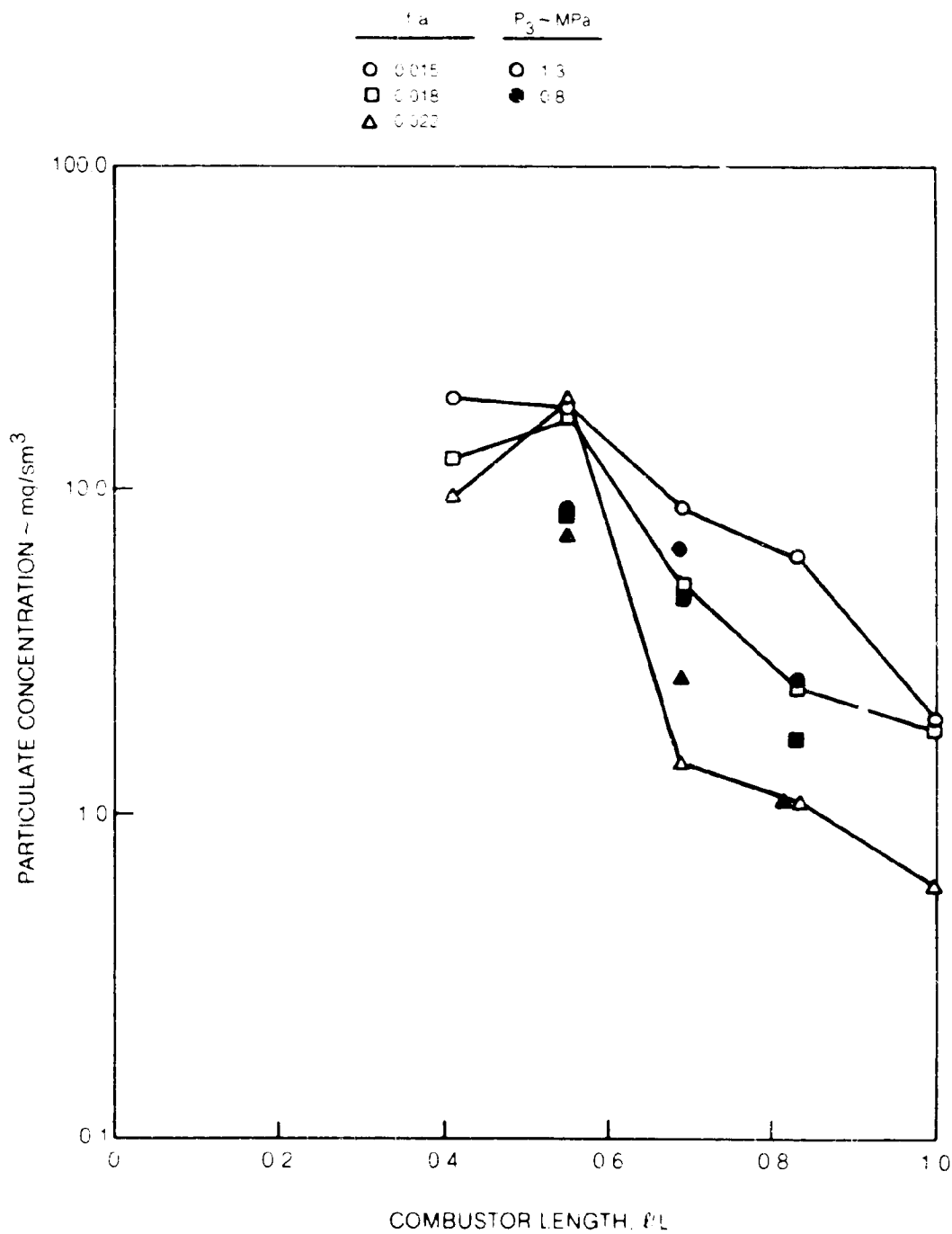
Fig. 20. Soot loading for ERBLS-2 fuel
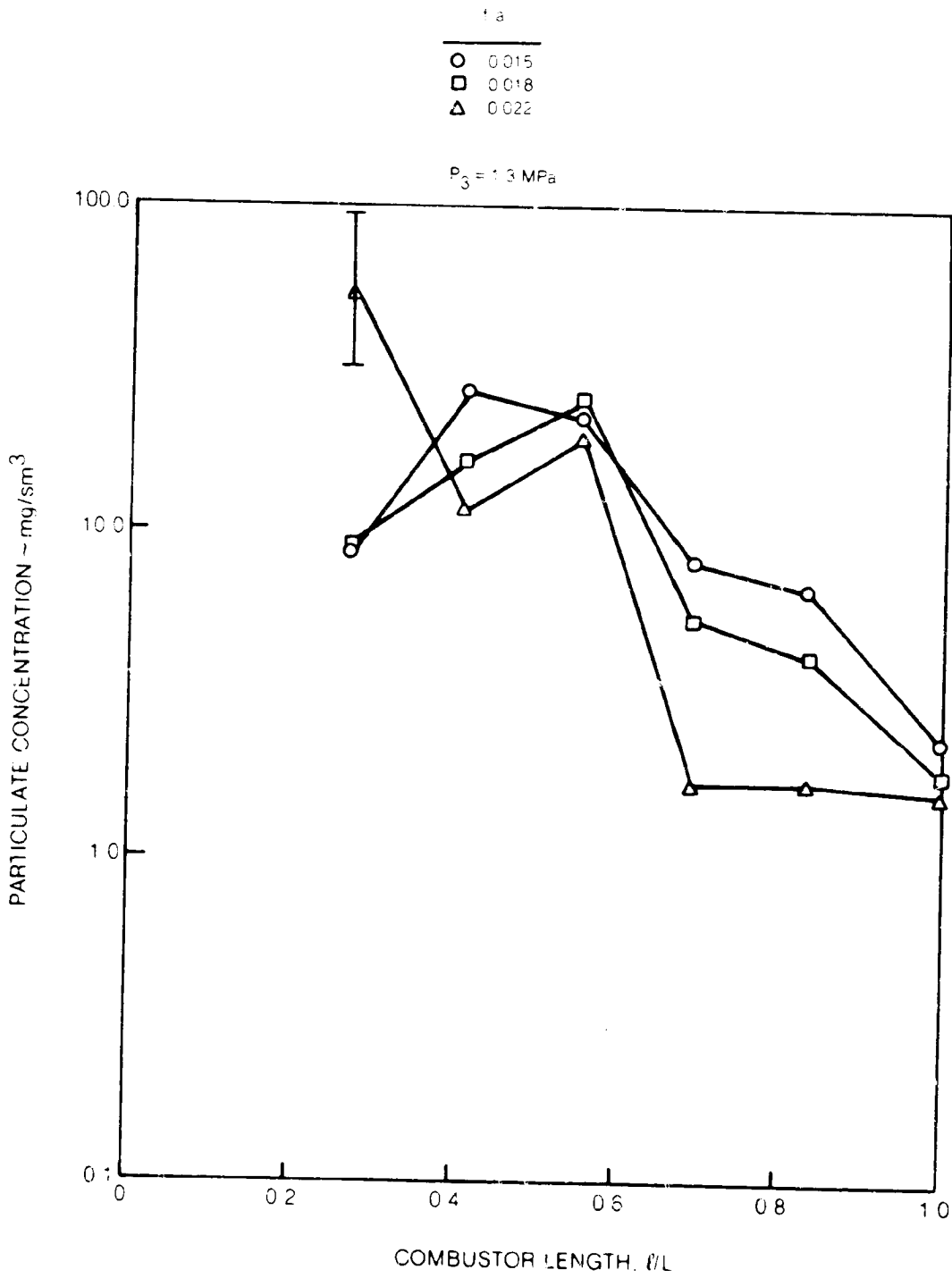
Fig. 21. Soot loading for XTB fuel
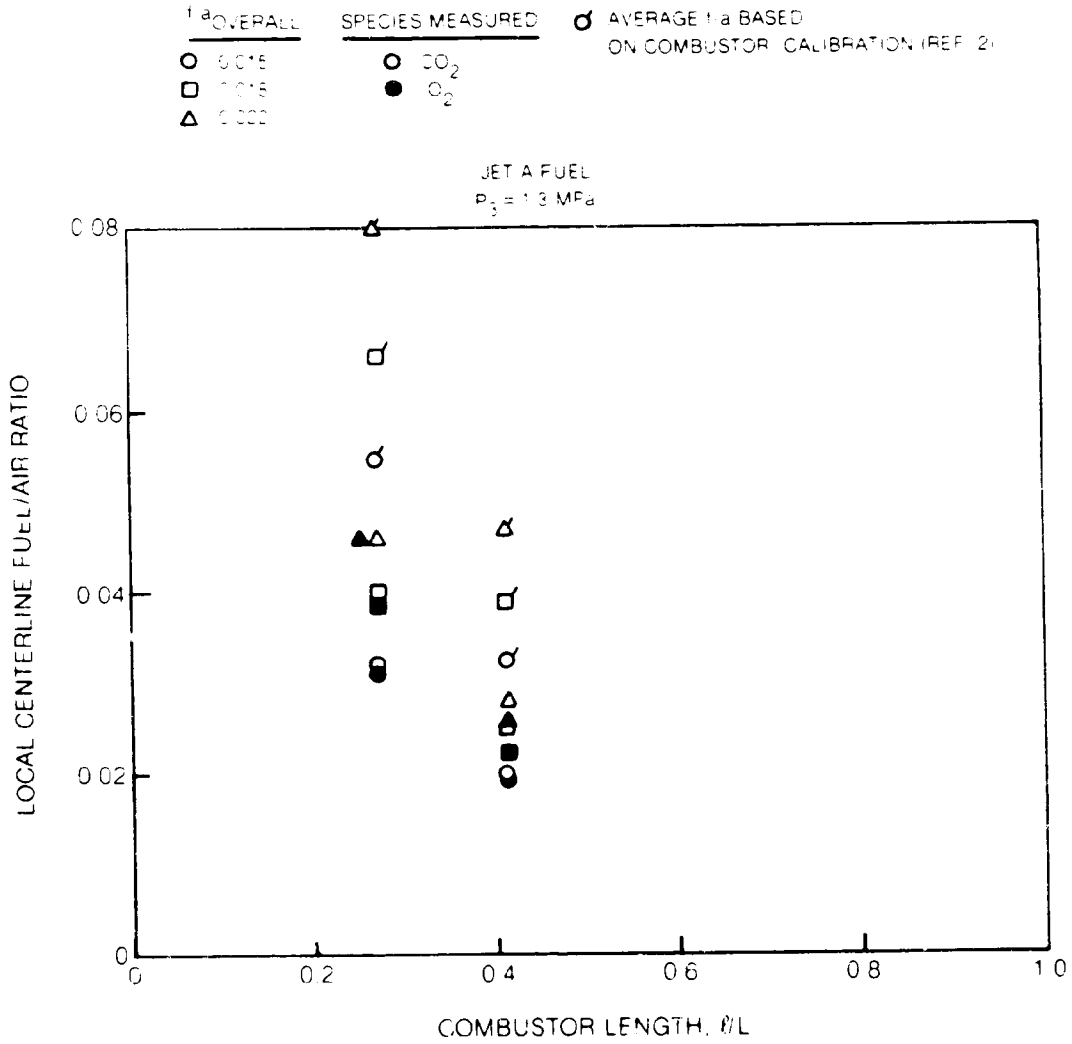
Fig. 22. Local centerline fuel-air ratio based on gas emission measurement
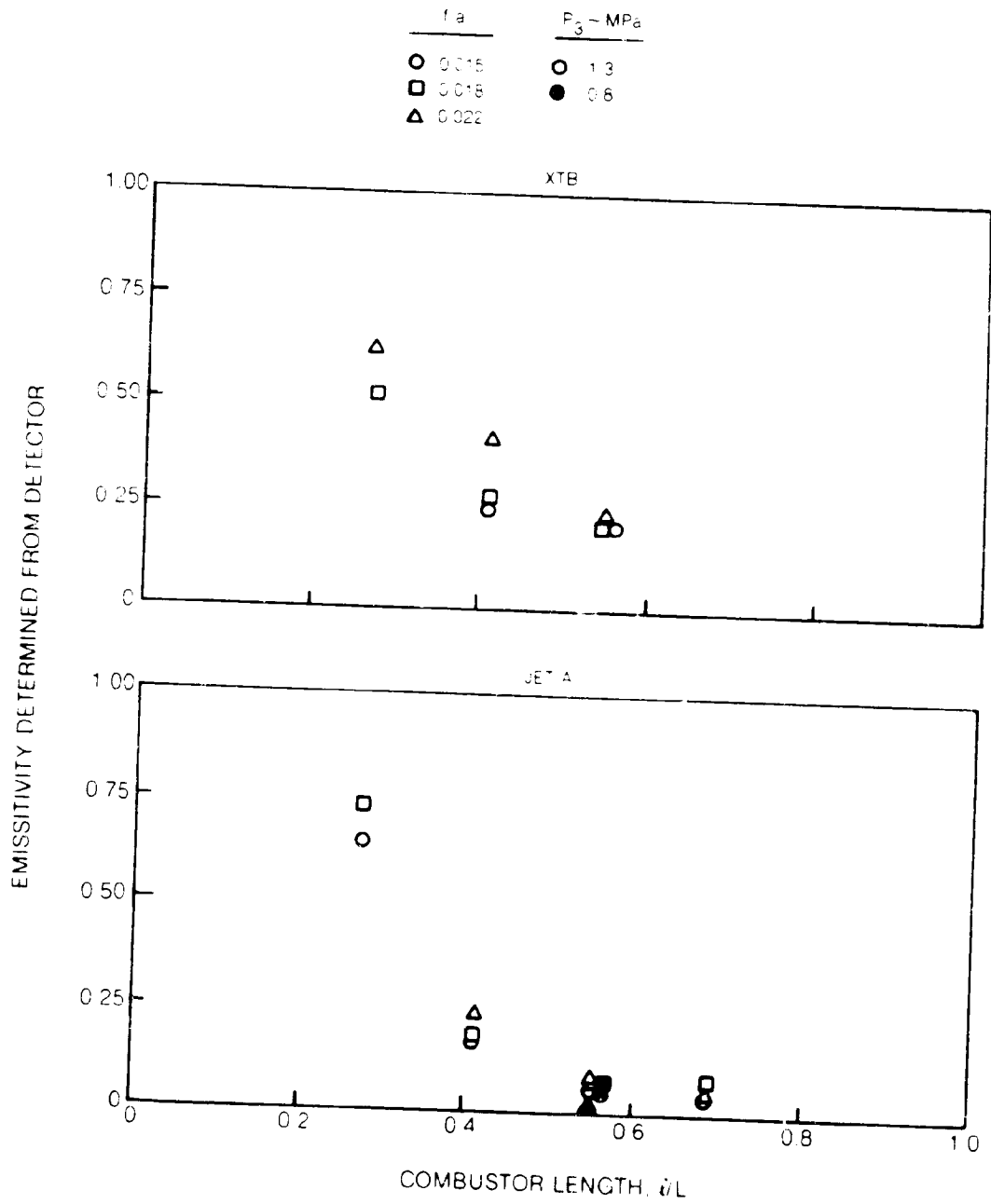
Fig. 23 Emissivity at combustor exit

$P_3 = 1.3$ MPa

f/a

○ 0.015
□ 0.018
△ 0.022

XTB
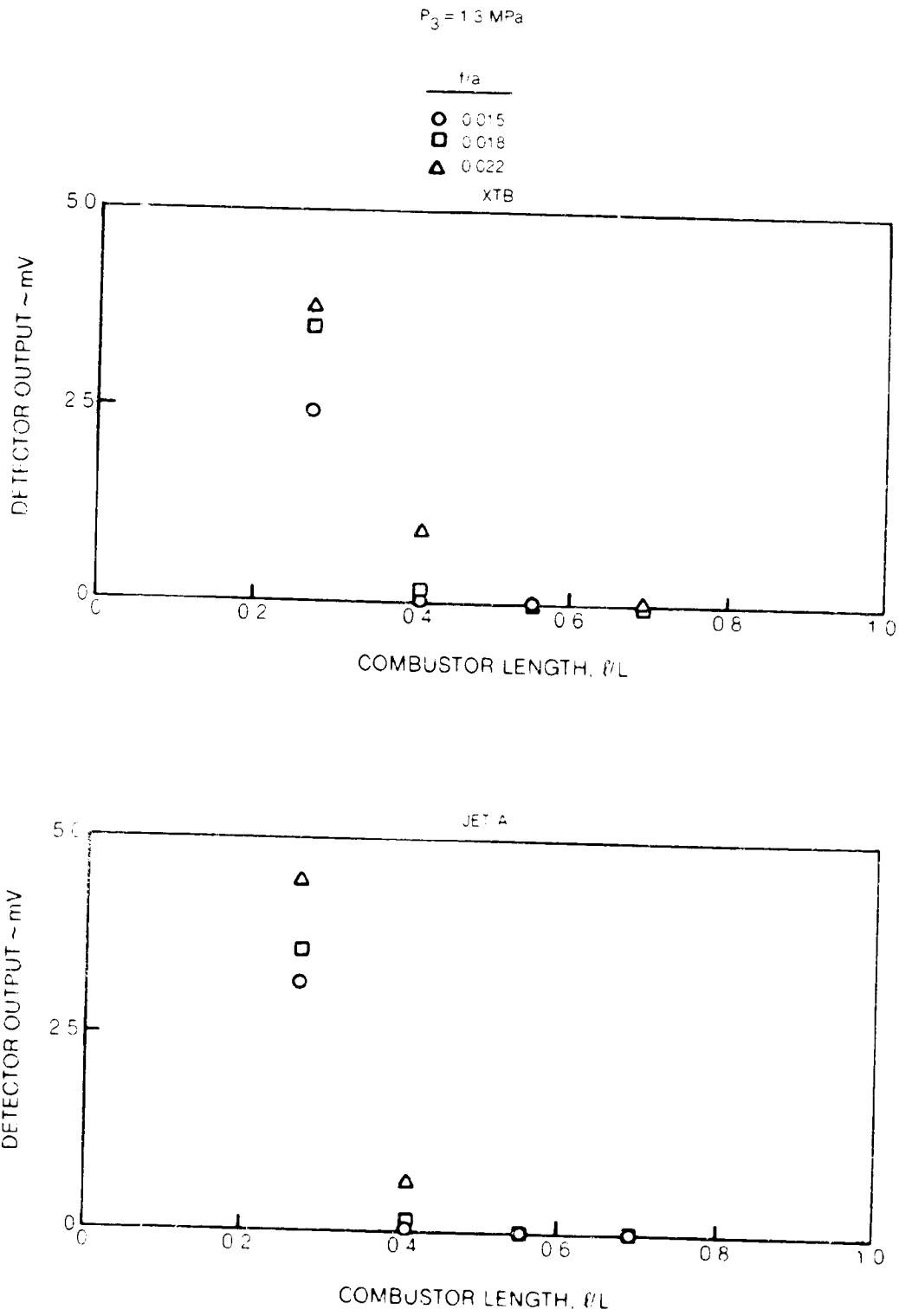
JET A

Fig. 24   Radiation at combustor exit
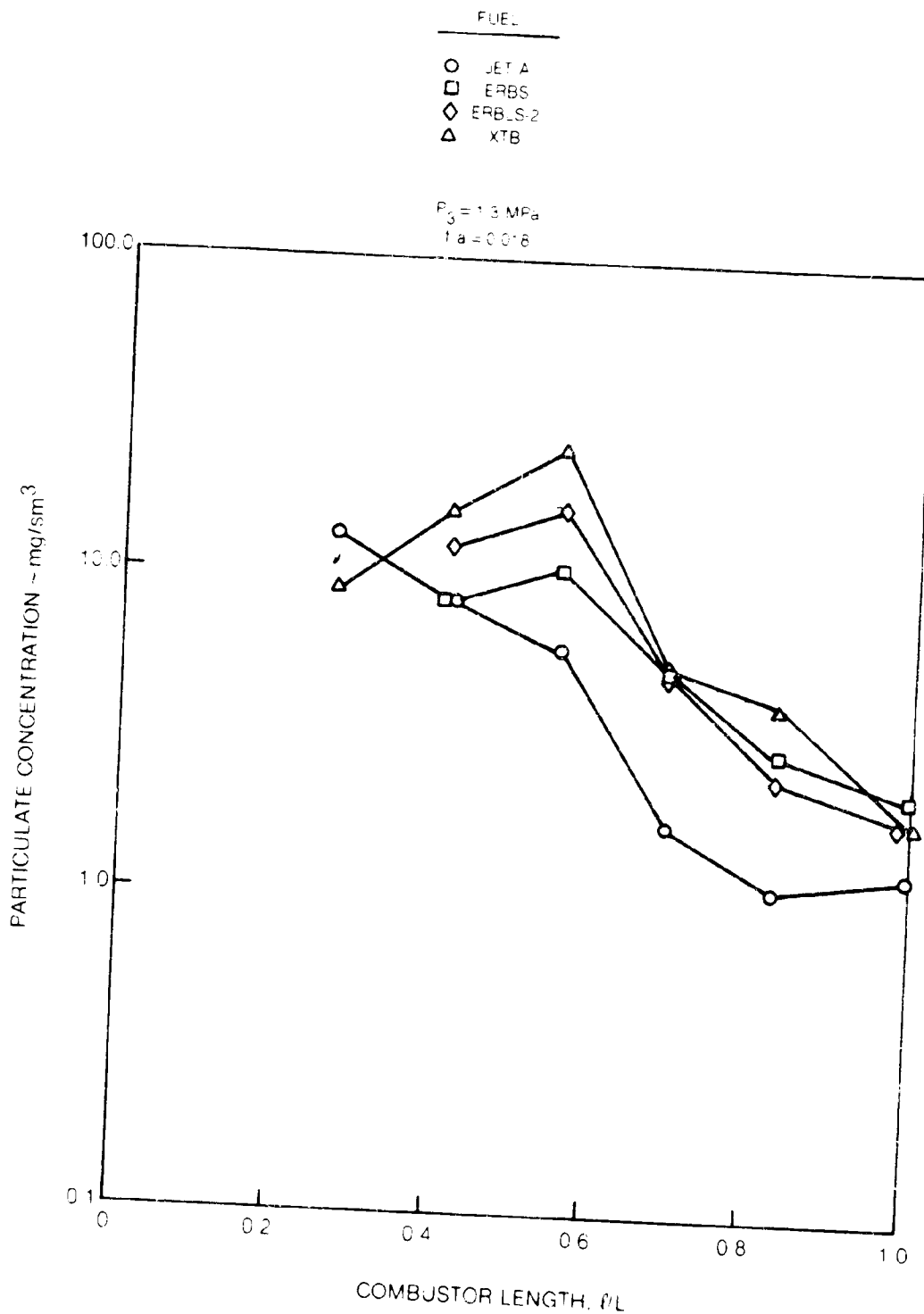
Fig. 25 Fuel effects on particulate concentration
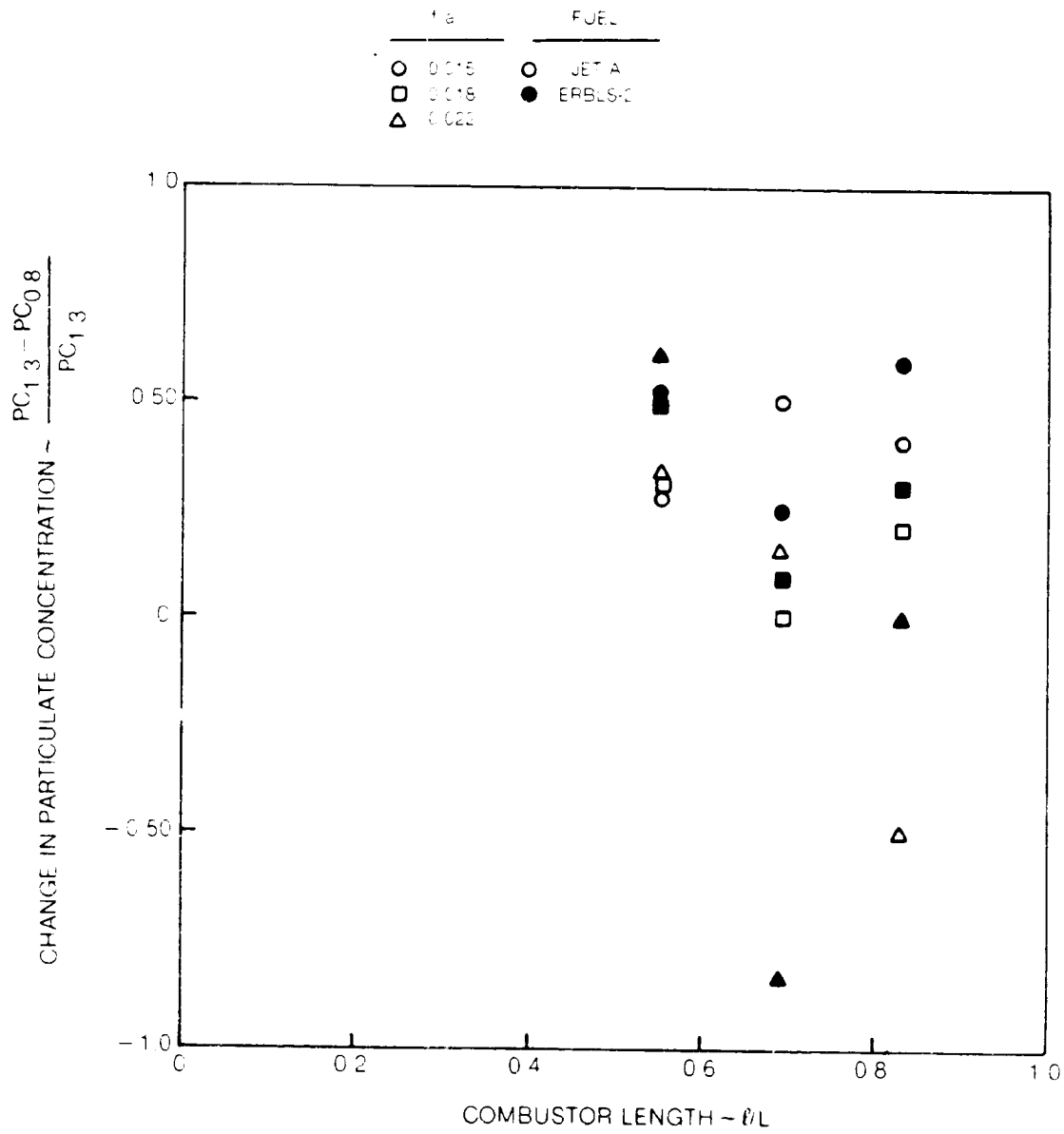
Fig. 26 Effect of combustor pressure on particulate concentration

σ DATA FROM REF. 2

$P_3 \sim MPa$		f/a
O 1.3	O	0.015
● 0.8	□	0.018
	△	0.022
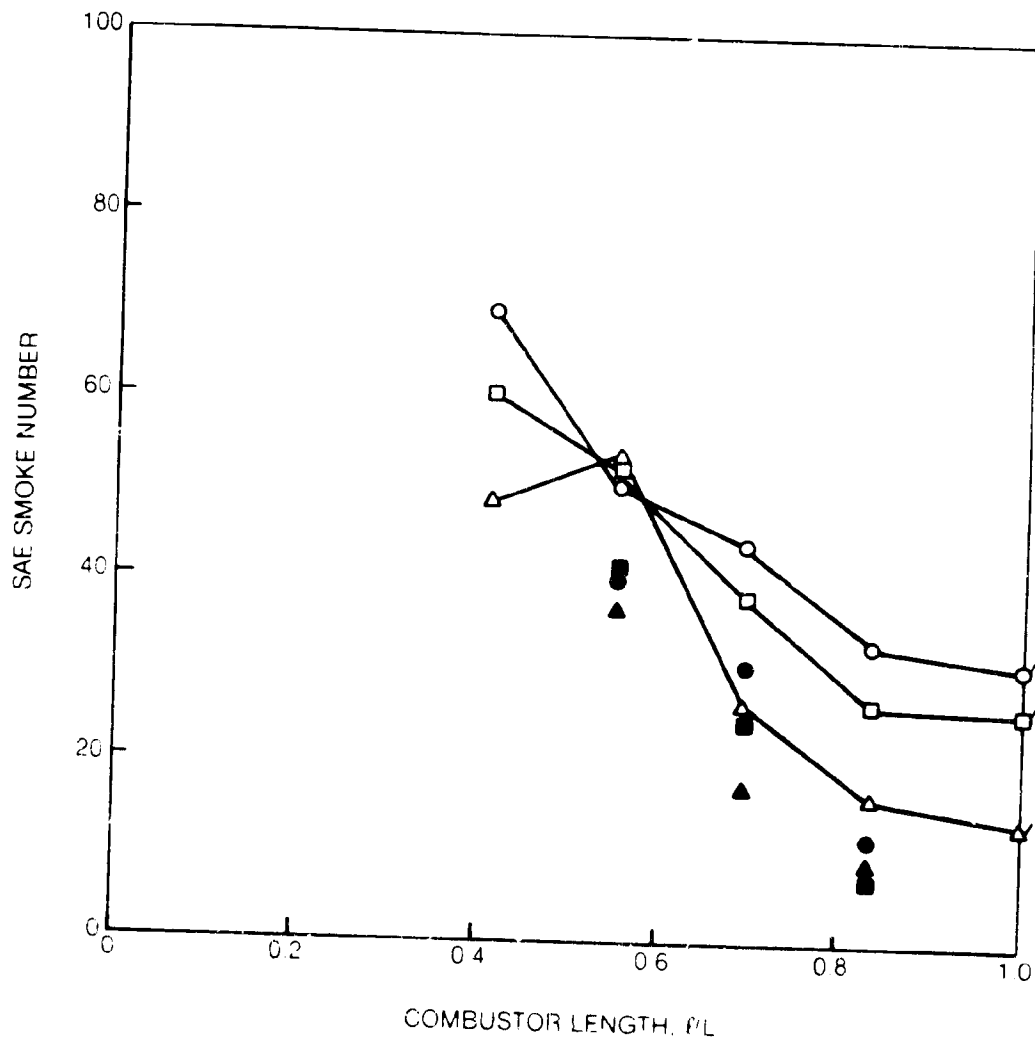
Fig. 27 SAE smoke number for Jet A fuel

♂ DATA FROM REF 2

	f/a
○	0 015
□	0 018
△	0 022

$P_3 = 1 3$ MPa
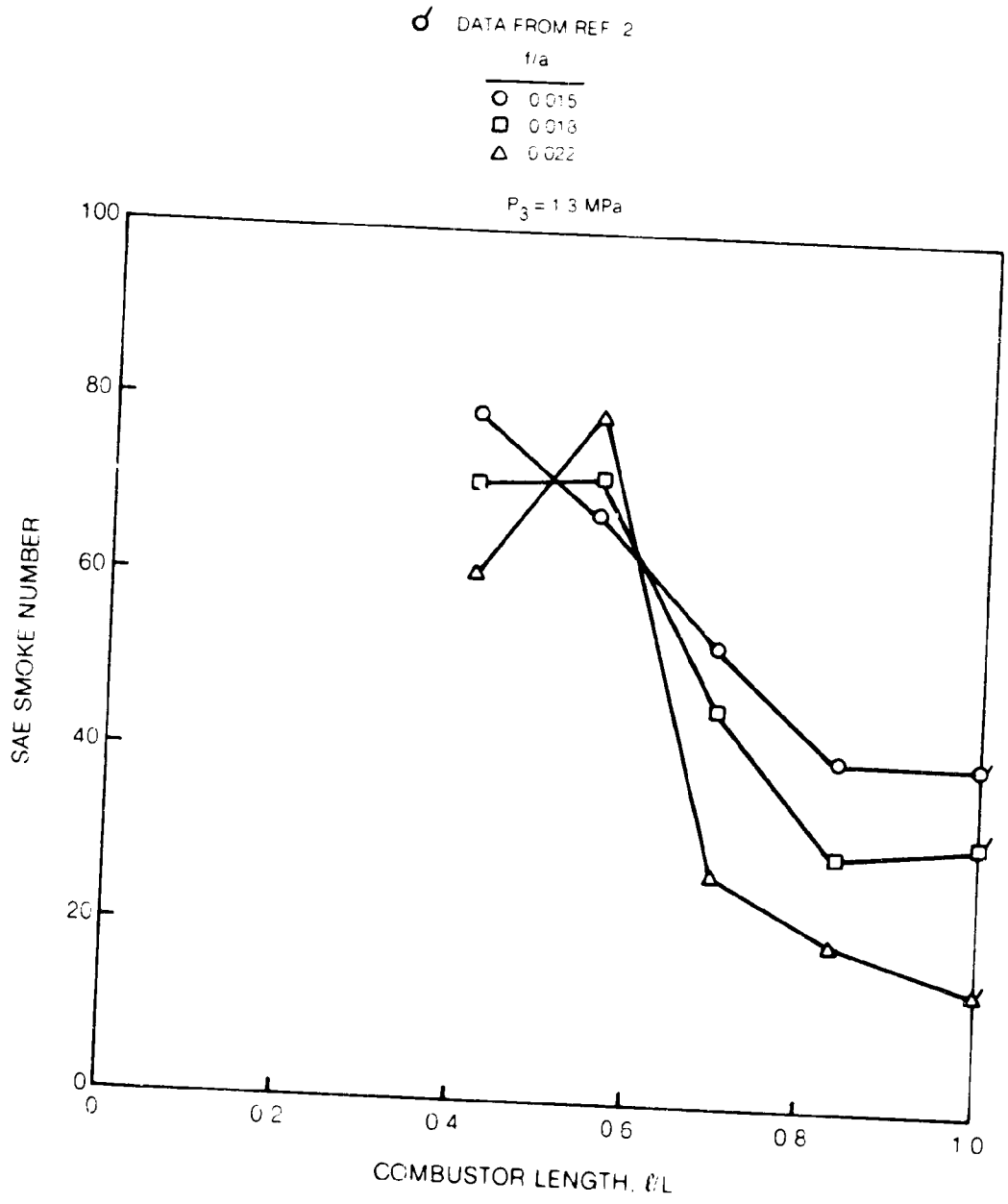
Fig. 28 SAE smoke number for ERBS fuel

85-9-29-13
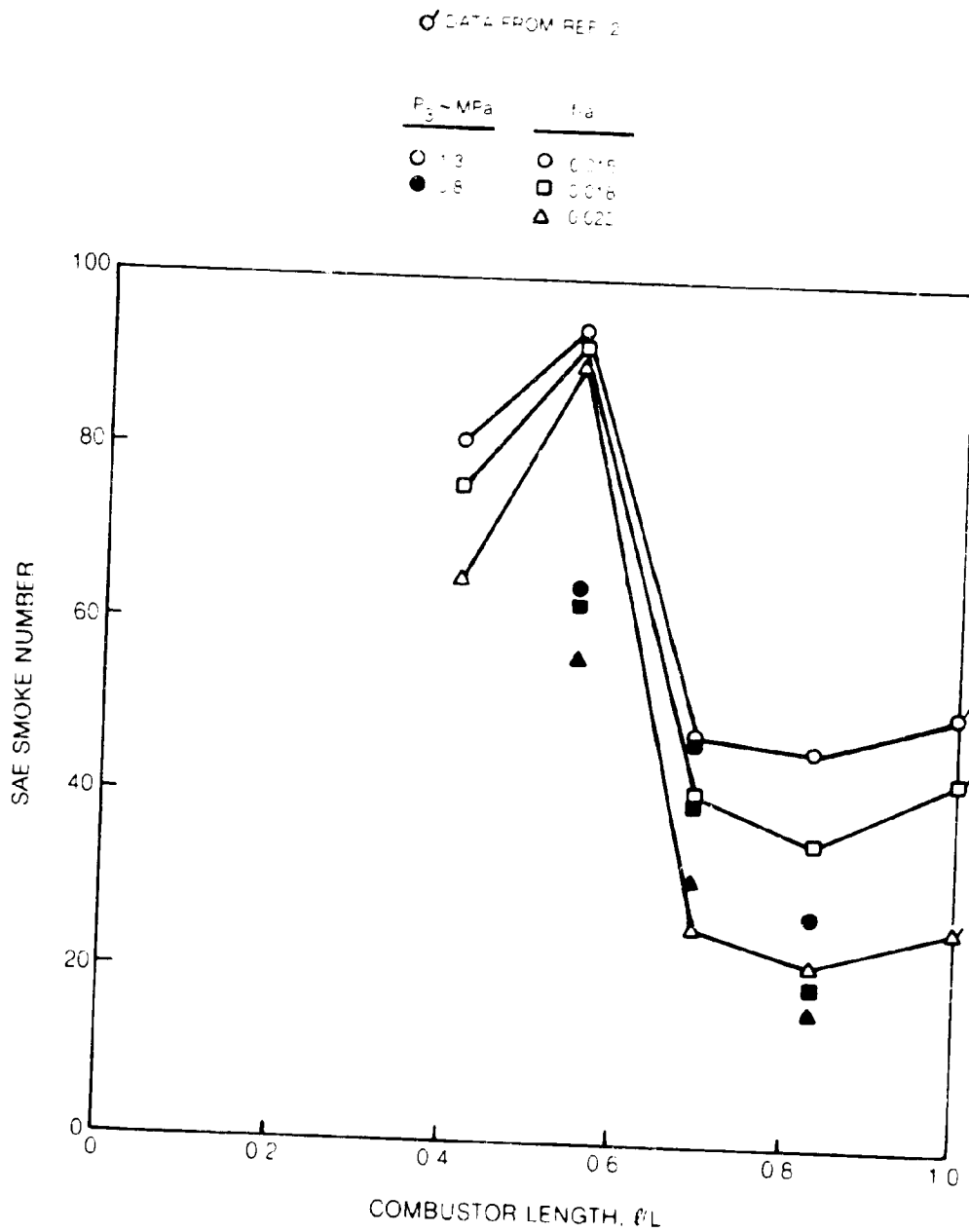
Fig. 29 SAE smoke number for ERBLS-2 fuel
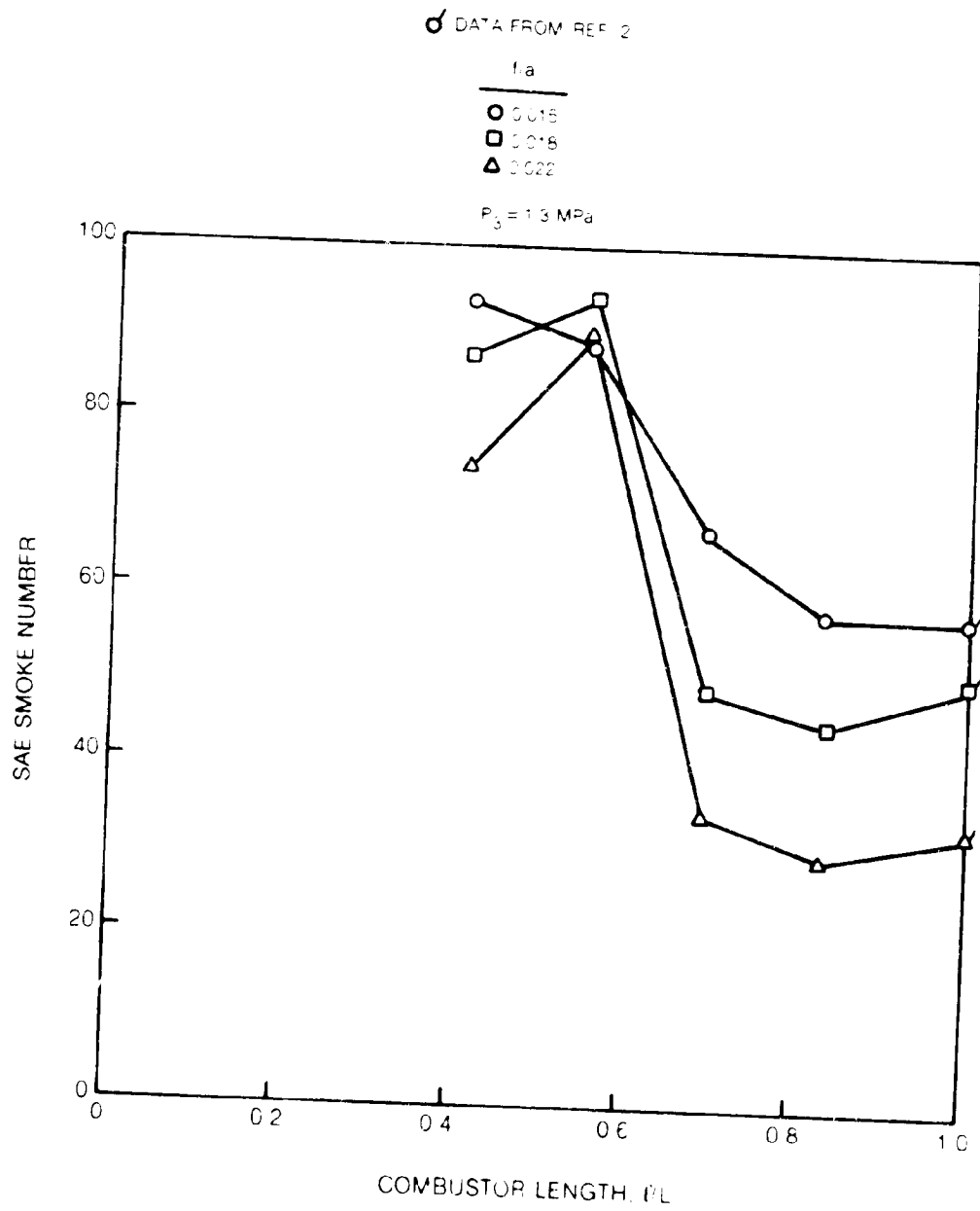
Fig. 30 SAE smoke number for XTB fuel
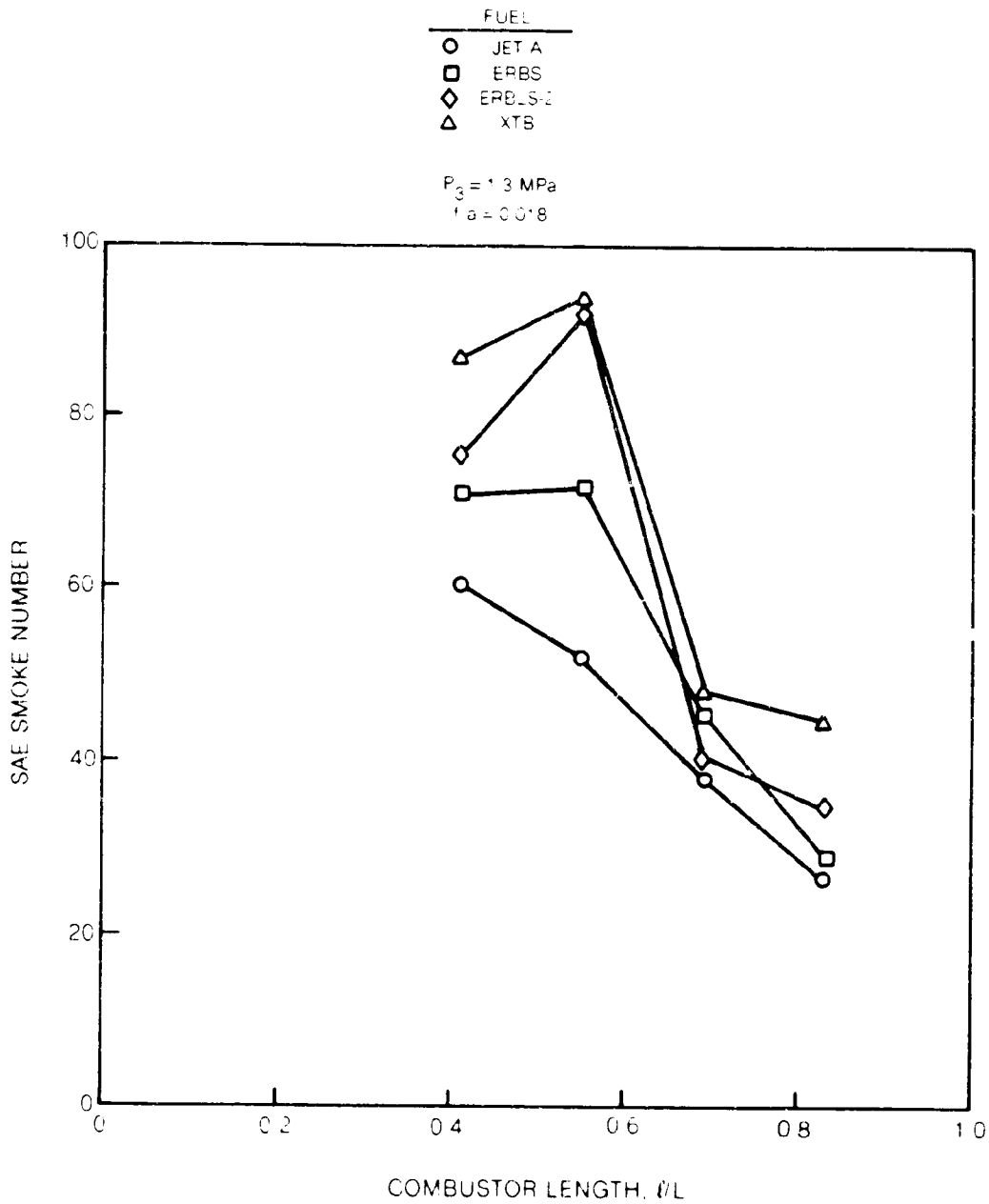
Fig. 31 Fuel effects on SAE smoke number
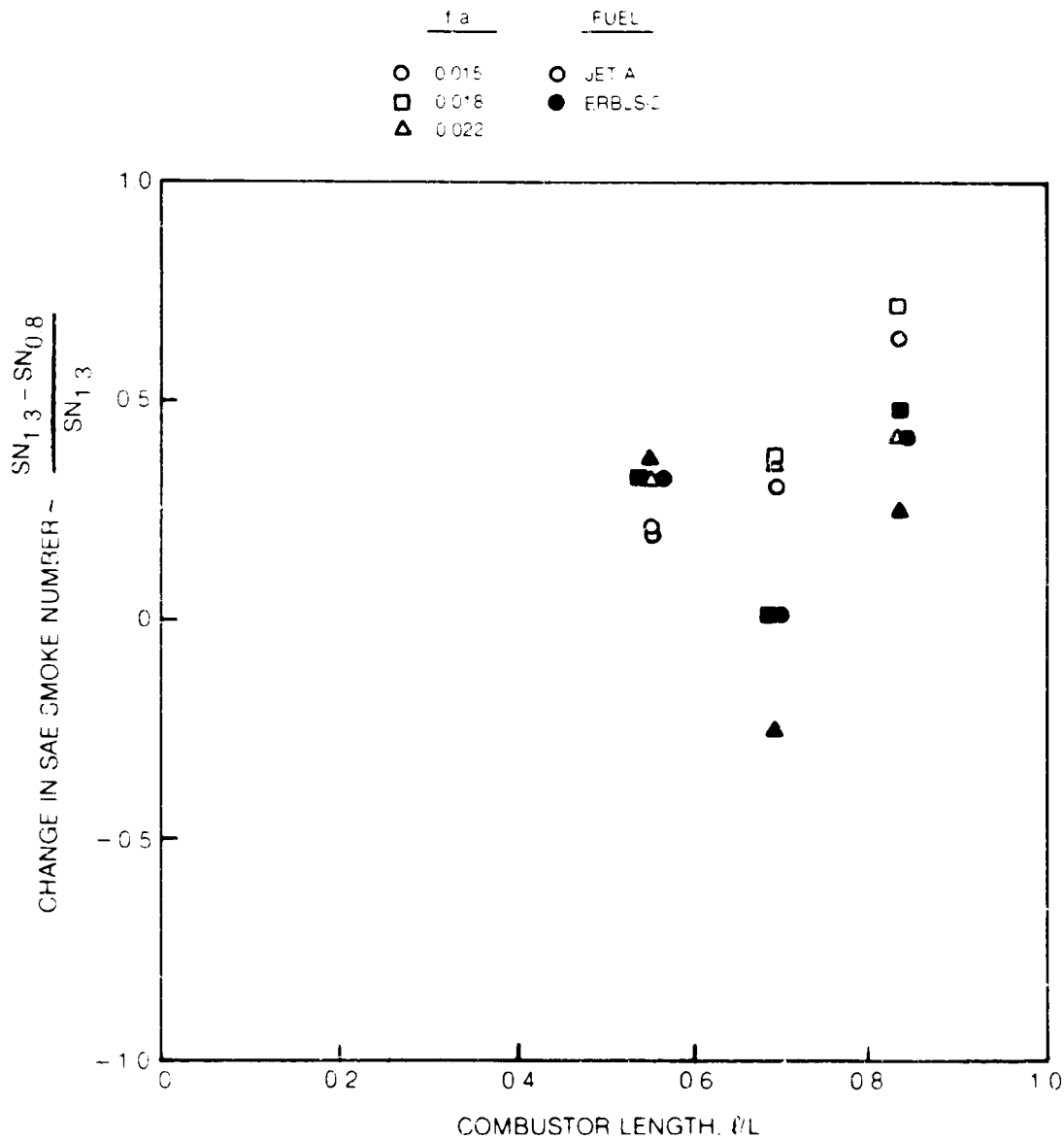
Fig. 32 Effect of combustor pressure on SAE smoke number
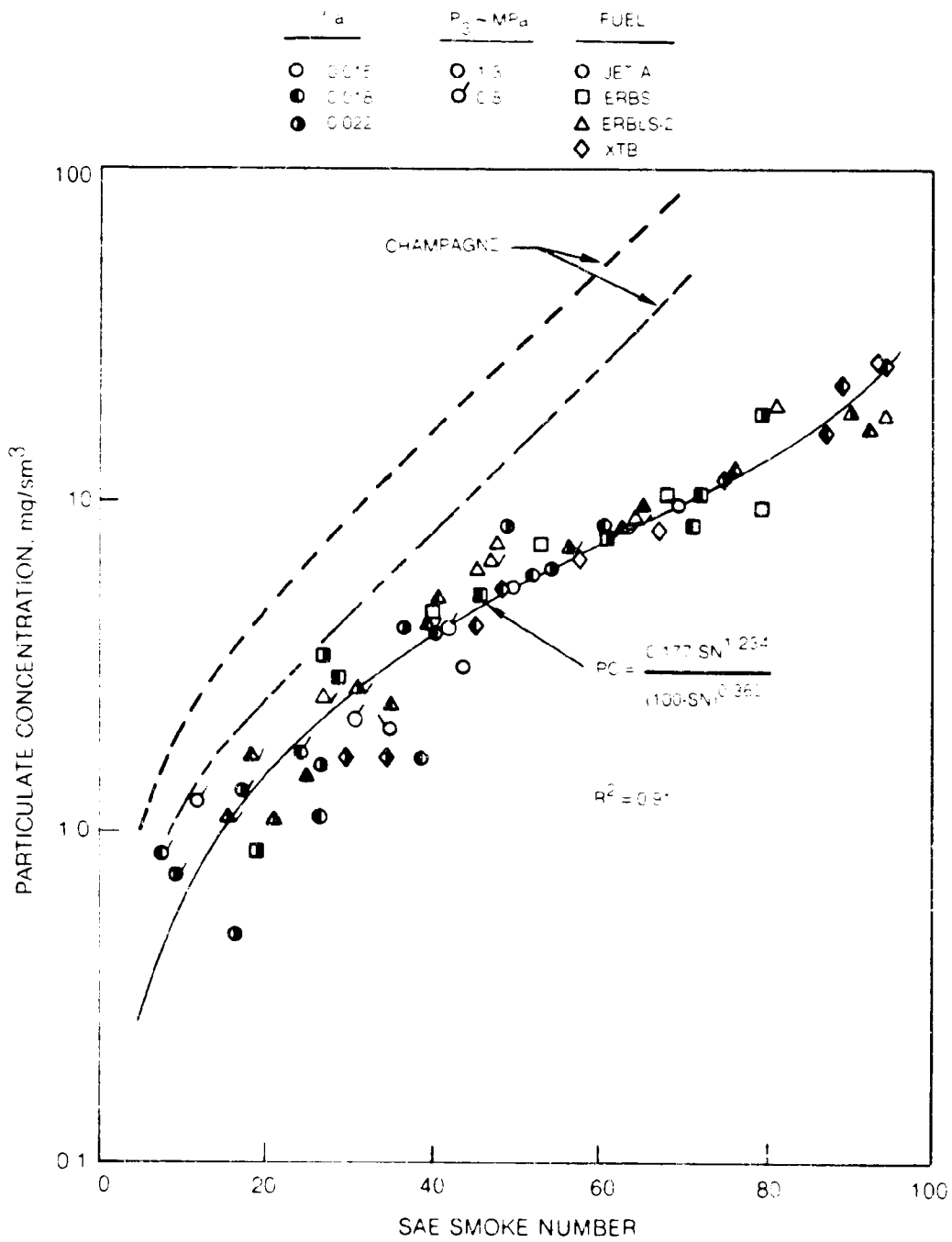
Fig. 33 Relationship between particulate concentration and SAE smoke number
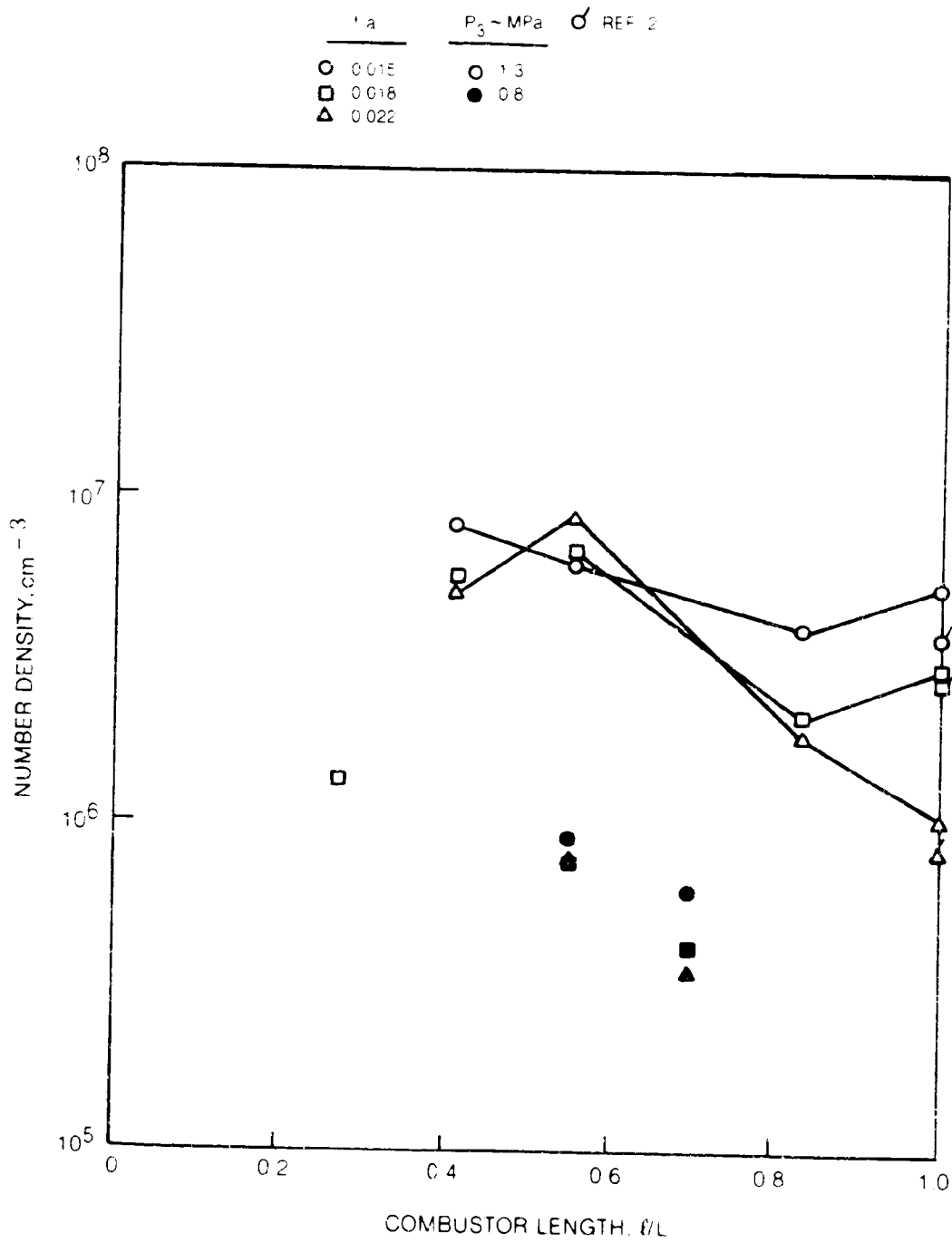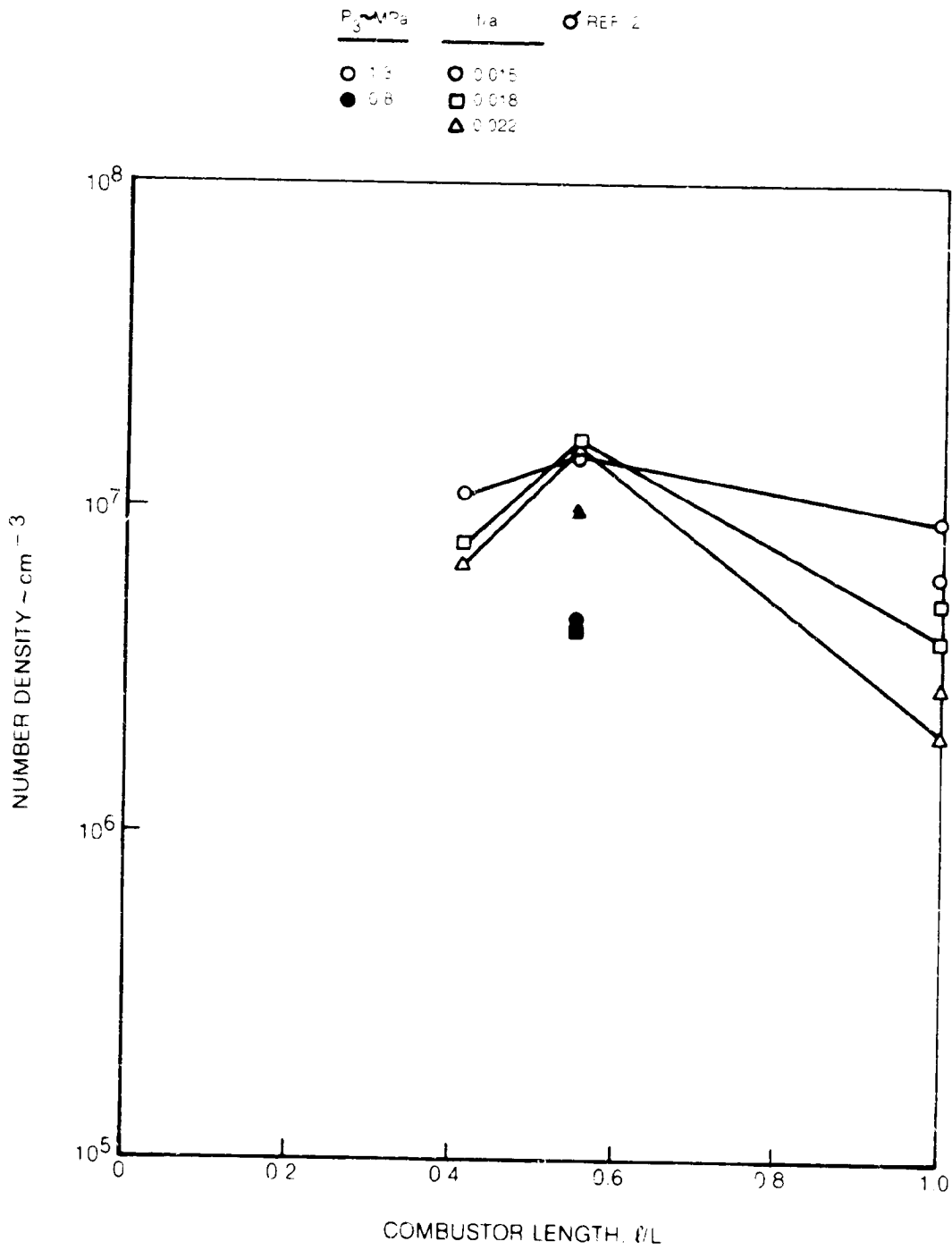
Fig. 34   Number density for Jet A fuel

f/a

○ 0.015   ♂ REF 2
□ 0.018
△ 0.022

$P_3 = 1.3$ MPa
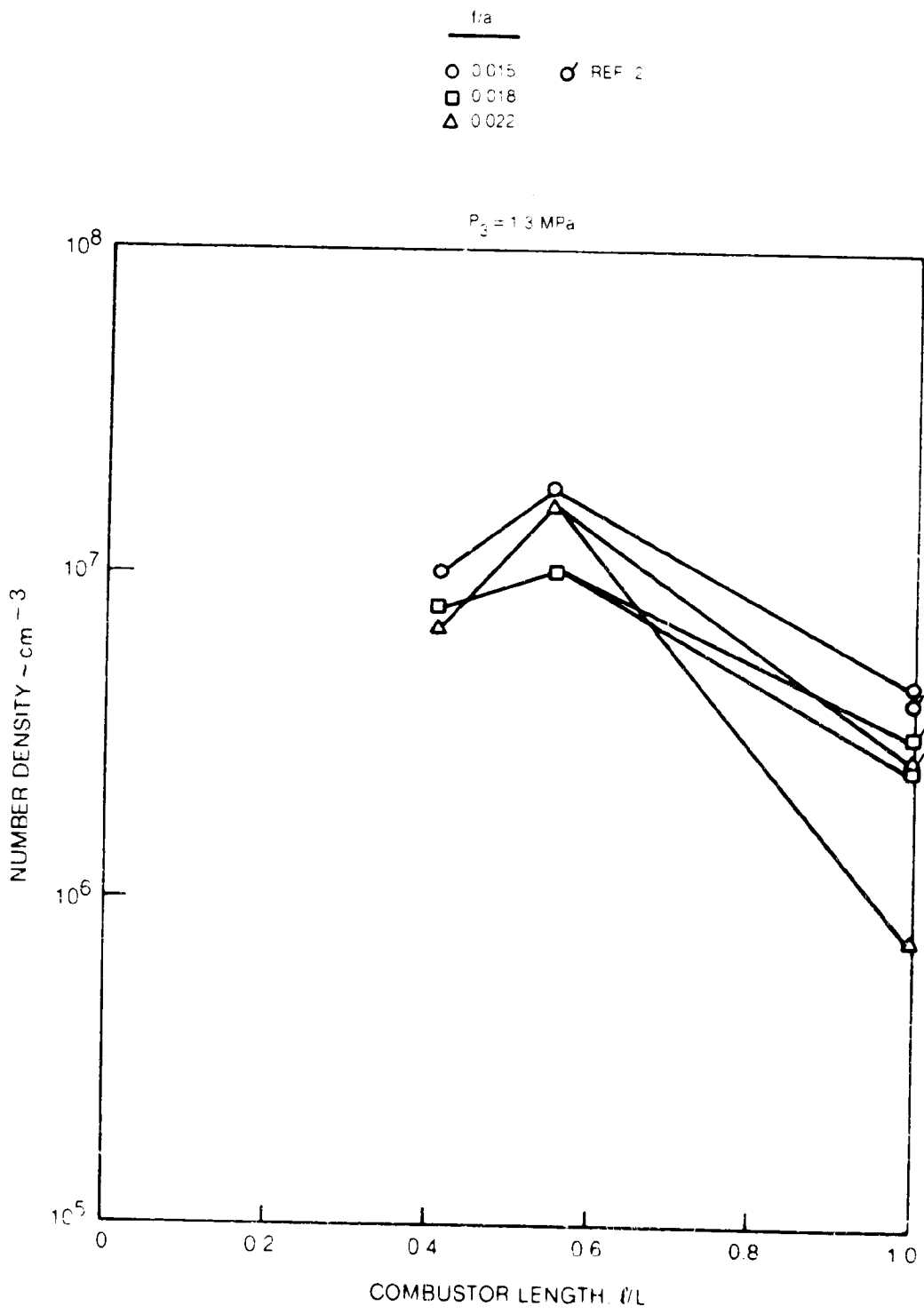
Fig. 35   Number density for ERBS fuel

Fig. 36   Number density for ERBLS-2 fuel

f a

O 0.015   ♂ REF 2
□ 0.018
△ 0.022

$P_3 = 1.3$ MPa

NUMBER DENSITY ~ cm^{-3}

COMBUSTOR LENGTH, ℓ/L
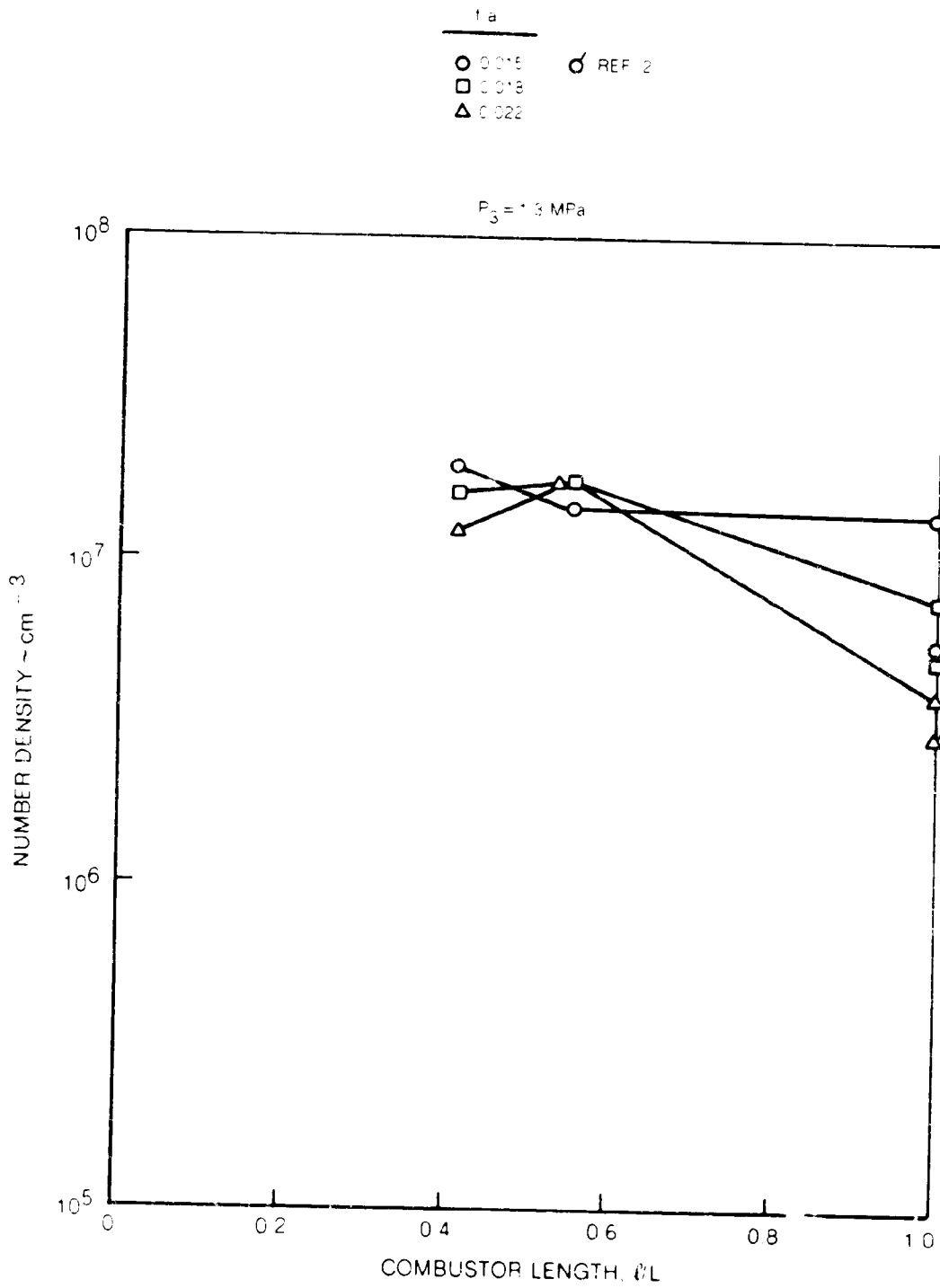
Fig. 37   Number density for XTB fuel

FUEL

○　JET A
□　ERBS
◇　ERBS-2
△　XTB

f/a = 0.019
P_3 = 1.3 MPa
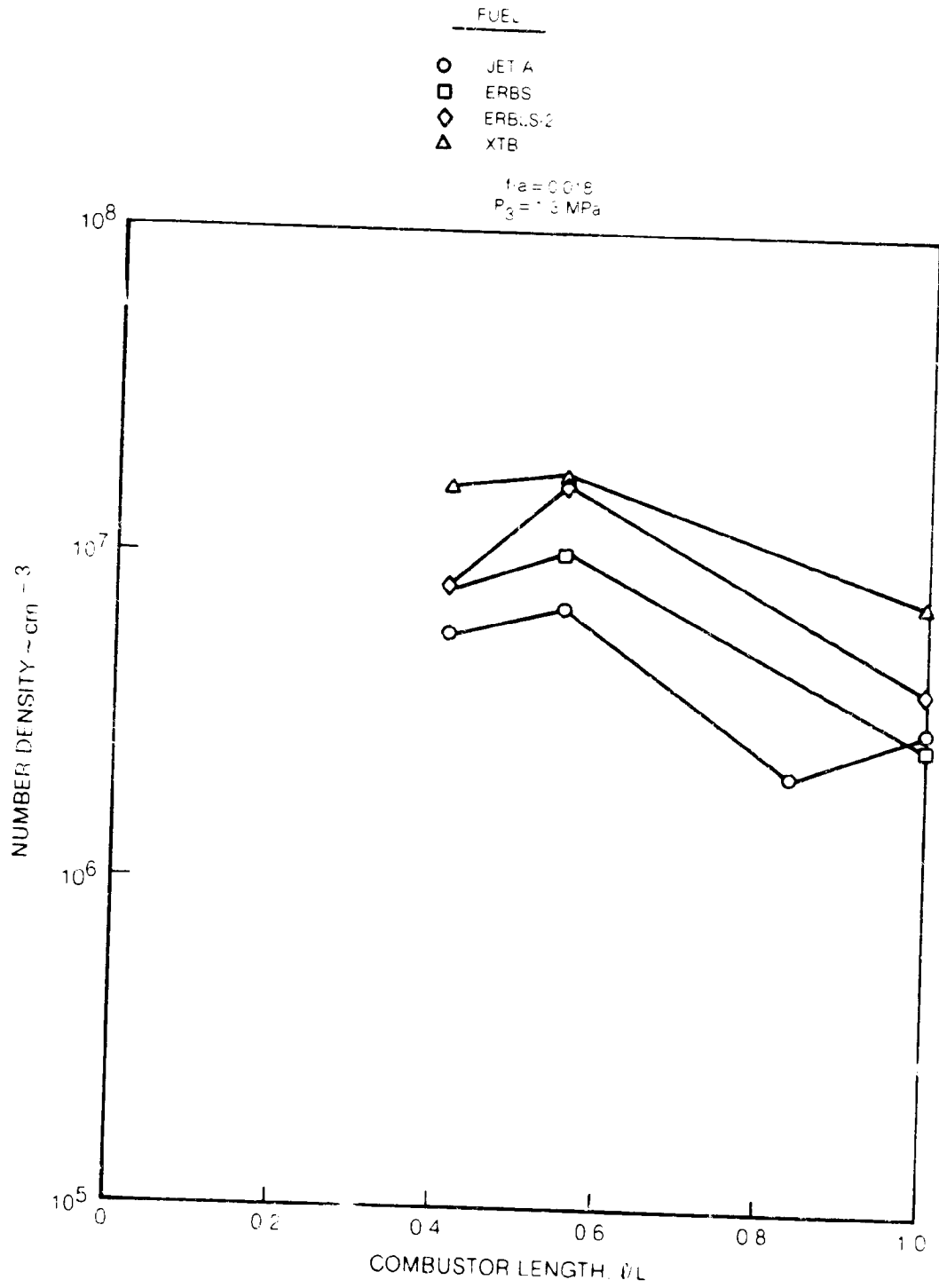
Fig. 38　Effect of fuel on number density
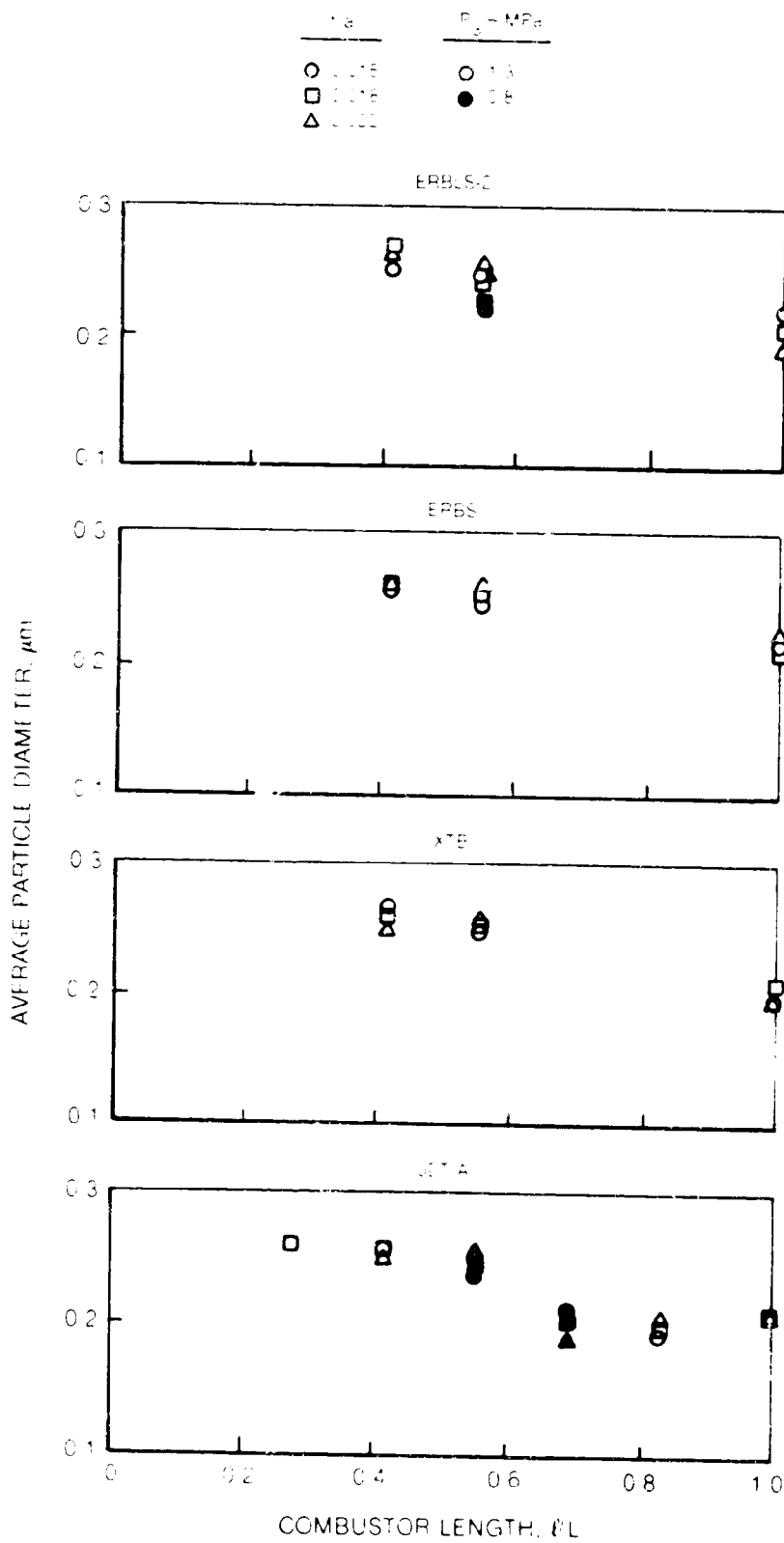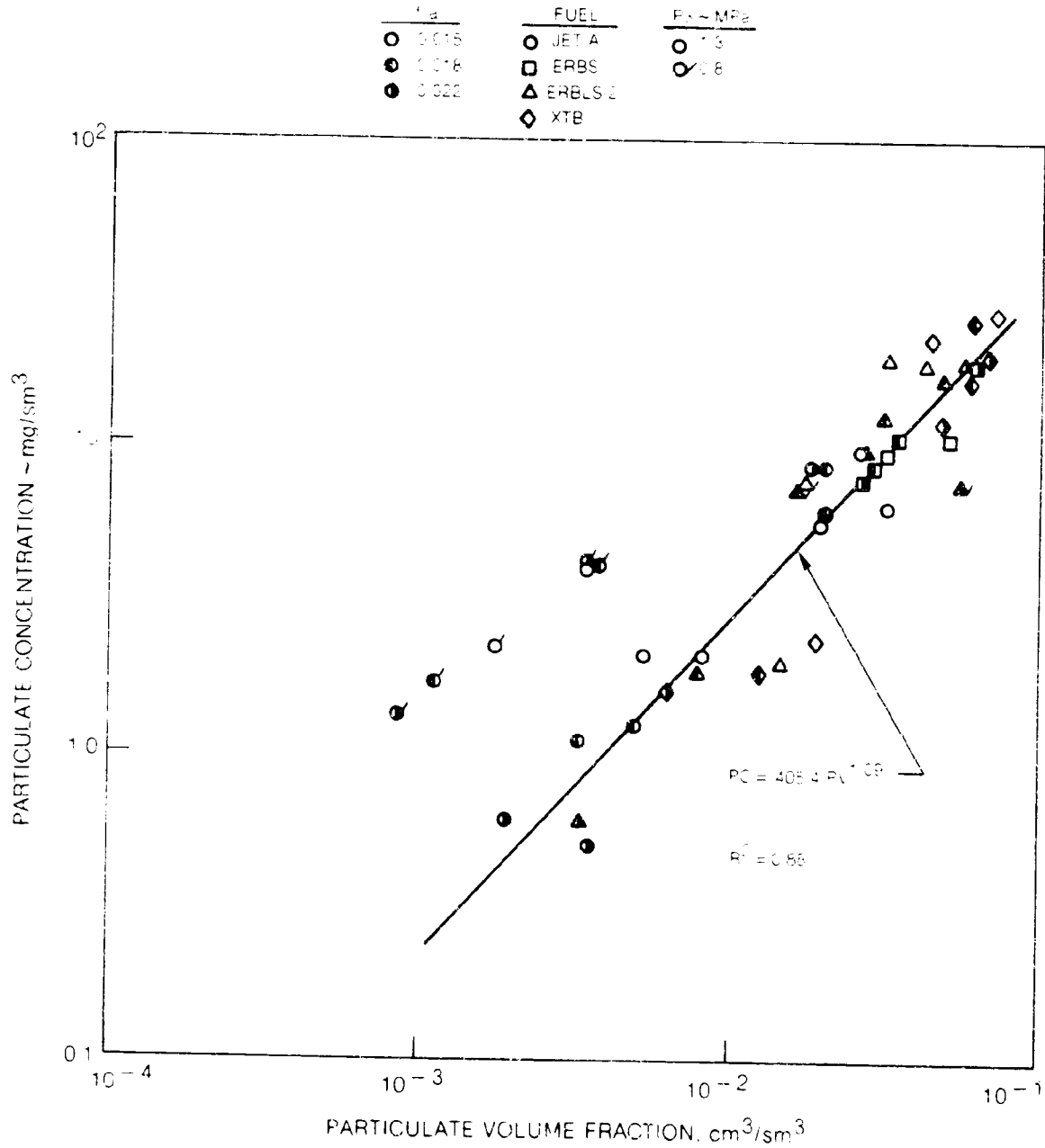
Fig. 39 Average particle diameter at combustor exit

85-9-29-23

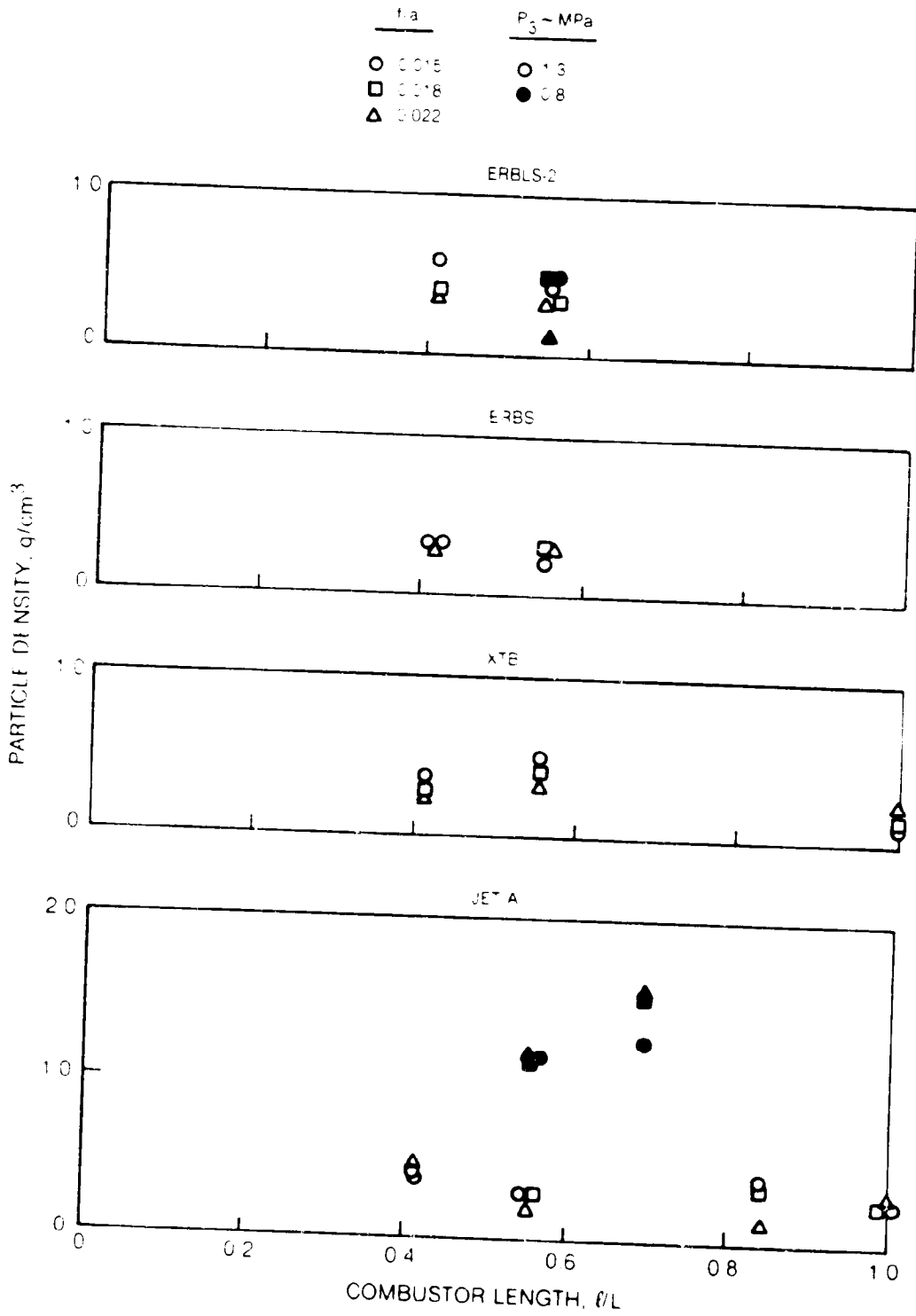Fig. 40.   Relationship between particulate concentration and particulate volume

Fig. 41 Particle density at combustor exit

C - 2

1. Report No. NASA CR-175030	2. Government Accession No.	3. Recipient's Catalog No.
4. Title and Subtitle "Optical and Probe Determination of Soot Concentrations in a Model Gas Turbine Combustor"		5. Report Date January, 1986
		6. Performing Organization Code
7. Author(s) W. A. Eckerle T. J. Rosfjord		8. Performing Organization Report No. UTRC R85-956760-21
9. Performing Organization Name and Address United Technologies Research Center Silver Lane East Hartford, Connecticut 06108		10. Work Unit No.
		11. Contract or Grant No. NAS3-24223
12. Sponsoring Agency Name and Address NASA Lewis Research Center 21000 Brookpark Road Cleveland, OH 44135		13. Type of Report and Period Covered Contractor Final Report
		14. Sponsoring Agency Code

15. Supplementary Notes

Program Manager - J. Biaglow

16. Abstract

An experimental program was conducted at UTRC to track the variation in soot loading along the centerline of a generic gas turbine combustor. The burner was a 12.7-cm dia cylindrical device consisting of six sheet-metal louvers. Determination of soot loading along the burner length was achieved by acquiring measurements first at the exit of the full-length combustor and then at upstream stations by sequential removal of liner louvers to shorten the burner length. Alteration of the flow field approaching and within the shortened burners was minimized by bypassing flow that would have passed through removed louvers in order to maintain a constant liner pressure drop. The burner exhaust flow was sampled at the burner centerline to determine soot mass concentration and smoke number. Characteristic particle size and number density, transmissivity of the exhaust flow, and local radiation from luminous soot particles in the exhaust were determined by optical techniques. Four test fuels were burned at three fuel-air ratios to determine fuel chemical property and flow temperature influences. Data were also acquired at two combustor pressures. Particulate concentration data indicated a strong oxidation mechanism in the combustor secondary zone, though the oxidation was significantly affected by flow tempeature. Soot production was directly related to fuel smoke point. Less soot production and lower secondary-zone oxidation rates were observed at reduced combustor pressure.

17. Key Words (Suggested by Author(s)) Gas Turbine Combustors Soot Concentration Fuel-Effects	18. Distribution Statement Unclassified - Unlimited		
19. Security Classif. (of this report) Unclassified	20. Security Classif. (of this page) Unclassified	21. No. of Pages	22. Price*

* For sale by the National Technical Information Service Springfield. Virginia 22151

NASA-C-158 (Rev. 6-71)